TECHNISCHE UNIVERSITÄT MÜNCHEN

LEHRSTUHL FÜR HOCHSPANNUNGS- UND ANLAGENTECHNIK

Factors of Influence on the Erosion of Epoxy Resin Insulating Material by Corona Discharges

Mostafa Mohamed Abdo Refaey

Vollständiger Abdruck der von der Fakultät für Elektrotechnik und Informationstechnik der Technischen Universität München zur Erlangung des akademischen Grades eines Doktor-Ingenieurs genehmigten Dissertation.

Vorsitzender:	Univ.-Prof. Dr. sc. techn. Andreas Herkersdorf
Prüfer der Dissertation:	1. Univ.-Prof. Dr.-Ing. J. S. Kindersberger
	2. Univ.-Prof. Dr.-Ing. Michael Kurrat Technische Universität Braunschweig

Die Dissertation wurde am 25.09.2014 bei der Technischen Universität München eingereicht und durch die Fakultät für Elektrotechnik und Informationstechnik am 04.12.2014 angenommen.

"Gedruckt mit Unterstützung des Deutschen Akademischen Austauschdienstes"

Acknowledgements

This dissertation is an outcome of the work done as a scientific assistant at Institute for High Voltage Engineering and Switchgear Technology of TU München which I have joined in April 2011. A thesis is seldom the work of a single person rather than the result of a research activity involving a bunch of people. I am pleased now to acknowledge those who have, in various ways, contributed to this work. I owe a great debt of gratitude to all of them.

First and foremost, it has been a pleasure working with Prof. Dr.-Ing Josef Kindersberger. His sharp eyes and superb analytical skills were instrumental in the success of this thesis. I would like to express my sincere gratitude, deep appreciation and thanks for his patience, concern, directions, continuous supervision and encouragement during the entire period of my PhD.

I am also grateful to Prof. Dr.-Ing Michael Kurrat from TU Braunschweig for his interest in this research area and kindly accepting to be the co-referee for my dissertation. Special thanks also go to Prof. Dr. sc. techn. Andreas Herkersdorf for being the chairman of the examination committee.

Without financial support, research becomes difficult. Accordingly, thanks to the Ministry of Higher Education of the Arab Republic of Egypt (MOHE) and the Deutscher Akademischer Austauschdienst (DAAD) for supporting the research work during my PhD.

Special thanks goes to Huntsman GmbH (Switzerland) for offering the epoxy resin specimens. I'm very grateful to prof. Dr. Sebastian Günther, in the Chemistry Institute at the TU München for the opportunity to use the XPS (ESCA) machine for investigating polymer surface composition.

I would like also to express my gratitude to all the colleagues at the institute of high voltage technology, their friendship and professional collaboration meet a great deal to me.

Many special thanks go to my lovely wife for being the person she is and being a constant source of strength for everything I do. She was always there cheering me up and stood by me through the good times and bad.

Last but not least, I feel myself blessed to have parents who were there always for me with their love. I would like to thank my parents for their love and support throughout my life. Thank you both for giving me strength to reach for the stars and chase my dreams.

قال تعالى '... وَمَا أُوتِيتُم مِّنَ الْعِلْمِ إِلَّا قَلِيلًا'

الآيه ٨٥ , سورة الإسراء

„..., und euch ist vom Wissen nur wenig gegeben.“; (85)(Al-Israa)

Zusammenfassung

In Hochspannungsisolierungen können innere und äußere Teilentladungen auftreten. Insbesondere bei der Verwendung von polymeren Isolierwerkstoffen, kann das Auftreten von Oberflächenentladungen zu Erosion führen. Bei hoher Entladungsintensität und -dauer kann es bei den meisten polymeren Isolierwerkstoffen auch zur Kriechwegbildung kommen. Eines der häufigsten Probleme von Isolierwerkstoffen bei der Anwendung für Hochspannungsisolierungen liegt in der Erosionsanfälligkeit unter dem Einfluss von Oberflächenentladungen.

Trotz der Bedeutung des Erosionsverhaltens gibt es noch kein genormtes Prüfverfahren, um Werkstoffe hinsichtlich ihrer Erosionsbeständigkeit zu prüfen. Derzeit wird in der Regel ein Versuchsaufbau nach IEC 60343 verwendet, um die Erosionsbeständigkeit von Werkstoffen zu prüfen, obwohl die Norm für einen anderen Anwendungsbereich entwickelt wurde. Darüber hinaus sind die Mechanismen, welche zur Erosion führen noch unbekannt und somit die dominierenden Einflussfaktoren nicht bekannt. Für die Entwicklung neuer Isolierwerkstoffe oder der Verbesserung bestehender Isolierwerkstoffen ist es notwendig, die Mechanismen der Erosion zu verstehen, die Einflussfaktoren zu identifizieren und deren Wirkung zu quantifizieren.

Die Art und der Umfang der Erosion, die bei Isolierungen unter Betriebsbedingungen auftreten, sind vielfältig. Teilentladungsaktivität führt zu verschiedenen Phänomenen der Erosion in Abhängigkeit von Form und Frequenz der angelegten Spannung, der Temperatur, und der Luftfeuchte. Um die Isolierwerkstoffe hinsichtlich ihrer Beständigkeit gegenüber Oberflächenentladungen zu prüfen, wurde ein Versuchsaufbau entwickelt, der in Bezug auf die Betriebsbeanspruchungen repräsentative Belastung ermöglichet und mit dem reproduzierbare Ergebnisse erzielt wurden.

Es wurden Prüfungen durchgeführt, um die Einflussfaktoren zu trennen und deren Wirkung zu quantifizieren. Dabei wurden die Auswirkungen unterschiedlicher Belastungen auf die Werkstoffoberfläche in Bezug auf die Entladungs- und Erosionseigenschaften quantifiziert. Mit Hilfe eines weiteren Versuchsaufbaus wurde die mit den Oberflächenentladungen verbundene UV-Strahlungsbelastung identifiziert. Die Intensität und Reichweite der UV-Strahlung wurde an Hand der erfassten UV-Bilder quantifiziert.

Auf Basis dieser Ergebnisse wurden statistische Modelle entwickelt, um einen genaueren Einblick in den Mechanismen der Erosion zu erhalten. Zusätzlich wurden die Isolierwerkstoffe einer Elektronenspektroskopie Analyse (ESCA) unterzogen. Diese Analyse dient der Identifikation der Materialzusammensetzung der erodierten Oberfläche und der Quantifizierung dominierenden Einflussfaktoren auf die Schädigung der Isolierstoffoberfläche. Die Ergebnisse und Schlussfolgesagen dienen dem Verständnis der Erosionsmechanismen unter Einwirkung von elektrischen Entladungen an der Oberfläche polymerer Isolierstoffe.

Abstract

High voltage insulations are subject to internal and external partial discharges. In particular with the use of polymeric insulating materials the occurrence of corona discharges may lead to erosion. At high discharge intensity and duration, erosion may turn into tracking (i.e. the formation of conductive paths) for most insulating polymers. The susceptibility of insulating materials to the occurrence of erosion under the influence of corona discharges is an issue for their use in high voltage insulation.

Despite the importance of the matter there is still no standardized test procedure to test materials for this specific performance. Up to now, usually an experimental set-up according to IEC 60343 is used to test for this performance although the standard has a quite different scope. Moreover, the mechanisms causing erosion are still unclear and hence the main factors of influence are unclear. They need to be identified and their influence needs to be quantified. In conclusion, for the development of new insulating materials or the improvement of existing insulating materials it is necessary to understand the mechanisms of erosion, to identify the factors of influence and to quantify their effect.

The kind and degree of erosion occurring on insulations under service conditions are manifold. The consequence of discharge activity leads to various phenomena of erosion, depending on the shape and frequency of applied voltage, the temperature, the humidity, the ambient gas, etc. In order to test materials with respect to their resistance to corona discharges a novel experimental setup is applied, which allows getting results reproducible and representative to those phenomena occurring under service conditions.

Then, tests have been performed with the aim to separate the factors of influence and to quantify their effect. Tests have been carried out with the variation of the main parameters of influence. The impact of different stresses on material surface is quantified in terms of discharge and erosion characteristics. Another experimental setup is utilized to separate UV radiation associated with the corona discharges in order to identify the influence of UV stresses on material surface. In the same context, an algorithm is applied to the captured UV images for the sake of quantifying UV radiation in form of intensity and spread.

Based on these results statistical models have been developed to get a closer view of the mechanisms of erosion. Additionally, electron spectroscopy chemical analysis (ESCA) has been performed on the insulating material. This analysis aims at identifying the material composition of the eroded surface and quantifying the influence of different stresses on material surface. Gathering all the obtained results and holding a correlation in between will help to achieve the goal of understanding the mechanisms of erosion under the influence of electrical discharges on the surface of polymeric insulating materials used in high voltage applications.

Contents

1. Literature Review

1.1. Introduction

Erosion susceptibility of high voltage electrical insulation is a prime factor that can significantly influence the reliability performance and the costs of maintaining high voltage equipment. At this time there is limited knowledge of factors affecting the life time of the polymeric high voltage insulation where the material is exposed to various stresses, e.g. UV radiation from the sun and from corona discharges on insulator surfaces. The focus of this research is on the fundamentals of the phenomena by which high voltage corona discharges lead to erosion of polymeric insulating materials under different ambient conditions. The fundamental factors that contribute to the understanding of the erosion mechanism of polymeric insulating materials under the influence of electrical discharges can be consequently clarified. The correlation study between corona discharge stress and the resulting material damage represented by surface erosion is still unclear.

The selection and the acceptance of insulators in high voltage applications rely on the assurance of good and long term stable properties of these products. Life time ranging for a few decades and very low failure rates is desired. Polymeric insulators have become more popular in high voltage applications. This can be obviously seen from increasing their share on the insulators market when compared to the traditional ceramic insulators made of porcelain or glass. The construction of polymeric insulators, based on a load bearing glass fiber reinforced (GFR) epoxy rod or tube covered with an elastomeric housing, provides attractive properties [MAR-08]. Compared to the traditional glass and ceramic insulators, modern polymeric insulators are significantly reduced in weight.

Different polymeric materials have been used for the housings of non-ceramic high voltage insulators for assuring a good protection against external environmental factors. Among the materials, the ones based on polydimethylsiloxane (PDMS) and commonly named as silicone rubber (SIR). Other materials used are ethylene-propylene-diene monomer rubber (EPDM), ethylene-vinyl-acetate (EVA) and so-called alloy rubbers, the latter being blend of EPDM and silicone. Polymeric insulators made from structural materials, e.g. epoxy resin (EP) must be also taken into consideration because of their importance in the high voltage insulating materials [ARO-11]. Now a broad range of insulator types is available, including line insulators, hollow-core insulators and apparatus insulators, for voltage levels ranging from distribution voltage to the highest transmission voltages [MAR-08].

Within utilities and industry an urgent need was indicated for material standards, which define the important physical properties of polymers applied for high voltage insulation. Thanks to the long experience, IEC 62039 has been achieved and considered adequate for this criterion. Nevertheless, manufacturers have therefore used their own selection criteria to choose suitable materials. Some utilities have also elaborated specifications for material properties to be proven by insulator suppliers.

1.2. Polymeric High Voltage Insulators

Polymeric insulators are increasingly being used in both the distribution and transmission voltage ranges and are steadily capturing a wider share of the market [HAL-93]. The primary impetus for their increased acceptance by the usually cautions electric power utilities are their substantial advantages compared to inorganic ceramic insulators which have primarily been porcelain and glass [HAC-99], [MAC-97], which are:

1. Better performance in the presence of heavy pollution [SOR-97a], [SOR-97b].
2. Non-ceramic insulators offer a high mechanical strength-to-weight ratio, which permits longer spans and less expensive structures.
3. Polymer insulators also facilitate new compact transmission line design with reduced electromagnetic field effects.
4. Low surface energy of polymer insulating materials results in maintaining a good hydrophobic surface property in the presence of wet conditions such as fog, dew and rain [KIM-92]. This limits the probability of dry band formation, which requires a higher impressed voltage to cause flashover. Compared to porcelain, some polymer materials typically have much better flashover resistance, even when aged.
5. Light weight results in more economic designs of the towers or alternatively enabling to upgrade the voltage of the existing systems without changing the tower dimensions. An example of this was a case in Germany; where the highest voltage of equipment was increased from 245 kV to 420 kV [KIN-96].
6. Easy installation; where there is no need to use heavy cranes for their handling and installation which results in saving in installation and labor costs.
7. Polymer insulators are advantageous to use in dense urban areas and offer advantages in narrow rights of way.
8. As polymer insulating housings are typically molded, it is not difficult to fabricate parts on a cost effective basis that have a higher creepage distance per unit length than porcelain. Weather shed profiles with alternating diameter can be made more complex without production or yield problems. This improves the ac wet flashover by avoiding bridging of all sheds simultaneously during heavy wetting conditions.

Because of the above mentioned points these polymeric insulators are gaining popularity worldwide and replacing the conventional ceramic insulators. However, in the presence of severe contamination and sustained moisture dry band arcing may occur that under certain conditions could lead to tracking and erosion and finally to a failure of the polymeric insulators.

The most common method of classifying the solid insulating materials, based upon their application, distinguishes mainly between indoor and outdoor insulating materials. Both classes are generally subjected to electrical discharge stresses. Nevertheless, outdoor insulators are susceptible to water drop corona as well as pollution initiated discharge activity, which are out of the scope of this study. As a matter of fact the main stress of interest in this work is electrical discharges generated from field enhancement at electrode sharp edges, called further on corona.

1.3. Epoxy Resin Systems and Their Properties

1.3.1. Why the Focus on Epoxy Resin

Epoxy resin is one of the most commonly used thermosetting materials in high voltage apparatus as insulation due to its excellent mechanical, electrical properties and chemical stability. Insulators, bushings, apparatus, etc. can be made from epoxy resin. It can also be used for encapsulation of electronic components, generator windings and transformers. It is used for bonding of very diverse materials such as porcelain, wood, metals, plastics, etc. In any laboratory or industry in which electrical or electronic equipments or components are handled or manufactured, numerous occasions arise wherein epoxy resins can be used with an advantage saving time, labor and money. Filled epoxy resins are extensively used in high voltage insulations such as impregnation of transformer or generator windings or as insulating spacers in SF_6 Gas Insulated Substations (GIS), SF_6 Gas Insulated Transmission System (GITS) and SF_6 circuit breakers.

1.3.2. Epoxy Resin Chemistry

The word “epoxy” is derived from the Greek prefix “ep,” which means over and between, and “oxy,” the combining form of oxygen. By strict definition, epoxy resins refer only to uncross-linked monomers or oligomers containing epoxy groups. It should be noted that very high molecular weight epoxy resins and cured epoxy resins contain very little or no epoxide groups. The vast majority of industrially important epoxy resins are bi- or multifunctional epoxides. Epoxy resins are polymeric compounds that contain at least a very reactive terminal epoxy group, relatively unstable triple ring, and in some formulations hydroxyl groups (see figure 1.1).

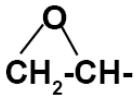

Figure 1.1: Epoxy Group [GRI-06]

Most commercially important epoxy resins are prepared by the coupling reaction of epichlorhydrin with compounds containing at least two active hydrogen atoms (polyphenols, terminal hydroxy substituted polyethers, mono- and diamines, etc.) followed by dehydrohalogenation. About 85% of the recent used epoxy resins [GRI-06] are based *on Diglycidyl Ether Bisphenol A* (DGEBA), and are hereinafter as bisphenol A resins designated. The market dominance of bisphenol A based epoxy resins is a result of a combination of their relatively low cost and adequate-to-superior performance in many applications [HER-04]. Other types, such as bisphenol F epoxy resins, aliphatic, heterocyclic and thermoplastic epoxy will not be discussed in detail as they were not used in the present work, they are only mentioned for completeness.

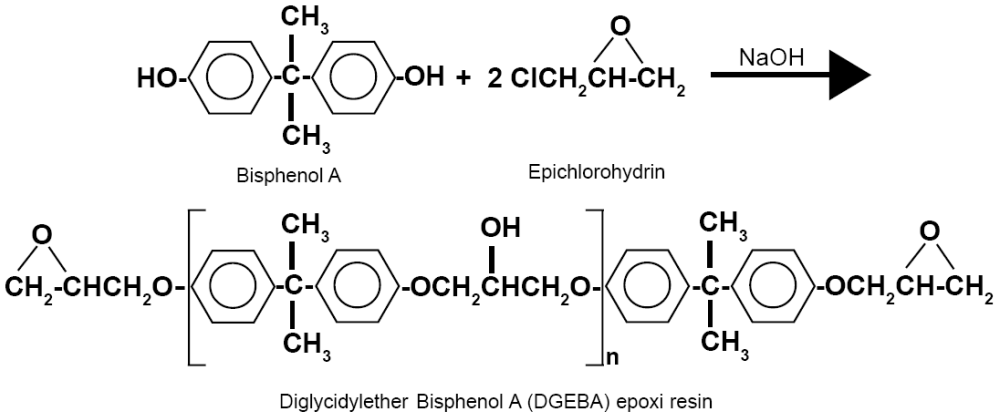

Figure 1.2: Formation reaction of diglycidylether in the manufacture of liquid resins [AUG-04]

When bisphenol A reacts with an excess of epichlorhydrin and alkali hydroxide at about 65°C (figure 1.2), it forms a liquid epoxy resin, which consists of about 50% of DGEBA. The theoretical molar ratio of epichlorhydrin to bisphenol A in the preparation of the diglycidyl ether is 2:1. In practice, however a higher ratio is required, because the stoichiometric ratio provides an epichlorhydrin recovery of only 10%. It is therefore selected as two to three times the stoichiometric amount [DOM-92].

When using "pure" epichlorhydrin it is necessary to use water for the acceleration of the reaction. Water must be added in excess to maintain the formation of high molecular weight reaction products within limits. Regained or recycled epichlorhydrin usually contains sufficient quantity of water. The degree of polymerization is in the range of $0 \leq n \leq 14$, where n is the average number of repeating structural monomer units. With n = 0, the product is diglycidyl ether, and the molecular weight is 340 g/mol. With n = 10 results in a molecular weight of about 3000 g/mol, which is a high figure for resins. Hence, it can be said that in the uncured stage, the epoxy resins are polymers with low degree of polymerization. For the production of resins with $0 \leq n \leq 4$ usually called Taffy process is used, while higher molecular weight resins are produced in the fusion process [GRI-06].

1.3.3. Epoxy Resins used for High Voltage Insulation

The most important epoxy resin used as electrical insulating material, bisphenol A epoxy resin, prepared by reaction of acetone and phenol. [BRY-99] and [BEY-86] have reported a fairly large number of synthetic epoxy resin compounds other than normal diglycidyl ether resin being developed for their appropriate and specific applications in high voltage insulation. Such non-glycidyl ether epoxides are generally prepared by epoxidizing unsaturated compounds using hydrogen peroxide or peracetic acid. Some of them most widely used in high voltage applications are as follows:

- ***Bisphenol A epoxy resins***, these are the most commonly used epoxy resin for coatings. Bisphenol A resins are available in a large range of molecular weights. It is the reaction product of phenol and acetone, and then it is further reacted with epichlorohydrin. Bisphenol A epoxy has good broad range chemical resistance and

good physical properties. The aromatic matrix systems lead to very good mechanical, electrical and dielectric characteristics and show a high resistance to thermal aging [SEI-98] due to their high crosslinking [BOL-95]. In spite of a favorable balance of dielectric, mechanical and thermal properties; the most obvious disadvantages of Bisphenol A resins are the unsatisfactory UV resistance, poor erosion tracking resistance and poor performance in arc and spark discharges [SEI-98]. Upon the occurrence of high energy arcs, internal or surface partial discharges, there is a risk of burning the benzene ring-containing matrix to the conductive graphite structure of carbon [DAK-74]. Due to these stability problems and the susceptibility to erosion and tracking aromatic matrix systems are not suitable for outdoor applications [HUI-91]. Aromatic resins are used in indoor high voltage insulation as well as in GIS systems [SEI-98].

- ***Novolac epoxy resins***, which are prepared by reacting phenol with formaldehyde under acidic conditions, show better thermal properties in final forms [ARO-11]. Novolacs have more reactive groups along their chemical backbone resulting in a more highly cross-linked polymer than either Bisphenol A or Bisphenol F epoxies. This much higher crosslink density produces coatings with much greater chemical resistance than Bisphenol A resins. The large quantity of aromatic ring structures increase the heat resistance of Novolac epoxies when compared to Bisphenol A resins.
- ***Hydantoin epoxy resins***, the non-aromatic hydantoin ring together with non-aromatic hardeners leads to epoxides with significantly improved UV resistance, better thermal properties and improved dielectric strength compared to conventional epoxy resins. Significant withstand characteristics to arcs and tracking currents in SF_6 insulated systems [ELI-86]. It is also used as embedding material for high voltage connection in transformers [ELI-86].
- ***Cycloaliphatic epoxy resins***, for example, dicyclopentadiene dioxide, which contain a ring structure as well as an epoxide group in the molecule, have a higher creepage current resistance, a desirable property for application in transmission lines [ARO-11]. In contrast to aromatic matrix systems above, cycloaliphatic epoxy resins exhibit good tracking and arcing resistance [STA-68], good UV resistance [SHU-95] and high resistance to moisture [SEI-98]. They are developed specifically for outdoor high voltage insulations [BAT-63] and strong arc and tracking currents applications [SEI-98], [HUI-91]. The disadvantages of the cycloaliphatic matrix systems lie in their high raw material costs, their brittleness, and susceptibility to cracking [STA-68] as well as the poor mechanical strength [SHU-95].

1.3.4. Curing Epoxy Resins

The curing process of the reaction resin compositions based on epoxy resins is performed by accelerator initialized polyaddition of the resin and curing agent and is carried out without the generation of volatile products and without pressurization. A large duromer macromolecule is the end result of a complete cure [DAK-74]. In practice, however a complete curing condition is neither intended nor achieved technologically [STA-68]. The main curing types are "*hot curing*" by carboxylic acid, "cold hardening" by organic

polyamines as well as the metal-catalyzed curing [SHU-95]. For anhydride curing of the epoxy resins, a large number of carboxylic acid anhydrides are used as hardening agents. Curing temperatures required with such hardeners are much above 100°C and the casting requires long time [ARO-11]. On the contrary, the amine hardeners cure almost spontaneously at room temperatures. The reaction of pure epoxy resins with primary amines is relatively sluggish compared to the reaction with anhydrides, so technical epoxy contains OH groups, which accelerate the crosslinking reaction [KAT-87].

A vast variety of chemical and physical properties of the finished products are obtained by using different hardeners. During curing, the monomers are converted into an infusible 3-D crosslinked structure. The choice of the curing agent affects the crosslinking density and chemical structure, and allows the achievement of the desired molding properties. Multifunctional hardener such as amine and anhydride hardener are often used due to their processing characteristics [ASH-88], [MAY-88]. For applications in the high and medium voltage technology is only the carboxylic acid anhydride curing of importance.

Anhydride curing

By casting and impregnation applications carboxylic anhydrides are preferably used as hardeners, since they result in mold materials with good thermal aging resistance [GRI-06]. Curing with anhydrides is carried out at elevated temperatures. After a post cure of typically 10 hours at 140°C the molded materials ensure very good short term and long term temperature resistance and excellent mechanical and electrical properties. The benefits of anhydride curing are the relatively low viscosities of the systems at usual processing temperatures, high thermal resistance and mechanical strength.

A detailed description of the different curing reactions is given in [BOL-95]. In general, the carboxylic acid anhydride curing is a process, by which in original state low viscosity, easy-to-cast and technologically well controllable formulations exist; leading to high-quality molded materials [SEI-98]. To avoid proteolysis danger from the interactions of the active ingredients with humidity, materials specially applied for outdoor applications are carried out with a slight curing deficiency [HUI-91]. Thus, a potential ionic conduction problem is eliminated by hydrolysis of excess hardener molecules. However, the glass transition temperature is lowered due to the reduced curing degree through the curing deficiency. An essential advantage of the carboxylic acid anhydride curing is the reaction process that is optimally controlled by the temperature [GRI-06]. The anhydride curing results in materials with good thermal, electrical and dielectric characteristics [SHU-95].

Since the reaction of epoxy resin with an anhydride is particularly relevant for this work, the principle of cross-linking of epoxy resin is explained in this example by [HAR-08]. In case of curing with uncatalyzed anhydride curing, the anhydride ring is opened by a hydroxyl group of the epoxy resin (figure 1.3 (a)), wherein a monoester is formed. Subsequently the monoester carboxylic acid group initiates a reaction with the epoxide group of the epoxy resin and forms a diester (figure 1.3 (b)). The polymerization process continues either by esterification with a further anhydride molecule (figure 1.3 (c)) or etherification with an epoxide group (figure 1.3 (d)). More reactions for development of a network are thus

possible through the created the hydroxyl group as well as the groups labeled "R1" and "R2". The etherification is the preferred mechanism, so that in practice 0.85 anhydride equivalents are required for an optimal crosslinking density [GRI-06]. In practice, accelerators are often added in order to achieve a faster esterification [HAR-08] when using anhydride hardeners.

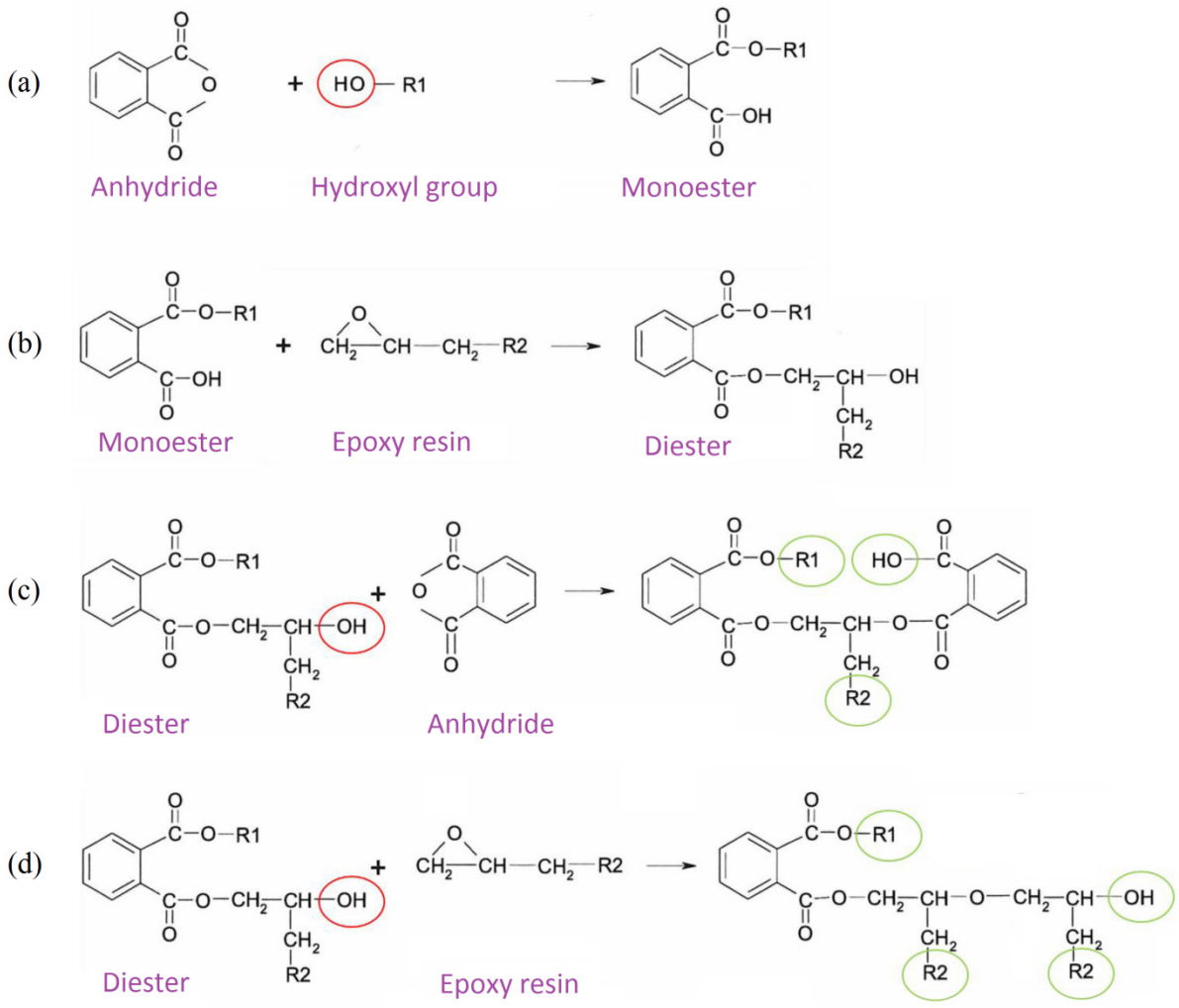

Figure 1.3: Fundamental hardening reaction of epoxy resin using acid anhydride [HAR-08]

1.3.5. Fillers

Dispersive mineral fillers are incorporated in epoxy resin matrices to equip epoxy resin materials with specifically required characteristics and strengths; hence these materials fit to the industry requirements. In addition to reinforcing fillers such as quartz, wollastonite, dolomite and alumina there are also functional fillers such as titanium dioxide and aluminum hydroxide (specially applied for increasing the arc resistance and reducing the risk of fire) [SEI-98]. Fillers are fundamentally different from each other by their chemical structure, their particle shape, size and size distribution. The selection of the fillers is made by considering four factors that affect the efficiency of the fillers; the ratio of length to diameter (aspect ratio), the filler surface, particle size distribution and the surface energy [DOM-92].

The importance of mineral fillers has changed considerably during the years. First, they were pure filler; the main purpose was reducing the cost of the final product. Only later has been recognized that through the use of fillers, the properties of thermosets can be selectively modified [HER-04]. Fillers generally introduce mechanical reinforcements through the increase of the density, elastic modulus, compressive and flexural strength, and hardness of the thermosets. Mineral fillers result in a reduction of the susceptibility to cracking, overheat, the volume shrinkage and the total cost [SEI-98]. Epoxy resins are particularly suitable for the inclusion of inert fillers. These reduce hardening shrinkage and the thermal expansion, and improve the thermal conductivity [DAK-74] and increase the compressive strength [HER-04].

Epoxy resin materials for use in high voltage insulations are preferably filled with siliceous fillers, most commonly silica flour (SiO_2 with large specific surface areas). Generally high filler contents (50/70 mass percent) are aimed, in order to save costs [GRI-06]. Quartz flour result in a longer gel time, lower glass transition temperature and improve the mechanical properties of epoxy resin materials, especially the compressive strength, modulus of elasticity and abrasion resistance [SEI-98]. The addition of quartz flour reduces shrinkage and the thermal expansion coefficient of the epoxy resin. Particularly advantageous for epoxy resins filled with quartz flours is the improvement of the electrical insulating strength, aging resistance [SEI-98] and the thermal conductivity [DOM-92].

In EP-matrices, technological Wollastonite (crystalline calcium silicate $CaSiO_3$) results in a high mechanical reinforcement. Due to their grain geometry characteristics and their associated grain anisotropic behavior, these fillers increase the tensile, compressive and bending strength and reduce the susceptibility to cracking. Wollastonite filled EP among all of mineral filled epoxy resin materials occupy the best mechanical properties [SEI-98].

Particularly advantageous in using aluminum oxides fillers (Al_2O_3) is the mechanical reinforcing of EP-matrices and the increase in the thermal conductivity (utilized in many applications) with very good electrical insulating properties [SEI-98]. In SF_6 Gas Insulated Systems (GIS) having epoxy resin spacers, aluminum oxide (Al_2O_3) is used as filler material. Unlike the silicon-containing fillers (quartz flour and wollastonite), aluminum oxides have good resistance to SF_6 decomposition products [BEY-86], [SEI-98].

1.4. Corona Discharge

Corona discharges are localized gaseous breakdowns which can occur within any plant system provided the electric stress conditions are appropriate. *Why are corona discharges of importance to high voltage engineers?* Their activity might be both a symptom of degradation in the insulating systems of power plant, irrespective of the causative stress, and a stress factor in itself. Wherever degradation occurs in electrical insulation system, due to electrical, mechanical, thermal or chemical/ambient conditions, it is mostly accompanied by the generation of discharges. Once present, these then tend to dominate as the stress degradation mechanism. It can therefore be appreciated why understanding the processes by which corona discharges lead to material erosion is so important to the development of new insulating systems capable of withstanding this stress. In addition, it can also be appreciated why

understanding the correlations among the measurable parameters of discharge activity and the nature, form and extent of degradation present is so important to the engineer responsible for the maintenance and asset management of existing plant systems.

In uniform field and weakly non-uniform field gaps the onset of measurable ionization leads to complete breakdown of the gap. In strongly non-uniform fields various manifestations of luminous and audible discharges are observed long before the complete breakdown occurs. The phenomenon is of particular importance in high voltage engineering where non-uniform fields are unavoidable. It is responsible for considerable power losses from high voltage transmission lines and often leads to deterioration of insulation by the combined action of the discharge ions bombarding the surface and the action of chemical compounds that are formed by the discharge. It may lead to interference in communication systems [ABD-00].

Electrical discharges result from processes in which atoms or molecules become electrically charged due to ionization, mostly starting in gaseous environment. Electrical discharges that do not bridge the electrodes or any pair of electrical contacts in electrical insulation systems are called *partial discharges*. In fact, all partial discharges involve gas discharges. Partial discharges can be classified into four types (see figure 1.4) [KAO-04]:

1. Corona discharges: These generally refer to discharges occurring in the vicinity of a sharp point or edge of a metallic electrode or in the vicinity of a conducting particle in extremely high and divergent electric field.
2. Surface discharges: Discharges occur on the surface of a solid insulating material.
3. Internal discharges: These discharges occur in inclusions or cavities originally existing in an insulating material.
4. Electrical treeing: Internal discharge in insulating materials with voids may results in disintegration of molecular chains and then formation of ramified conductive channels. The spreading of spark channels in the form of the branches of a tree is called treeing. Electrical treeing may be considered a combination of corona and internal discharges.

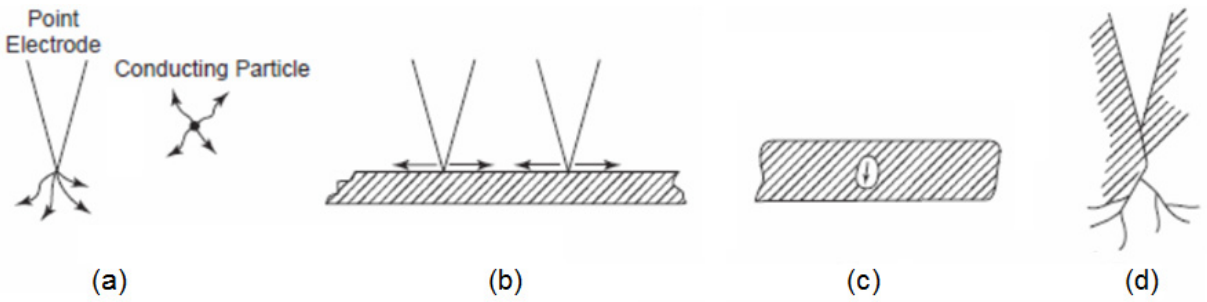

Figure 1.4: Four types of partial discharges: (a) corona discharges, (b) surface discharges, (c) internal discharges, and (d) electrical treeing involving corona and internal discharges [KAO-04]

All electrical discharges are detrimental to insulating materials. They may cause permanent changes in chemical structure or in constituent elements of the material's molecules. Both the surface and the corona discharges involve external discharges, implying that such discharges are associated mainly with gas discharges. Surface discharges may occur when there is a component of electric field parallel to the insulating material surface high enough to cause discharges. Usually corona discharges occur at the edges or imperfections of electrodes. External discharges can give rise both to surface breakdown and to penetration of the insulating material specimen.

Surface breakdown means the development of a conducting channel between two electrodes on the insulating material surface. This can be in the form of either flashover or tracking. Flashover essentially involves a gas discharge but does not necessarily impair permanently the insulating properties of the surface. Tracking essentially requires conducting channel on insulating material surface, which would suffer damage from the tracking process.

Corona discharges occur around sharp points or edges at high voltages in air or other gases. For AC voltages, they occur often during the negative half-cycle of the sinusoidal wave. Then, for a point–to-plane electrode configuration in gas, corona discharges occur near the point, resulting in the formation of a positive ion space charge in the vicinity of the point. The positive ions may impinge the point electrode, releasing more electrons. According to Townsend gas breakdown mechanism this would produce a cloud of positive ions near the point and negative electrons away from the point, gradually forming a cloud of negative ions due to the attachment of the electrons to oxygen molecules in low field regions.

During the discharge process, radiation due to recombination takes place, producing photoionization toward the point and extending the ionized region laterally until the cathode spot is formed, from which the corona discharge emanates. This process will go on until enough negative space charge is accumulated to reduce the field near the point to a value too low to produce further ionization. Then, the discharge extinguishes. After extinction, the negative space charge moves to the positive plane electrode and becomes neutralized there. Then, the electric field rises, and the next discharge starts [KAO-04]. Because of the distinctly different properties of coronas under the different voltage polarities it is convenient to discuss separately positive and negative coronas.

1.4.1. Positive or Anode Corona

In discussing the corona characteristics and their relation to the breakdown characteristics it is convenient to distinguish between the phenomena that occur under pulsed voltage of short duration (impulse corona) and under long lasting voltages (static field corona). The observations have shown that when a positive voltage pulse is applied to a point electrode, the first detectable ionization is of a filamentary branch nature. This discharge is called a streamer and is analogous to the case of uniform field gaps at higher partial discharge values. As the impulse voltage level is increased, the streamers grow both in length and their number of branches as indicated in figure 1.5. One of the interesting characteristics is their large number of branches which never cross each other.

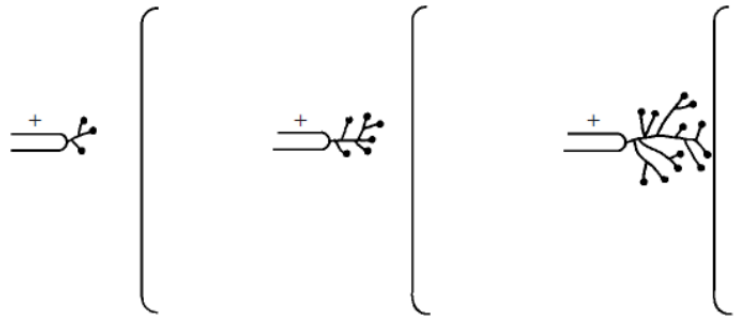

Figure 1.5: Schematic illustration of the formation of streamers under impulse voltage-progressive growth with increasing pulse duration-positive rod-to-plane gap [KUF-00]

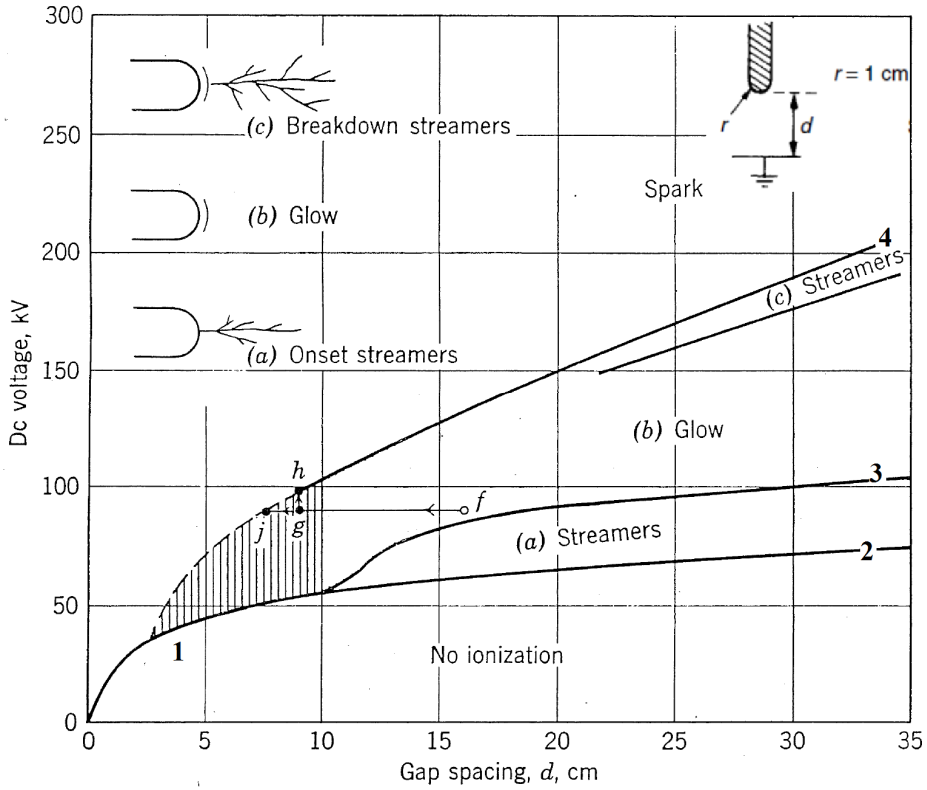

Figure 1.6: Threshold curves for various modes of anode corona and for spark breakdown for a hemi-spherically capped anode and plate cathode under atmospheric conditions [NAS-71]

When the voltage is applied for an infinitely long time the ionization products will have sufficient time to build up in the gap and accumulate in space, causing a distortion in the original field. To study this phenomenon, [NAS-71] assumed the rod-to-plane gap with the rod tip of radius of 1 cm as shown in figure 1.6 and studied the various discharge modes together with the breakdown characteristics for this arrangement in atmospheric air.

Then, if the gap length is small (less than ~2 cm) and the voltage is gradually raised no appreciable ionization is detected till breakdown. As the gap is increased, the field distribution becomes more inhomogeneous, and on increasing the voltage at first a transient slightly branched filamentary discharge appears. These discharges have been shown to be identical with those observed under impulse voltages and are also called streamers. Under steady state the streamer develops with varying frequencies, giving rise to currents that are proportional to

their physical length. These streamers are called onset streamers or burst pulses as shown in figure 1.7 (a). It is characterized by a series of consecutive positive charge clouds moving along the discharge gap from the anode to the cathode [KUM-09]. Figure 1.7 (b) demonstrates formation and propagation of a positive charge cloud during a single burst pulse.

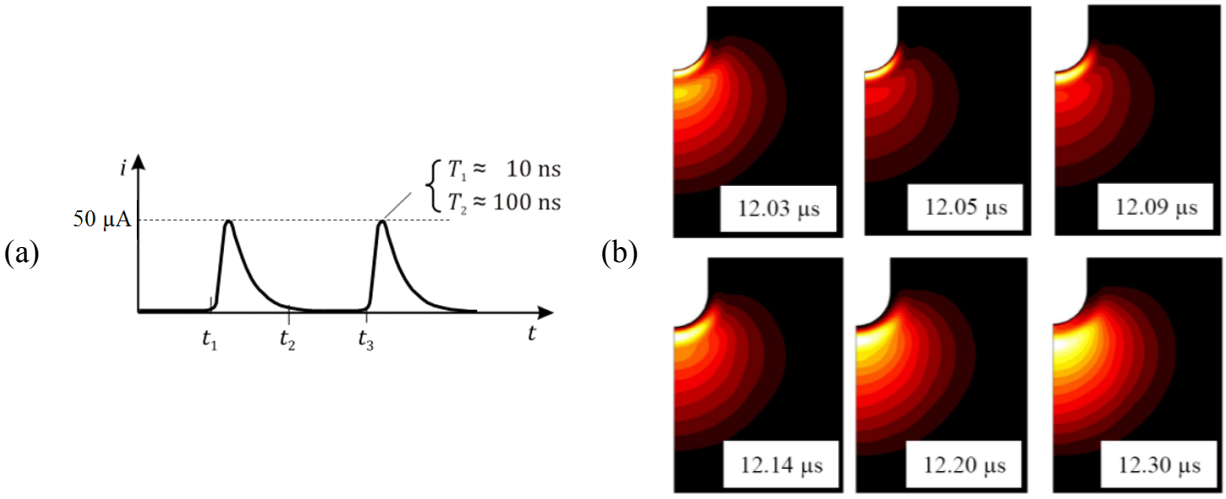

Figure 1.7: Burst discharges in non-uniform electric fields. (a) Ideal shape of burst pulses with rise time T_1 of ~10 ns, time to half value T_2 of ~100 ns and peak value of ~50 µA [KIN-13]. (b) Dynamics of positive ions during development of a single burst pulse; normalized (actual/maximum) densities are shown (light color corresponds to maximum and dark color to minimum); with application of the short, 12/50 µs, impulse voltage of 5 kV amplitude [KUM-09]

The onsets of the various discharge modes observed, as the gap length is increased, are illustrated schematically in figure 1.6 together with the corresponding discharge characteristics. At the smaller spacing when the voltage is still reasonably uniform the streamer is capable of penetrating the weaker field, reaching the cathode and initiating breakdown in the same manner as in uniform field gaps as shown by curve 1 of figure 1.6. With the larger spacing above 5 cm, streamers appear that do not cross the gaps as shown by curve 2.

Curve 3 represents transition from streamers to steady glow corona without sparking. At gap distance larger than 20 cm there is a considerable spread in the voltage at which breakdown streamers develop preceding the complete breakdown of the gap. The dashed area represents the region of uncertain transitions; which indicates the onset of streamers followed immediately by transition to spark. If the voltage is raised across a gap of 16 cm to 90 kV, a glow is established materializes at the anode (point ***f***). Then, by remote control and keeping the voltage, the gap can be decreased gradually to 9 cm (point ***g***), which is definitely above the normal sparking threshold, nonetheless, no spark occurs thanks to the stable glow at the anode preventing streamers to develop and trigger spark. Sparking under such condition will occur only if the voltage is raised to point ***h*** or if the distance is reduced to point ***j***. At both points a glow-spark transition develops (curve 4) [NAS-71].

1.4.2. Negative or Cathode Corona

With a negative polarity point-to-plane electrode arrangement under static conditions above the onset voltage the current flows in very regular pulses, which indicates the nature of a single pulse and the regularity with which the pulses are repeated as shown in figure 1.8. The pulses were studied in detail by Trichel [TRI-39] and are named after their discoverer as 'Trichel pulses'. The onset voltage is practically independent of the gap length and is close in value to the onset of streamers under positive voltage for the same arrangement. The pulse frequency increases with the voltage and depends upon the radius of the cathode and the gap length. The frequency of these current pulses may vary from a few kHz to MHz [ARO-11].

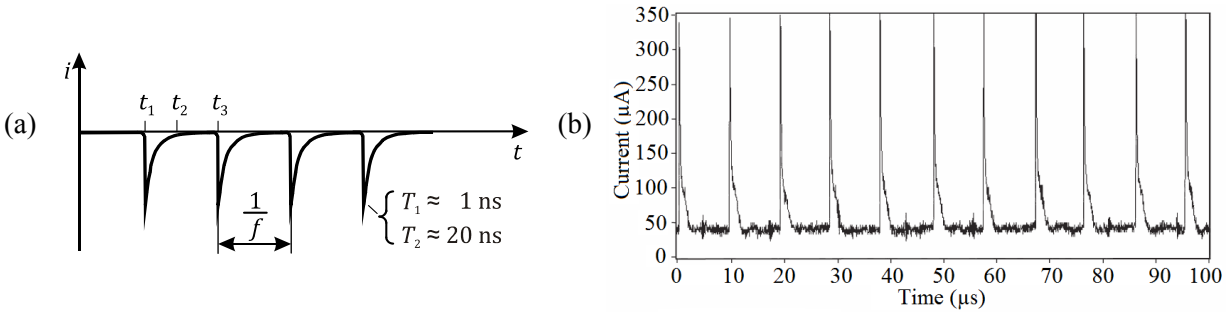

Figure 1.8: Impulse form of discharge current "Trichel Pulses". (a) Ideal shape of Trichel pulses with rise time T_1 of ~ 1 ns, time to half value T_2 of ~20 ns and peak value of ~500 μA [KIN-13]. (b) Trichel pulses measured at needle - plane electrode system on applying negative DC voltage [ARO-11]

The relationship between the pulse frequency and the gap voltage for different gap lengths and a cathode point of 0.75 mm radius in atmospheric air is shown in figure 1.9. A decrease in pressure decreases the frequency of the Trichel pulses [KUF-00]. Figure 1.9 (b) illustrates the onset voltage of different negative coronas plotted as a function of electrode separation for a typical example of a cathode of 0.75 mm tip radius. The lowest curve illustrates the onset voltage for Trichel pulses which is not greatly affected by the gap length. The mode of the pulses is not influenced by voltage rise over a wide voltage range. Eventually at a much higher voltage a steady glow discharge is observed.

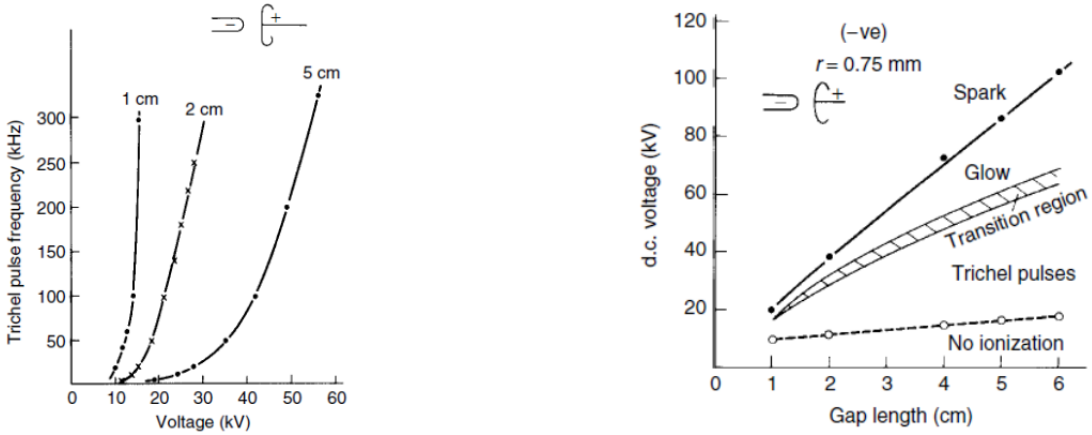

(a) Trichel pulse frequency–voltage relationship *(b) Negative discharge modes*

Figure 1.9: Negative corona discharge for rod to hemi-spherically capped electrode arrangement in atmospheric air [KUF-00]

On increasing the voltage further, the glow discharge persists until breakdown. It should be noted that breakdown under negative polarity occurs at considerably higher voltage than under positive voltage, except at low pressures; therefore, under alternating power frequency voltage the breakdown of non-uniform field gap invariably takes place during the positive half-cycle of the voltage wave.

1.4.3. Polarity Effect in Strong Inhomogeneous Field

In the following the positive and negative polarity effect of a needle-to-plate electrode arrangement on the electric field is presented. The mechanism of a positive needle tip arrangement is analyzed in figure 1.10 (a). The electrons formed in front of the needle tip by collision ionization are drawn away by the anode. A positive space charge remains, which reduces the electric field strength at the needle tip without resulting in a breakdown. When the voltage is increased further, short duration discharges appear in the weakly glowing space charge region and the ionization boundary is displaced. The frequency and range of the discharges increase with increasing voltage, until finally there is a complete breakdown.

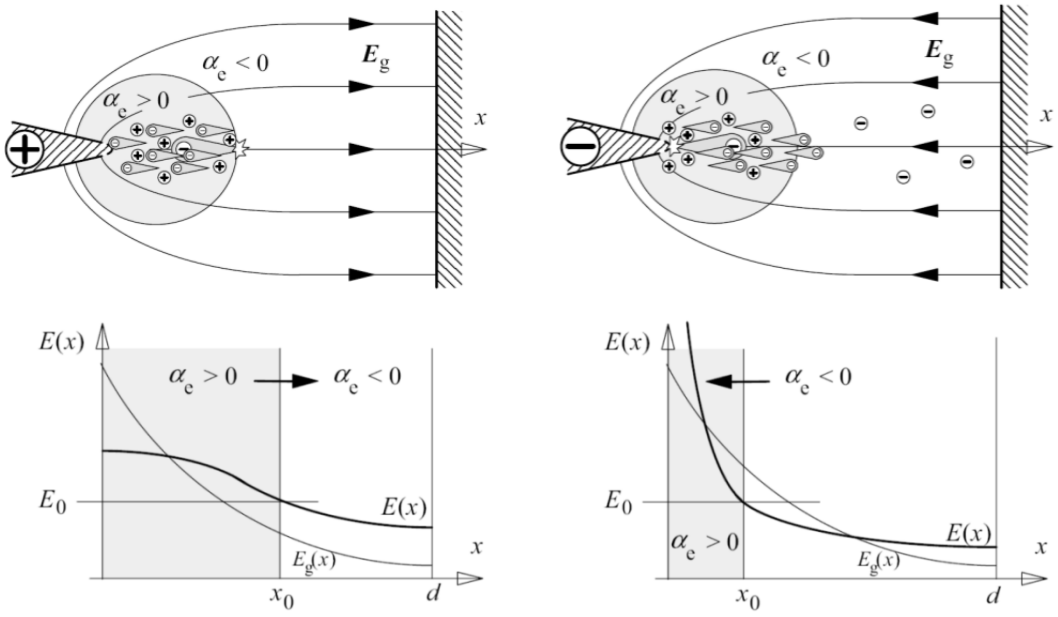

a) positive needle tip *b) negative needle tip*

Figure 1.10: Polarity effect in strong inhomogeneous field with positive and negative tip, Eg(x): electric field strength distribution along x-axis without space charge, E(x): electric field strength distribution along x-axis considering space charge, and E_0: electric field strength of the ionization boundary [KÜC-09]

In the configuration with a negative needle tip and grounded plate, in figure 1.10 (b), a positive space charge evolves in front of the needle tip when the inception voltage is exceeded, but the electrons drift in the direction of the plate electrode. In air a space charge consisting of negative ions is formed which can reduce the electric field strength between the needle tip and the space charges to such a small value that the collision ionization is stopped and the ionization boundary is displaced to smaller values. The discharge starts again when the negative space charge travels away, which leads to a pulse type mechanism with regular

current pulses of 10 ns duration. Of particular interest for discharges are the characteristic differences between the positive-point and negative-point discharges that can occur in the same cycle on AC power systems. The rate at which each type of discharge occurs will most likely contribute to the rate of degradation of an insulator surface.

1.5. Atomic Emissions from Electrical Discharges

1.5.1. Emission Principles

In a discharge, gases in the high field region are subject to inelastic collisions from high speed electrons. Energy transferred to molecules in the air by these electrons causes excitation, dissociation, and ionization. Energy is released as the molecule or atom cools. This may be in the form of photons which are unique to each type of atom or molecule. The electromagnetic radiation emitted in the visible and UV part of the spectrum comes from fast changes in electron orbit configurations. Most of the radiation emitted from electrical discharge is in UV part of the electromagnetic spectrum for photons with wavelengths from 240 nm (5.13 eV) to 480 nm (2.57 eV). The visible portion of the electromagnetic spectrum lies between 380 nm (3.26 eV) for violet and 780 nm (1.59 eV) for far red [FAN-06].

1.5.2. Data for Air and Other Materials

The atomic emission spectra are produced by the gases involved in the discharge and the gases most likely to be involved in atmospheric air are those in the high voltage field gradients surrounding the pointed electrode. Apart from the metal vapor at the surface of the metal electrode the atmosphere surrounding the electrode consists mainly of nitrogen 78%, oxygen 21%, argon 0.9%, and smaller quantities of other gases including carbon dioxide 0.03%, krypton, xenon, neon, helium and moisture. Thermal bond dissociation energy and ionization energy are listed in the Table 1.1. For example, N_2 has thermal bond dissociation energy 945 kJ/mol which is equal to electrical energy units of 9.79 eV. This is the minimum equivalent energy required to dissociate a nitrogen molecule. If more than 15.58 eV of energy is transferred to a N_2 molecule then the molecule will ionize.

Electron affinity is the interesting property of atoms and molecules that enables them to attach an electron to become a stable negative ion it defines the energy released when the atom or molecule gains an electron. This occurs in electrical discharge when oxygen molecules in the gap gain free electrons following the first avalanche process. Nitrogen becomes unstable with the addition of an electron, in contrast to the oxygen ion which has a lower preferred state than the neutral oxygen. So, the oxygen easily becomes negatively ionized which encourages the development of the space charge cloud that reduces the electric field intensity at the tip of the point electrode during the Trichel pulses production in case of negative polarity at the tip.

1.5.3. Dissociation of Molecules by Electron Impact

Not all the energy from the high velocity electrons in the high field region of corona discharges causes dissociation of gas molecules. In a study of the efficiency of the dissociation of air molecules for industrial processes, using an electron beam, [ELE-85] found that the type of gas mixtures can have a dramatic effect on the dissociation process efficiency. The process efficiency was defined as the ratio of energy introduced into the system to the amount of energy to produce the atoms by the dissociation process.

Table 1.1: Properties of elements and compounds associated with corona discharges [HIN-09]

Gas	Atomic No	Portion in Air (%)	Dissociation Energy (ΔeV)	Ionization Energy (eV)	Electron Affinity (eV)	Electro-negativity (Pauling)	
N_2		78	9.79	15.58	not stable		Gases present at sea level
O_2		21	5.16	12.07	0.45		
CO_2		0.03	5.51	13.77	1.59		
H_2O		RH	5.15	12.62			
Ar	18	0.90		15.76	not stable	-	
Ne	10	0.00182		21.56		-	
He	2	0.000534		24.59		-	
Kr	36	0.000114		13.99		-	
Xe	54			12.13		2.6	
N	7			14.53	not stable	3.04	Atoms of dissociated air molecules
O	8			13.62	1.46	3.44	
C	6			11.26	1.26	2.55	
H	1	0.01		13.6	0.754	2.2	
Na_2				4.89	0.430		Sodium and chlorine associate with salt
Cl_2				11.48	2.38		
Na	11			5.14	0.5479	0.93	
Cl	17			12.96	3.612	3.16	
N_2O				12.886	-0.03		byproducts for air corona discharge
NO_2				9.59	2.273		
NO			6.54	9.26	0.026		
OH			4.46	13.02	1.82765		
CO			11.16	14.01	1.59		
O_3				12.43	2.1028		
C–H			3.50				Gas degradation byproducts of SIR
H–CH_2			4.79				
Si–C			4.67				
Si–O			8.28				
Si	14			8.15	1.38	1.90	

During heating, the gaining of energy for molecular dissociation proceeds via the increase of vibrational energy levels within the molecule. Besides the electric discharge and gas heating other causes of dissociation were also examined [ELE-85], including UV radiation, and focused electron beam excitation. The most effective process for dissociation was shown to be by photon excitation when the surrounding gases are transparent and provide little attenuation to the critical dissociation wavelengths. The second highest efficiency for dissociation of air molecules was found to be heating by passing the gas over a hot plate.

1.6. Electrical Discharge Erosion Mechanisms

Corona discharges may introduce some alterations in the characteristics of insulating material surface [AMI-06]. Discharges could lead to material discoloration or chalking; i.e. appearance of a rough and whitish powdery surface giving the insulator a chalky appearance. Additionally, surface micro-fractures may be initiated either as shallow or deep cracks. Another impact from corona discharges is the hydrophobicity deterioration resulting in the formation of hydrophilic surface. Under high discharge activity conductive carbon tracks may appear on the surface which cannot be easily removed. All the above symptoms of material aging under the influence of electrical discharges are out of scope in this work. The focus of this study is to examine surface erosion severity along with stresses of electrical discharges.

Electrons, ions, atoms, radicals and excited molecular species produced in corona discharge move variously under the influence of the following forces:

- Thermal excitation (undirected motion)
- Particle impact stress
- The electric field (directed motion)
- The electric wind, generated by the collision of the ionic species, moving under the influence of the electric field, with the molecules of surrounding gas.

Although, for the sake of convenience, these various forms of stress which apply during electrical discharges stressing can be compartmentalized, it is the synergetic interaction of these stresses which results in degradation. Different materials, gaseous atmospheres, contamination levels, discharge magnitudes all will result in a unique combination of stress effects at a discharging surface. Electrical discharges are known to cause deterioration to solid insulating materials by several means [KRE-89], [ANG-08], [ANG-12]:

- Heating the insulating material boundary
- Charges reaching the insulator surface
- Attack by Ultraviolet rays
- Formation of chemicals such as nitric acid and ozone.

Corona discharges attack insulation directly by charged particle bombardment, as well as indirectly by the resulting byproducts formed by discharge. The existing degradation mechanisms to the insulating materials due to electrical discharges are still not clear and need more identification. This is for the sake of formulating the exact mechanism which offers a better understanding of the electrical discharge phenomenon. The majority of the research in the discharge initiated erosion on the surface of insulating polymers is concerned with the material resistance with respect to the examined characteristics. Whereas the erosion mechanism and the stress factors have a poor research results for corona discharges.

Erosion of solid insulating materials by electrical discharges has been examined by Koyanagi et al. [BAR-87]. The behavior of the epoxy resin samples was examined while exposed to discharges in dry air at room temperature and at 90°C. There was an observed weight gain for the samples tested at room temperature due to oxidation that was not observed

at higher temperature. Koikov et al. attempted to make a correlation between the weight loss for PE films and discharge characteristics [BAR-87]. It was found that weight loss as well as the discharge characteristics increases when increasing the test voltage. They concluded that significant erosion is mainly the result of the discharges and oxygen.

Bui-Ai et al [BUI-69] have proposed a proportional relationship between the eroded volume from epoxy resin insulating material under the impact of corona discharges and the energy of discharges. The relation is given as [BAR-87]:

$$\frac{dv}{dt} = k\, n\, dw \qquad [1.1]$$

Where v is the eroded volume, t is time, n is the number of discharges per second, dw is the rate of change in discharge energy per pulse, and k is the proportionality constant, which is equal to 2.01 x 10^{-12} m^3/J in case of epoxy resin.

McMahon [MCM-68] has also examined corona-stress cracking of polyolefin resins according to IEC 60343. The results indicated that the occurrence of corona discharges is the vital agent for an accelerated deterioration. Under oil or vacuum corona is suppressed and the degradation is not greatly accelerated by increasing the voltage. The material degradation in air, nitrogen and argon were found to be almost similar, indicating that the corona is the most deteriorating agent and not the ozone generated in the oxygen medium. When part of the specimen was under corona stress and the remainder exposed to gaseous byproducts from corona discharge, only the former exhibited cracking.

Anglhuber et al [ANG-08], [ANG-12] have examined the influence of corona discharges on the surface PE insulating material in terms of both the erosion and the electrical parameters of the corona discharges were measured in a test program. A good indicator has been introduced for erosion degree instead of maximum erosion depth, which is the "95% erosion depth". The curves of erosion and the discharge characteristics were examined for correlations. It was found that the test voltage magnitude exhibits a direct correlation trend with both erosion degree and discharge intensity.

Tanaka et al [TAN-07], [TAN-08a] have studied the erosion resistance of epoxy/clay nano-composite prepared by organic modification and different solubilization methods. Rod-to-plan electrode arrangement, which consists of a tungsten rod electrode of 1 mm diameter with 0.5 mm radius of its tip, and a brass plane electrode with 1.2 mm. A specimen of 1 mm thickness is inserted between the tip of the rod electrode and the surface of the counter plane electrode to allow an air gap of 2 mm. They examined the influence of material compositions along with the degree of the resulting erosion represented by maximum erosion depth.

1.7. Influencing Factors on the Erosion of Insulating Material Surface

Polymeric Insulators are widely used in high voltage electricity networks where they are exposed to environmental, mechanical and electrical stresses which the non-ceramic insulating housing must endure. Some typically well-known factors are [HIN-09]:

1. Electrical discharges: a. discharge in vicinity of surface, b. discharge on surface (i.e. water drop corona, sharp edges electrodes, metallic particles…)
2. Humidity level of the medium in which the insulating material exists.
3. Heat from solar radiation, supported conductor operated temperature, and elevated air temperature from nearby bushfires as well as thermal radiation from nearby high temperature industrial processes such as those used in thermal power stations.
4. UV radiation acting on the insulator surface.

1.7.1. Environmental Factors

As a matter of fact discharge intensity depends mainly on the test voltage, electrode arrangement and electric field distribution. However, discharge gas characteristics may also have an impact on discharge intensity and in turn on erosion behavior. In most of the previous work [MOR-00], [MOR-01a], [MOR-01b], [LIA-04], [YOS-99], there is almost no elucidation on the correlation between environmental factors (i.e. temperature and humidity) and corona discharge intensity as well as surface erosion. The effect of the stressing factors on discharge intensity and discharge gaseous byproducts is expected to play an important role in material erosion [DIS-92].

1.7.1.1. Humidity

The effect of humidity as one of the most important environmental factors has been analyzed. It has been proven that higher levels of moisture act as a catalytic element for chemically induced polymer degradation processes. The effect of humidity, in terms of degradation rate, manifested itself in generally somewhat shorter times to the surface deterioration on tests run under high humidity conditions.

Moreno an Gorur [MOR-00], [MOR-01a] performed high voltage humidity tests on EPDM, SIR, a blend of EPDM with silicone rubber (blend ratio ~95:5 in %wt.) which showed the influence of humidity on the amount of observed degradation. Samples were exposed to point-to-plane discharges with 1 mm gap distance under both low (35 to 40%) and high (95 to 100%) relative humidity (%RH) conditions for 500 hours at a constant fog input rate of 500 g/m^3.hour. A heating resistance fog generator was used to create the high relative humidity environment by boiling de-ionized water. The average temperature increase inside the test cell was measured to be ~3 to 5K above the ambient temperature. AC voltage (7.2 kV_{rms}) was applied to the discharge electrode throughout the test period.

Samples were tested with and without application of bending mechanical stress to investigate the interaction of the mechanisms involved in such process. The applied mechanical stress had an impact on the damage degree of the material surface, where more intensive cracking was detected on the samples at the end of the test time compared to the samples tested with no mechanical stresses

Table 1.2: Summary of evaluation results as observed for each material group [MOR-00], [MOR-01a]

Test condition	Material	Observations
High relative humidity (95-100%), bending mechanical stress	SIR EPDM blend	Deep cracking (~3 mm in depth), surface whitening Surface darkening, shallow cracking Deep cracking (~1.5 mm in depth), surface whitening
High relative humidity (95-100%), no mechanical stresses	SIR EPDM blend	Deep cracking (~2 mm in depth), surface whitening Surface darkening, slight roughening Shallow cracking (~0.5 mm in depth), surface whitening
Low relative humidity (35-40%), no mechanical stresses	SIR EPDM blend	Deep cracking (~2.5 mm in depth) Surface darkening, slight roughening Shallow cracking (~0.5 mm in depth), surface whitening

The influence of humidity was manifested primarily by noticeable differences on the PD magnitude and frequency, and hence on the computed values of cumulative charge computed for each polarity. Regarding the effect of humidity levels and externally applied mechanical stress on surface morphology, it was observed that exposure of samples to the combined effect of both factors resulted in a noticeable increase of the severity of degradation at the end of the test period. Nevertheless, under low relative humidity conditions (35-40%) without application of mechanical stress, the influence of humidity is insignificant in terms of surface degradation compared to the high relative humidity test conditions. In Table 1.2, a summary of the varying degrees of damage observed on every material group with respect to each test condition is presented.

1.7.1.2. Temperature

One of the most significant factors of influence on material degradation of insulating materials is when exposed to thermal stresses. The influence of temperature has been intensively examined in terms of material aging and specifically on hydrophobicity. Despite the importance of temperature, it could hardly found in the literature as influencing factor affecting surface erosion of insulating polymers under the influence of electrical discharges.

1.7.1.3. Role of ozone in discharge degradation

One of the most noticeable effects from an electrical discharge in air is the production of ozone. Ozone is a pale blue highly reactive gas in which three oxygen atoms combine to form one ozone molecule. The ozone molecule is made from a double bonded pair of oxygen atoms, and a weakly bonded third oxygen atom. Thermal bond energy of the double oxygen bond is 5.16 eV whereas the bonding energy of the third oxygen atom to O_2 is only 1.05 eV [KAN-03]. The weak bond means that oxygen radical can be easily released and this makes ozone a very reactive oxidizing agent. Oxygen does not need to be ionized to form ozone

although some ionization is necessary to produce a corona discharge. From table 1.1 only 5.16 eV of dissociation energy is required for an oxygen molecule to produce 2 oxygen atoms.

In figure 1.11 the color shading depicts the strength of the electric field; deep red is the region of highest field gradient which is against the tip electrode. The process shown involves two free electrons generated by the ionization process, and three O_2 molecules, to make two O_3 molecules. In 1 an oxygen molecule captures a low speed electron to form an oxygen ion O_2^-. In 2 an oxygen molecule is dissociated by a high speed electron; one of the dissociated oxygen atoms captures the electron to form O^-, the other oxygen atom is in the excited state O*. In 3 and 4 ozone O_3^- is formed but from slightly different ways. The ozone ions neutralize by giving up their electrons at the plane metal electrode after drifting across the gap under the influence of the electric field. Once neutralized, the ozone molecule can drift out of the discharge gap. Oxygen O_2^- and O^- can also reach the plane electrode and neutralize without forming ozone.

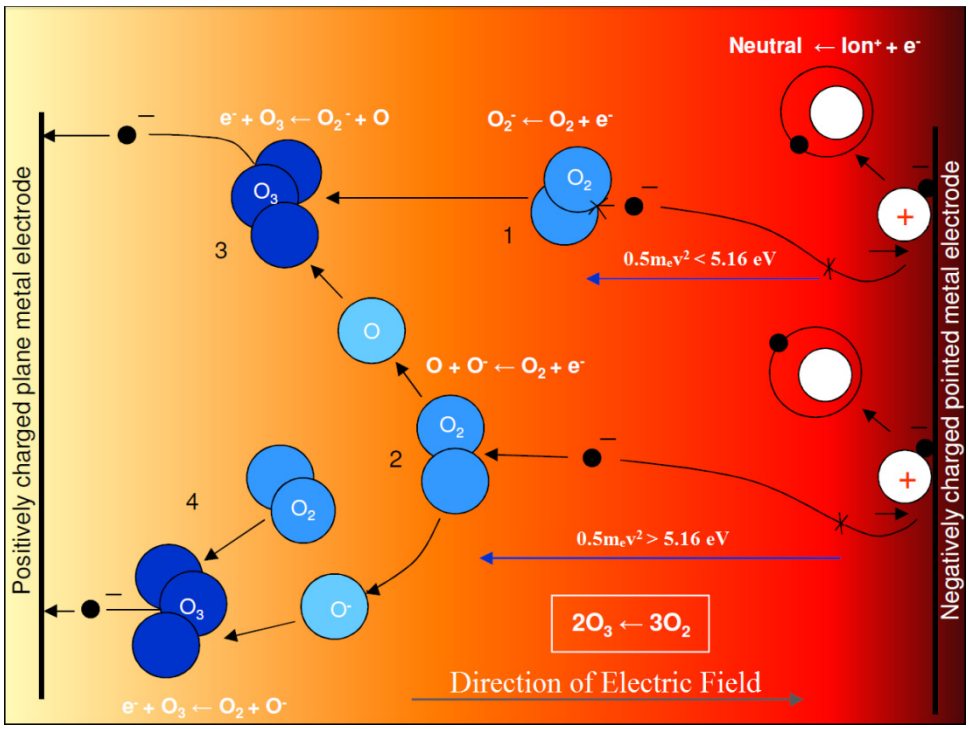

Figure 1.11: An interpretation of the formation of ozone in a dry point-to-plane discharge gap showing the conduction process of the electrons [HIN-09]

The impact of ozone on polymeric insulating materials was compared to the action of discharges, which involves ozone as well [COO-60]. Cooper and Prober used LDPE in their study. One specimen was placed between the electrodes with a gap distance of 6 mm between the electrode and the insulating material surface, and therefore exposed to the corona discharge. A duplicate specimen was placed at the bottom of the test cell and was exposed only to the ozone generated by the discharges, not to the discharges itself. Discharge treated samples had lost weight; however the ozone exposed samples showed a very slight increase in weight because the oxidation products continued to form and accumulate during exposure.

While ozone is not the only agent involved in discharge degradation of PE, the oxidation taking place during discharge stressing is mainly due to ozone attack.

1.7.1.4. Oxygen impact

Polymer degradation is commonly observed if autoxidation occurs. Autoxidation refers to reactions of materials with molecular oxygen which proceeds as chain reactions. At ambient temperatures the chemical structure of most polymers are quite stable against any attack of molecular oxygen. According to the present state of knowledge, the most prominent modes of initiation refer to the generation of free radicals capable of reacting rapidly with molecular oxygen. These modes of initiation comprise thermolysis and photolysis induced reactions. In addition, free radical formations are feasible processes pertaining to electrical phenomena such as corona discharge and electrical breakdown, since electrical processes result in both thermolysis and photolysis [SCH-81].

Chemical modes of initiation pertain to chemical reactions generating free radicals. Actually, many direct oxidation processes may involve free radicals as intermediates. The latter may be capable of reacting with O_2, forming radicals of peroxy type $ROO^{\bullet}$. As far as commercial polymers are concerned, the decomposition of hydro-peroxides is considered to be of utmost importance. Many hydro-peroxides decompose at relatively low temperatures according to the following reaction:

$$ROOH \rightarrow RO^{\bullet} + {}^{\bullet}OH \qquad [1.2]$$

The hydroxide radicals ${}^{\bullet}OH$ are very reactive and react with many organic substances with encounter controlled rate constant. Commonly they either abstract hydrogen atoms (in case of aliphatic compounds) or undergo addition reactions (in case of aromatic compounds). Concerning polymer degradation, H atoms abstraction processes proceeding according to the following reaction are most important.

$$RH + {}^{\bullet}OH \rightarrow R^{\bullet} + H_2O \qquad [1.3]$$

At sufficiently high oxygen concentrations, reaction will be followed by propagation steps of autoxidation processes as follows:

$$R^{\bullet} + O_2 \rightarrow ROO^{\bullet} \qquad [1.4]$$

$$ROO^{\bullet} + RH \rightarrow ROOH + R^{\bullet} \qquad [1.5]$$

The ultimate products are R, RO, ROO, OH, and H; in which R indicate the polymer components. In the case of epoxy resin, C–C bonds, C–H bonds in CH_3 groups were cut off by electrical discharge, and they combined with the OH and OOH groups generated in the oxidation reaction. Cross-linking and branching reactions can also proceed between the OH and OOH groups and other functional groups.

An oxidized layer was formed on the surface of the discharge-aged epoxy resin specimen [ZHU-06a]. Thus, the by-products of aging, O–H bonds, which are formed instead of the hydrophobic CH_3 groups on the surface of the discharge-aged epoxy resin specimens, cause a deterioration of the polymeric materials. All these consequences lead to higher material susceptibility to surface erosion under the impact of electrical discharge.

1.7.2. UV Radiation

Polymer insulating compounds are exposed to ultraviolet (UV) radiation not only from sunlight, but also from corona and dry band arcing. Resistance to degradation resulting from ultraviolet exposure is an important factor in determining the service life of a polymer.

1.7.2.1. UV Radiation from sunlight

UV wavelengths from sunlight are an important component in outdoor degradation. The energy from sunlight is mainly visible light (700:400 nm), infrared, and UV light (400:10 nm). Although UV radiation amounts to only 3% of the total radiation that reaches the earth, it is energetic enough to cause chemical reactions of polymers [MAS-06].

The energy contained in UV radiation is capable of directly rupturing polymer chains (chain scission), and, in the presence of oxygen, UV radiation causes oxidation of polymeric insulating materials. The wavelengths that cause the most damage to polymers are in the UV range, 290:400 nm. At the shortest wavelengths in the UV region, the photon *energy* is of the same order of magnitude as the energies of the bonds in common polymers [PIN-02], [PIN-05]. Solar UV radiation spectrum is divided into three ranges. The wavelength regions of UV radiation and their characteristics relative to degradation of materials are listed below [MAS-06]:

- ***UV-A 400–315 nm:*** Always present in sunlight; 400 nm upper limit for UV-A is the boundary between visible light and UV light; energy at 315 nm boundary begins to cause adverse effects and pigmentation changes in human skin and some polymers.
- ***UV-B 315–290 nm:*** This range includes the shortest wavelengths found at the earth's surface; responsible for severe polymer damage; absorbed by window glass; UV radiation absorption by ozone varies with solar altitude;
    - 290–315 nm is completely absorbed at altitudes below 14°,
    - at 19° solar cutoff is 310 nm,
    - at 40° solar cutoff is 303 nm,
    - at solar altitudes between 60° and 90° maximum UV-B reaches the earth's surface with a solar cutoff at approximately 295 nm.
- ***UV-C 290–200 nm:*** The UV-C range is a sharp cutoff of solar radiation at the earth's surface due to complete absorption by ozone; found only in outer space.

1.7.2.2. UV radiation from electrical discharge

UV light contained in sunlight whose wavelength less than 290 nm is almost absorbed by ozone, so the wavelength of UV radiation that reaches the earth's surface is above 290 nm. On the other hand, UV radiation associated with electrical discharge ranges from 290 nm to 400 nm, in addition to a fraction ranging from 230 nm to 290 nm (i.e. solar blind zone) [PIN-02], [PIN-05], [LIU-06]. Figure 1.12 presents corona discharge electromagnetic spectrum describing the region called solar blind zone, in which solar radiation is almost negligible.

For solar blind zone in discharge induced UV radiation, the photon *energy* is ranging from 4.4 to 5.4 eV which is higher than the bond dissociation energies of the bonds in most polymers. Therefore, this energy band is the severest in the entire UV spectrum with respect to material damage. Moreover, the bond dissociation energy of oxygen molecules is about 5.16 eV, equivalent to 243 nm wavelength, which is only achieved under the influence of UV radiation from electrical discharge and not from sunlight. The effect of oxygen dissociation and UV radiation synchronously occur, referred to technically as photo-oxidation. Materials subjected to oxygen are degraded much faster in the presence of radiation than in its absence.

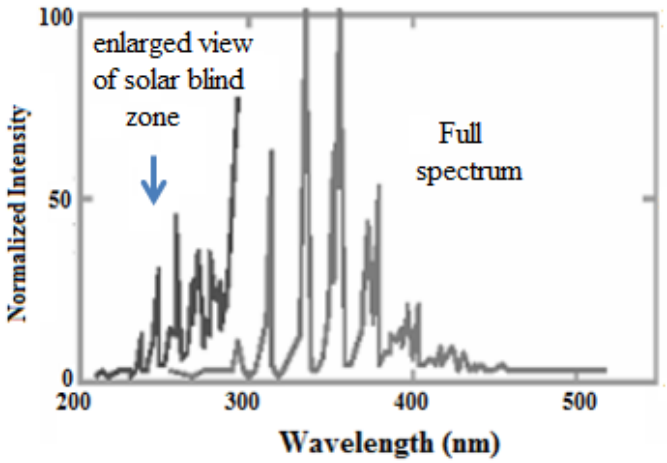

Figure 1.12: UV spectrum for electrical discharge; solar blind zone is the range of wavelengths blocked from reaching the earth from sunlight, i.e. wavelength from 230 nm to 290 nm [LIU-06]

From the above held comparison the main differences between sunlight and electrical discharge in terms of UV radiation characteristics lies in the following:

- Spectrum of electrical discharges covers also the solar blind zone with higher photon energies leading to more damage; whereas the same range of wavelengths contained in sun light is blocked by atmospheric ozone layer.
- Dissociation of oxygen molecules resulting in photo-oxidation of polymers is more probable and with higher rate in case of electrical discharge due to the higher magnitudes of photon energy.

Hence test environments used to produce UV conditions in the laboratory to reproduce natural UV stresses is not sufficient to test UV stresses from electrical discharges. The intensity of applied UV spectrum in such tests for wavelengths less than 270 nm is 0% and from 270 nm to 300 nm is 8% [CIG-04], [CIG-12].

1.7.2.3. Influence of UV radiation

[SON-08] stated that the ultraviolet radiation generated from corona discharge around transmission lines contains both UV-B and UV-C. The UV-B is absorbed by ozone and therefore it extends far from the discharge area, because the ozone density is low outside corona discharge zone. The absorption of this UV radiation results in mechanical and chemical degradation of the polymer structure that can affect the insulating material, physical and weathering properties. The rate at which the degradation occurs is dependent upon the intensity and wavelength of the radiation. These factors vary with season, time of day, elevation and latitude. Acceleration of the effects occurs in the presence of moisture on the polymer surface; which is considered one of the most important factors leading to material degradation. Polymer compounds for use in outdoor environments should, therefore, be evaluated under UV stress and high humidity.

SIR filled with *Aluminum Trihydrate* (ATH) (45 to 54%), EPR filled with ATH (56 to 61%) and SIR filled with silica quartz powder (46 to 50%) were exposed to UV radiation for 1000 hours and 2500 hours in an Atlas Twin Arc weather-ohmmeter and tested in a tracking wheel [CHE-81]. The test results indicated that UV radiation had no effect on the tracking endurance of the polymers. The EPR exhibited surface chalking and cracks.

Artificial exposure of RTV SIR and HTV SIR to UV combined with electric stress of 2.5 kV/cm and humidity of 70 to 90% at 50 to 70°C resulted in an increase in the loss factor ($\tan \delta$) and the relative permittivity (ε_r) but these were attributed to the absorption of moisture and not to the effect of radiation [SUW-98]. Subjecting HTV SIR, EPDM and EPR to multi stresses of electrical (0.5 to 1 kV/cm) and/or mechanical (stretching by 0, 30, 60%) and to UV radiation for 1000:5000 hours showed that there was a synergetic effect between exposure to UV irradiation and mechanical stress [DE-90]. However, a synergism was not present between UV radiation and electrical stress when corona discharges were absent.

In the work presented by [YOU-05] HTV SIR and EPDM were exposed to 5000 hours of accelerated UV weathering and the degree of degradation with time was analyzed. Surface morphology and chemistry of the UV treated samples were studied through scanning electron microscopy (SEM) and X-ray photoelectron spectroscopy (XPS) analysis. A weathering tester equipped with eight UV-B 313 nm fluorescent lamps was used for UV exposure of the samples. The wavelength region of the UV lamps is 280 nm to 415 nm. The distance between the lamps and the specimen surface was 50 mm. Only one side of the specimen was subjected to the UV. The test cycle was continuously repeated with 4 hours of UV irradiation and 4 hours of condensation with UV-Off.

Measurement of the surface resistivity and the surface voltage decay after corona charging were found to provide similar information on the UV treated materials. It was observed that EPDM suffers more loss of hydrophobicity and surface resistivity than HTV SIR under UV weathering conditions. Also, HTV SIR appears to undergo mainly cross-linking reactions whereas the damage on EPDM primarily occurs through chain scission reactions followed by the generation of free radicals and oxygen containing groups.

The study performed by [VEN-07] deals with the long term accelerated multi stress aging on full scale 11 kV distribution class composite silicone rubber insulators. In order to assess the long term synergistic effect of electric stress, temperature and UV radiation on insulators, they were subjected to accelerated aging for 3800 hours in a specially designed multi stress aging chamber, controlled thermal stress and different levels of UV radiation (8 UV fluorescent tubes and a UV-A lamp) either singly or simultaneously. It was noticed that substantial oxidation took place on the surface of the polymeric specimen at the current level of aging. A surface roughness increase and a reduction in contact angle have been observed.

1.7.3. Electrical Influencing Factors

1.7.3.1. Test voltage magnitude

The rate at which space charges accumulate within the polymer depends upon a number of factors. Among these, the type and magnitude of the applied electrical gradients and the amount of trapping sites present in the polymer can be mentioned. The type (AC/DC) and magnitude of the electrical stresses imposed on the insulating arrangement also will determine strongly the expected intensity and frequency of any corona discharging generated under specific operational conditions. Therefore, in defining the extent to which electrical discharges may provoke a degradation of the polymer physical and electromechanical properties, the polymer charging characteristics should be identified first in a comparative way for both AC and DC corona.

The degree of influence on AC and DC energized insulation, and a resulting comparative relationship on the expected electrical performance of polymer materials stressed with both types of voltage have been identified by [MOR-99]. In this study, the AC and DC (of both polarities) corona charging of the samples was performed at room temperature (20:25°C). A constant test voltage of 7.2 DC or 7.2 kV_{rms} AC with 1 mm electrodes gap distance and corona charging time of 3 hours were adopted. After exposure to corona, surface charge decay measurements were performed under both low humidity (19% and 35 %RH) and high humidity conditions (75 and 80 %RH). In this study, three completely different polymeric systems, namely HTV SIR, EVA and epoxy resin, were evaluated. Both the HTV-SIR and EVA samples are reinforced with *Alumina Trihydrate* (ATH). On the other hand, the epoxy resin compound contains silane treated silica as reinforcing agent.

From the results obtained, charging of insulating material surfaces exposed to AC and DC corona has been verified experimentally. Surface charge build-up under DC stresses was enhanced significantly with respect to the surface charge magnitudes recorded for the AC case. In general, it was observed that even under high humidity conditions the lifetime of corona implanted positive DC charge is longer than that of AC and negative DC charge.

Surface degradation of flat silicone rubber samples exposed to electrical discharge was studied by [ZHU-06a], [ZHU-06b], [ZHU-06c]. Voltages of 8, 8.5, 9, 9.5, 10, 10.5, and 11 kV at 50 Hz, were applied to generate the corona discharge from a multi needle-to-plate electrode arrangement for 3 hours at each voltage. Both electrodes are placed on the specimen surface with a gap of 20 mm in between.

Removing the by-products of aging from the eroded surface results in a weight loss of the specimen, which can indicate the extent of degradation of the SIR exposed to electrical discharges. Figure 1.13 shows the relationship between the cumulative charge of the discharge stress and the weight loss of the specimen at different applied voltages. It was observed that the cumulative charge increases with an increase in applied voltage; furthermore, the weight loss (from surface erosion) due to discharge was also proportional to the cumulative charge. The amount of cumulative charge indicates the intensity of the discharge stress. It appeared that the more intense the discharge stress, the larger was the weight loss.

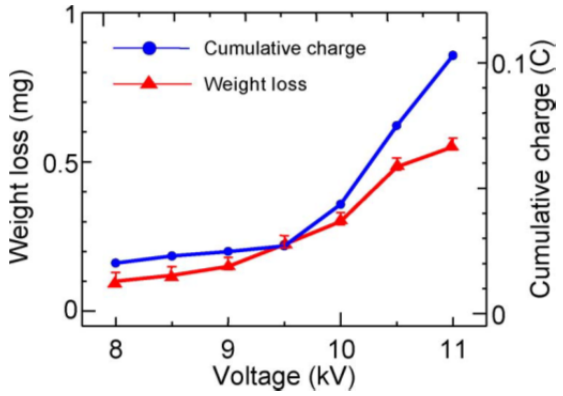

Figure 1.13: Cumulative charge and weight loss of silicone rubber samples under corona stress in a multi-needle-to-plate arrangement [ZHU-06b]

The influence of test voltage magnitude on discharge intensity as well as erosion severity has been investigated by [ANG-08], [ANG-12]. Anglhuber et al have tested polyethylene specimens with respect to their resistance to surface erosion. The electrode arrangement used in these investigations is according to IEC 60343 at 50 Hz test voltage of magnitudes 6, 10.5, 15 kV and for stress duration of 120 hours. All the resulting erosion characteristics as well as the cumulative discharge parameters were normalized with respect to the eroded volume under the lowest voltage stress condition; i.e. at 6 kV. It was found from the results that the discharge parameters in comparison to erosion characteristics exhibit a higher rate of increase with respect to the increase in the test voltage (figure 1.14).

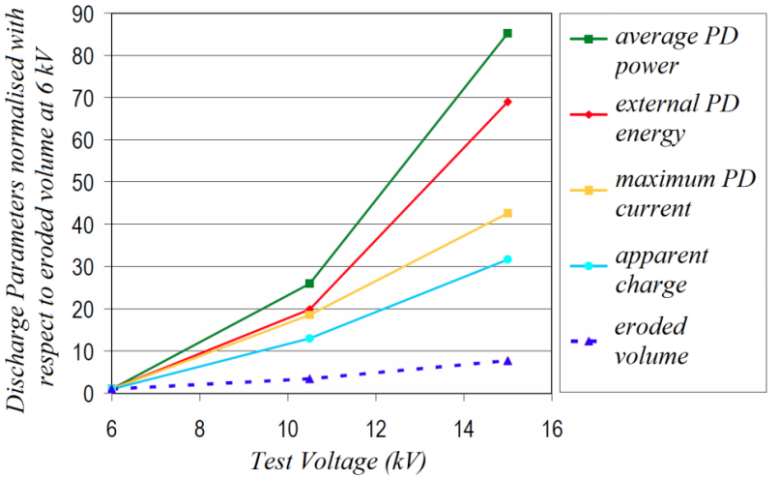

Figure 1.14: The influence of test voltage magnitude on erosion characteristics and cumulative discharge parameters for polyethylene samples tested according to IEC 60343 [ANG-08]

1.7.3.2. Test voltage frequency

For solid insulation in general the frequency of the applied voltage has to be regarded as a very important influencing factor on the performance as well as the degradation progress of the insulator. The increase of the insulating material heating with frequency may be significantly higher than can be expected from the linear frequency term in the following basic formula:

$$P_{loss} = 2\pi f V^2 C \, tan\delta \qquad [1.6]$$

Where, $\boldsymbol{P_{loss}}$, is the dielectric loss, $\boldsymbol{V}$ the voltage (RMS), and $\boldsymbol{C}$ the capacitance of the test specimen. This is due to the increase of the loss factor $\boldsymbol{tan\delta}$ which may occur in the kHz range. The result may be a higher probability of thermal breakdown and a reduction of the short-time dielectric withstand capability. For inhomogeneous gaps, the influence of the frequency on the breakdown voltages is much more significant than that for homogeneous one. The amount of the reduction of the breakdown voltages will be about 50%. The results are also strongly influenced by the electrode configuration [PFE-91].

Practical considerations make it desirable to accelerate the degradation and failure testing of polymer insulating material samples. Johnston et al [JOH-79] have reviewed the frequency acceleration of life testing. The rationale for accelerating the frequency is that if a given amount of damage due to discharges occurs during one cycle, then the life of the insulation is determined by the number of cycles, rather than the stressing time. Some questions have been raised as to whether the damage is linearly accelerated by frequency.

Ahmed et al [AHM-78] measured the temperature rise under discharge conditions and found that the rate temperature rise with voltage is increased at higher frequencies. However, another study has suggested that such a temperature rise may modify the characteristics of the discharge itself and lead to nonlinear acceleration [BAR-87]. Olyphant [OLY-67] inspected the surfaces of the samples eroded by electrical discharge. He found that, when there was a difference between the actual 60 Hz life time and the "equivalent 60 Hz life time" at 1440 Hz obtained by multiplying 1440 Hz failure by 24, there were readily detectable differences in the amounts of erosion.

If it can be assumed that discharge intensity along one cycle under constant test voltage is independent of the frequency, then stressing the insulating material surface under high frequency leads to achieving to a certain erosion degree in less time. This hypothesis is confirmed by the frequency acceleration tests performed by Tanaka et al. and Montanari et al. who have applied test voltages at high frequencies to achieve the same amount of discharge at shorter stress time duration [KOZ-05b], [TAN-06], [Tan-07], [TAN-08a], [TAN-08b], [FAB-09]. The low frequency equivalent time t_{low-eq} can be calculated from the following equation:

$$t_{low-eq} = \frac{t_{high} \cdot f_{high}}{f_{low}} \qquad [1.7]$$

Where, the high frequency f_{high} is applied for a stress time t_{high} which is indeed less than the low frequency equivalent time t_{low-eq}.

Tanaka et al [TAN-07], [TAN-08a] have examined the acceleration of epoxy erosion under the impact of test frequency. Nanocomposite specimens are prepared by the solubilization method and are cured either by amine or by acid anhydrite. Erosion evaluation is carried out with two frequencies, i.e. 600 Hz and 1.2 kHz as acceleration tests. It was suggested to select 600 Hz as acceleration frequency, since erosion is saturated in 1.2 kHz aging condition for the long run. Therefore, frequency acceleration was suggested to be done from 60 Hz to 1.2 kHz.

Here the acceleration of material aging under the impact of test frequency was examined at the same 60 Hz equivalent time. Acceleration factor is almost 2 between 600 Hz and 1.2 kHz, but it is much less than 10 between 60 Hz and 600 Hz as shown in figure 1.15. This performance was attributed to the modification of the electric field caused by shape change due to erosion. Although a stress time period of 120 hours was applied to all samples, the comparison in terms of erosion degree was performed for constant number of cycles and not for the same stress time duration.

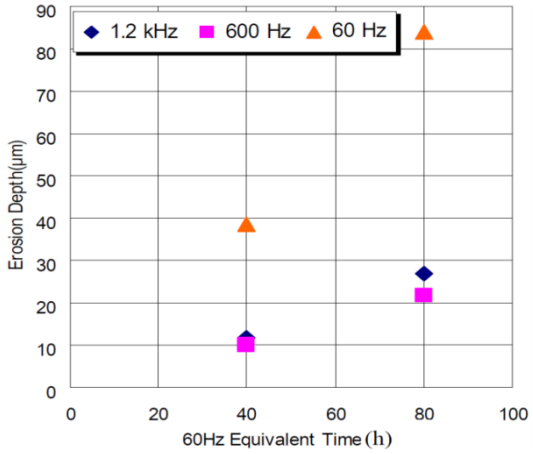

Figure 1.15: PD erosion depths for base epoxy hardened by acid anhydride under different frequencies, after [TAN-07], [TAN-08a]

1.7.4. Ion bombardment

Discharges in nitrogen result in craters or pits on the material surface which appear to be the result of ion bombardment [TAN-86], [GAM-87], [DIS-92]. Although individual ions may not necessarily have energies sufficient to break bonds, the concentrated bombardment from a streamer on a small area is sufficient to lead to that erosion. Mason [MAS-78] estimated that the resulting erosion of PE by internal discharges, after prolonged tests at a stress of 4 kV/mm, proceeded at a rate of approximately 10^{-12} m^3 per discharge

Mayoux [MAY-76] showed that the erosion due to electron bombardment was usually insignificant, because electron required energy greater than 500 eV to cause substantial damage. He suggested that the results of the ionic impact on PE could only account for a part

of the material erosion and that chemical degradation is also responsible. Whilst in electrical discharges ion Bombardment is unlikely to initiate significant damage, it may play a significant role in worsening the existing damage. For example, cracks may have been initiated by any other mechanism in which case energies of only a few electron volts are required to deepen the crack. Mayoux [MAY-76] has reported the results of a comprehensive study in which PE was stressed in air by UV radiation and by low energy (< 100 eV) electrons and ions supplied from electron and ion guns. The results were compared with the damage occurring under electrical discharge.

Electron irradiation was found to turn material surface brown and apparently did not penetrate the PE. For the ion bombardment, it also produced the brown color. Several different ions were used and it was found that the damage resulting from these ions increase with their mass, suggesting that they exhibit mechanical stresses. However, the mass of the O^+ ions is less than that of Ar^+ ions, the damage caused was more than that caused by the noble gas ions. So it was suggested that the oxygen ions have chemical effect in addition to the mechanical effect. UV irradiation resulted in degradation that was rather different from that produced by accelerated ions and electrons, being characterized primarily by unsaturated carbon groups. The authors concluded that ion bombardment could account for a large part of discharge degradation.

In another study Mayoux et al [MAY-73] examined the degraded surface of PE stressed by UV irradiation, electrons, and O^+ ions. Only O^+ ions produced material degradation can be resembled to that caused by corona discharge, but UV irradiation and electrons did not show considerable degradation.

1.8. Summary

- Epoxy resin is considered as one of the most reliable polymeric insulating materials used in high voltage applications; especially bisphenol A epoxy resin.
- Corona discharge proved to have a direct influence on insulating material surface in form of (chalking, crazing, cracking, erosion, tracking, hydrophobicity deterioration).
- There are many factors that could have an influence on surface erosion of discharge stressed materials; temperature, humidity, pollution, UV radiation, mechanical stresses and the characteristics of applied electric field.
- The impact of the influencing factors has been widely examined in terms of surface characteristics (i.e. hydrophobicity) except for surface erosion under discharge stress.
- A correlation study could hardly be found between corona discharge stress and the resulting material damage represented by surface erosion.
- Laboratory experimental setups are designed to examine the effect of UV radiation from sunlight; whereas those setups neglect the solar blind zone existing in the UV spectrum associated with corona discharge.

- Despite the importance of discharge initiated surface erosion, a standardized adequate test setup to examine materials for this specific performance has not existed till now.
- Different measurement techniques are applied after material stressing to introduce indicators on the level by which insulating material is impacted. Among those are chemical properties measurements; in which surface degradation is analyzed, and surface properties measurements; in which erosion severity is quantified in terms of erosion depth, eroded volume and weight loss.
- Ambient conditions (humidity, ozone, temperature, pressure, UV…) have been studied as factors of influence on the material degradation under corona discharges. Nevertheless, there is almost no correlation study hold between environmental factors and corona discharge intensity or surface erosion.

1.9. Thesis Objectives

- The main objective of this thesis is concerned with the erosion of polymeric insulating materials due to corona discharges. Actually, there is a significant lack of the knowledge concerning surface erosion mechanism of the polymeric insulating materials with respect to corona discharges.
- This research aims to understand the mechanisms of erosion under the influence of corona discharges on the polymeric insulating materials for use in high voltage applications. Here the material of concern under study is epoxy resin.
- To achieve this goal a suitable test procedure including a suitable experimental setup has to be developed and validated. This procedure concerned with testing materials with respect to their erosion resistance to corona discharges should be representative and gives reproducible results.
- Another experimental arrangement needs to be developed to study the influence of discharge initiated UV radiation on insulating material surface. In this way UV radiation, which is one of the stresses working together on material surface, can be identified separately in terms of material erosion.
- It is also mandatory for understanding the mechanism of erosion in the sake of the development of new insulating materials or the improvement of the existing ones, to identify the complex factors of influence causing erosion and to quantify their effect.

2. Test Technique

The main purpose of this chapter is to select suitable test setups and test procedures which allow holding a correlation study between the investigated phenomena and the resulting influences on material surface erosion. All the available information about the existing test stands concerned with testing materials to their surface erosion resistance are presented in this chapter. Taking all these stands in to consideration, certain test setup and test procedures can be chosen as described in the following sections.

2.1. Electrode Arrangement

To examine the influence of corona discharges on the properties of insulating materials, several different test setups should be compared. So the effects of electrical discharges from pointed electrodes based on structures with one electrode or with multiple ones were studied. On the other hand, test setups were used, in which discharges occur in an air gap far from insulating material to have its indirect impact; whereas others are in direct contact with material surface. Because of these different test setups and experimental parameters it is not possible to hold a direct comparison of those different methods.

Artificial tests have been developed employing continuous corona discharges from various electrode arrangements [KIM-99], [HIL-99], [HIL-01a], [HIL-01b], [KUM-03], [IJU-02], [MAL-03], [MEI-05], [OLA-05]. Nevertheless, these tests were applied to investigate the material surface degradation in terms of hydrophobicity, which is irrelevant for this study. Other applied test procedures concentrated on the impacts of long term corona discharges on the erosion of polymeric insulator surfaces and on clarification of the ageing mechanisms involved [MOR-99], [MOR-01a], [MOR-01b], [KOZ-04], [KOZ-05a], [KOZ-05b], [TAN-06], [TAN-07], [CAV-07], [ANG-08], [TAN-08b], [FAB-09], [TAN-11]. All of the proposed test setups concerned with erosion phenomena were designed to generate corona discharge near or in the vicinity of material surface to guarantee non-uniformity of the electric field and hence the acceleration of specimen erosion.

2.1.1. Investigating Different Electrode Arrangements

For the sake of construction and validation of test stands, different setups and test procedures which allow getting results representative to those phenomena occurring under service conditions are selected. All the investigated test stands in literature are summarized in table 2.1. At the beginning the selected promising test setups can be classified into two groups according to the location of electrical discharge with respect to the specimen surface, i.e. group A, in which electrical discharges are relatively far from material surface and group B, in which electrical discharges are generated and located directly on the material surface.

Table 2.1: Different test setups to investigate the influence of corona discharge on insulating materials

Group	***Literature***	***Specimen Size (mm)***	***Electrode Arrangement***	***Gap Distance***	***Test Voltage***	***Stress Time***
A	***HIL-98*** ***AND-07***	*Disc with diameter of 110 mm and thickness of 1.6 mm*	*Multi-needle to plane*	*40 mm*	*50 Hz* $20\ kV_{rms}$	*20 min: 200 hours*
	DU-08	*20 × 20 × 8*	*Multi-needle to plane*	*10 mm*	*50 Hz* $3\ kV_{rms}$	*10 hours*
	VEN-10	*Disc with diameter of 70 mm and thickness of 3 mm*	*Multi-needle to plane*	*5 mm*	*50 Hz* $8\ kV_{rms}$	*25, 50 hours*
	MA-10	*120×100×2*	*Multi-needle to plane*	*40 mm*	*50 Hz* $20\ kV_{rms}$	*100 hours*
B *with mainly a dominant* ***normal*** *field component and no gap between electrodes*	***IEC 60343*** ***KOZ-04***	*60 × 60 × 1*	*Rod to plane according to IEC 60343*	*0*	*60 Hz* $4{:}10\ kV_{rms}$	*1:48 hours*
	ANG-08	*100×100×2*	*Rod to plane according to IEC 60343*	*0*	*50 Hz; 6, 10.5,* $15\ kV_{rms}$	*24, 72, 120 hours*
B *with mainly a dominant* ***normal*** *field component and very small gap distance*	***MOR-99***	*50 × 50 × 6*	*Needle to plane*	*1 mm*	$7.2\ kV_{rms}$ *7.2 DC*	*3 hours*
	MOR-01a ***MOR-01b***	*30 × 50 × 6*	*Needle to plane*	*1 and 5 mm*	*50 Hz* $7.2\ kV_{rms}$	*3 hours*
	KOZ-05a T. Tanaka	*50 × 50 × 1*	*Needle to plane*	*0.2 mm*	*50 Hz* $6\ kV_{rms}$	*5:96 hours*
	KOZ-05b T. Tanaka	*50 × 50 × 1*	*Needle to plane*	*0.2 mm*	*720 Hz* $4\ kV_{rms}$	*20,60, 120 hours*
	TAN-06	*40 × 40 × 1*	*Needle to plane*	*0.2 mm*	*720 Hz* $4\ kV_{rms}$	*48 hours*
	TAN-07 ***TAN-08a***	*40 × 40 × 1*	*Needle to plane*	*0.2 mm*	$4\ kV_{rms}$ *60, 600, 1200 Hz*	*120 hours*
	TAN-08b	*30 × 30 × 1*	*Needle to plane*	*0.2 mm*	*600 Hz* $4\ kV_{rms}$	*12,24, 48 hours*
	CAV-07 G. C. Montanari	*60 × 60 × 1*	*Needle to plane*	*0.1 mm*	*50 Hz* $10\ kV_{rms}$	*Up to 2544 hours*
	FAB-09 G. C. Montanari	*60 × 60 × 1*	*Needle to plane*	*0.1 mm*	*250 Hz* $10\ kV_{rms}$	*Up to 2500 hours*
	TAN-11 G. C. Montanari	*60 × 60 × 1*	*Needle to plane*	*0.1 mm*	*250 Hz* $10\ kV_{rms}$	*Up to 150 hours*
B *with mainly a dominant* ***tangential*** *field component*	***ZHU-06a*** ***ZHU-06b*** ***ZHU-06c***	*60 × 50 × 2*	*Comb-shaped electrode with Multi-needle to plane*	*20 mm*	*50 Hz, 8, 8.5, 9, 9.5, 10, 10.5,* $11\ kV_{rms}$	*3 hours*

i. Group A

This group includes the test setup in which electrical discharges are relatively far from the specimen surface. The arrangement shown in figure 2.1 (a) [HIL-98] is for a multi-needle high voltage electrode 40 mm apart from the specimen surface. This arrangement was only used to study the effect of electrical discharge on material degradation in terms of hydrophobicity, surface resistivity, dielectric properties and mechanical properties. However, the most important restriction against this arrangement is that the structural analysis proves negligible erosion resulting from the electrical discharge which cannot be quantified [AND-07], [MA-09], [MA-10].

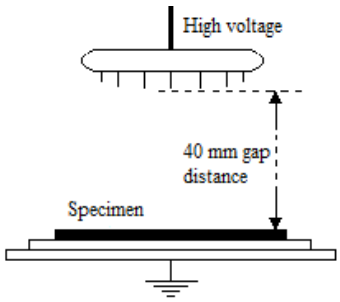

(a) Multi-needle H.V. electrode 40 mm apart from the specimen surface [HIL-98]

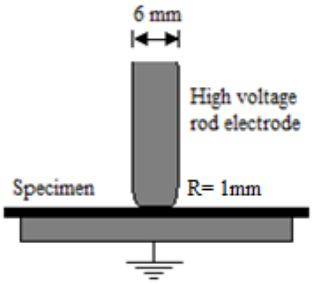

(b) Rod H.V. electrode touching the specimen surface and with mainly normal field stress [IEC 60343], [KOZ-04]

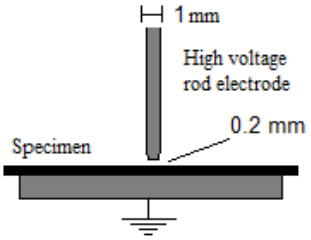

(c) Rod H.V. electrode 0.2 mm apart from the surface with mainly normal field stress [TAN-07], [TAN-08a]

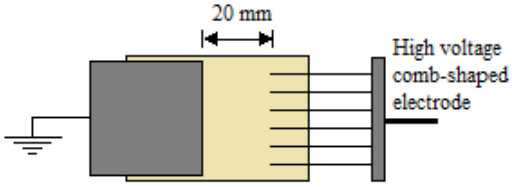

(d) Comb-shaped electrode applying corona discharges mainly through tangential field stress [ZHU-06a], [ZHU-06b], [ZHU-06c]

Figure 2.1: Different electrode arrangements in comparison

i. Group B

This group deals with those test setups applying electrical discharges directly on the surface of the specimen under treatment taking in to consideration that the main point is to produce measureable erosion. The corona discharges can be generated from test setups applying either normal or tangential field stress to the specimen surface.

1. Test setups applying mainly a normal field stress

The arrangement shown in figure 2.1 (b) produces mainly a normal field stress to the specimen surface. A high voltage rod electrode is touching the specimen surface resulting in a certain erosion region surrounding that region of contact. This arrangement can be modified as illustrated in figure 2.1 (c) by introducing a small air gap (0.2 mm) between the

electrode and the specimen surface. Hence the specimen surface is subjected to electrical discharges generated in the gap and the erosion zone will be that under the air gap. In other words this arrangement generates mainly discharges in the 0.2 mm gap, while the former (i.e. figure 2.1 (b)) brings about surface discharges.

The advantage of this test setup (figure 2.1 (b), (c)) is the resulted measureable erosion depth, erosion area and weight loss [IEC 60343], [TAN-07], [TAN-08a]. However, the disadvantage of this setup is the possibility of flashover occurrence in case of increasing the stresses (voltage, frequency, humidity, etc...). Additionally, if any of the stresses is decreased, there is a possibility that the intensity of corona discharge is not enough to cause significant surface erosion.

The electrode arrangement proposed by Tanaka for the purpose of PD resistance measurement shown in figure 2.1 (c) used test voltages up to 10 kV and specimens of size 40 mm x 40 mm x 1 mm. Montanari has noticed several flashovers without specimen breakdown due to small specimen surface. Beside that he noticed that PD activity was not enough intense to lead to a significant surface erosion for epoxy resin specimens. In order to solve these problems Montanari has introduced little modifications to the former electrode arrangement. Accordingly the specimen size was increased to 60 mm x 60 mm and the air gap between the high voltage electrode and the specimen surface was reduced to 0.1 mm [CAV-07], [FAB-09], [TAN-11]. In this way the possibility of flashover occurrence is reduced and the field stress is enhanced resulting in considerable surface erosion.

2. *Test setups applying mainly a tangential field stress*

The test setup illustrated in figure 2.1 (d) is for a comb-shaped high voltage electrode applies mainly a tangential field stress on the specimen surface. This tangential field supports the acceleration of surface degradation in a small time as well as reaching a considerable amount of erosion to be analyzed. The main problem in that test setup is that the use of multi-needle restricts the possibility of representative correlation between the applied test conditions and the resulted erosion effect. To avoid this problem only one needle was used as a high voltage electrode in this study. From that stand point the proposed test setup is a needle-to-plate electrode producing tangential field parallel to the surface of the material specimen. Beside that the test arrangement was accommodated in a glass vessel to control ambient conditions.

2.1.2. Applied Electrode Arrangement (Test Setup A)

Schematic view of the used setup is illustrated in figure 2.2. A stainless steel needle was used as a high voltage electrode, its cross sectional- and tip diameters are 0.8 mm and 0.4 mm respectively. On the other hand, (50 x 20 x 0.2 mm^3) aluminum sheet was used as the ground electrode. The needle electrode was supported in reality be plastic holder and the air gap between the needle tip and the ground electrode was adjusted at 15 mm. This value was chosen to avoid any flashover that could occur at smaller gaps. Both electrodes were fixed on the specimen surface to produce a tangential electric field parallel to the dielectric surface.

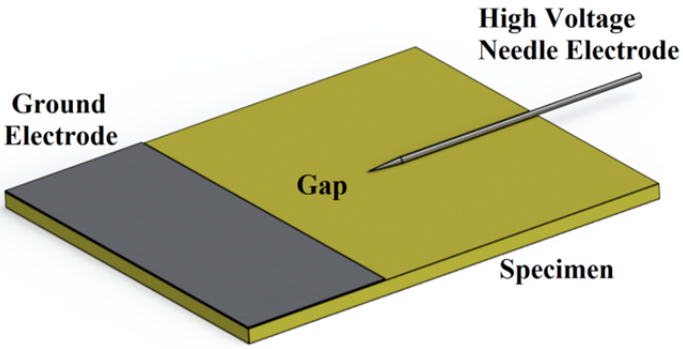

Figure 2.2: Schematic view of electrode arrangement for the corona discharge; Test Setup A

For each test series number of specimens with dimensions of 60 x 50 x 2 mm^3 (each with its high voltage and ground electrodes) were placed on (24 cm diameter) PLEXI disc. To isolate the lower surface of the samples from the ground; the disk was mounted on PE cylinders of 15 cm height. The whole experimental arrangement was then placed in a desiccator in order to allow the control of ambient conditions according to the test phase, see figure 2.10. It is made from Duran Borosilicate glass 3.3 and placed above a grounded plate.

As a matter of fact the time of voltage application plays an important role in the discharge process. Some of the test procedures suggested time intervals in the range of 100 hours to study the aging mechanism of dielectrics that requires a long time to progress. Hence, the selected stress duration is 96 hours, in order to achieve the aimed erosion. The proposed test setup with such electrode arrangements offers many advantages over that according to IEC 60343 as follows:

1. The severity of erosion is much higher for the same applied voltage in terms of eroded area and volume. This is referred to the area of discharge zone and the applied field tangential to specimen surface, which accelerates surface degradation at higher rate.
2. The possibility to use this test setup with little modification to study the impact of UV radiation separately on material surface as will be seen later in 2.1.4.
3. After the first hour of stress, the mean discharge parameters (charge and discharge energy) of the test setup in accordance with [IEC 60343] increase gradually with aging time [LUO-13]. This presents bad correlation between applied stresses and the resulting surface damage. On the other hand, the proposed electrode arrangement (figure 2.2) guarantees nearly constant mean discharge parameters after the first three hours of stress as shown in figure 2.3.
4. Thanks to this electrode arrangement there is a focus on a well-defined area with a local discharge activity.

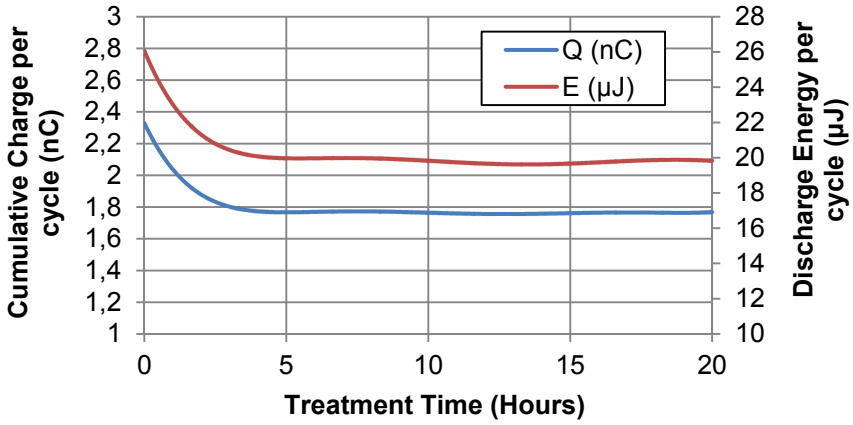

Figure 2.3: Discharge parameters of epoxy specimen under 12 kV_{peak}, 500 Hz, 20 ℃ and 33 %RH; cumulative charge and total discharge energy within one cycle of the applied voltage along with treatment time (test setup A)

2.1.3. Electric Field Simulation

Simulations of the electric field distribution were performed to determine if the selected gap distance between the needle and the plate electrodes is the optimum. A 3-D model of electrode arrangement was built, as illustrated in figure 2.4, and static finite element method (FEM) solutions of electric field strength at different distances from the needle tips were obtained. The model was solved with a simulated needle tip radius of 200 µm AC voltage 12 kV_{peak}. A static finite element method (FEM) solution of electric field strength was performed using COMSOL Multiphysics software.

Simulated field distribution on the surface of a specimen ($\varepsilon_r = 4$) is presented in figure 2.5, where it can be noticed that the maximum field strength was obtained in front of the needle tip. This is also clear from the electric field along the axis of the needle towards the grounded electrode; a little bit above the surface as in figure 2.6. Here, an enhancement in electric field is detected in front of needle tip and then it starts to decay by getting far till reaching the opposing ground electrode.

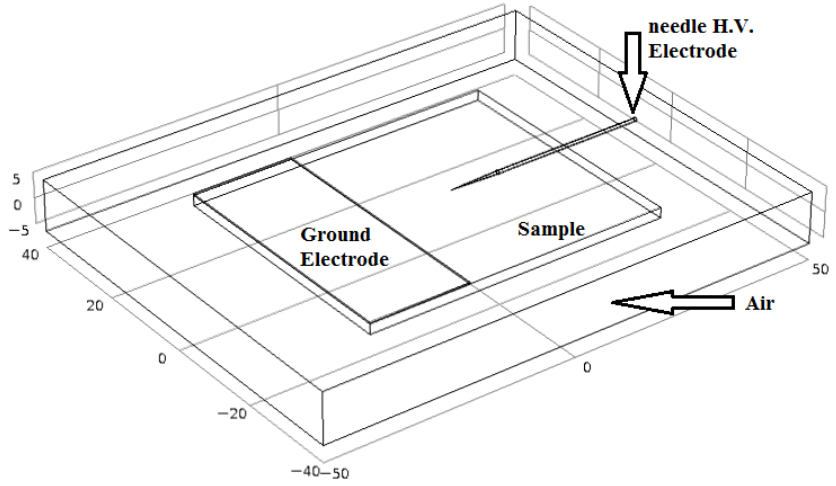

Figure 2.4: 3-D Model of corona discharge (test setup A)

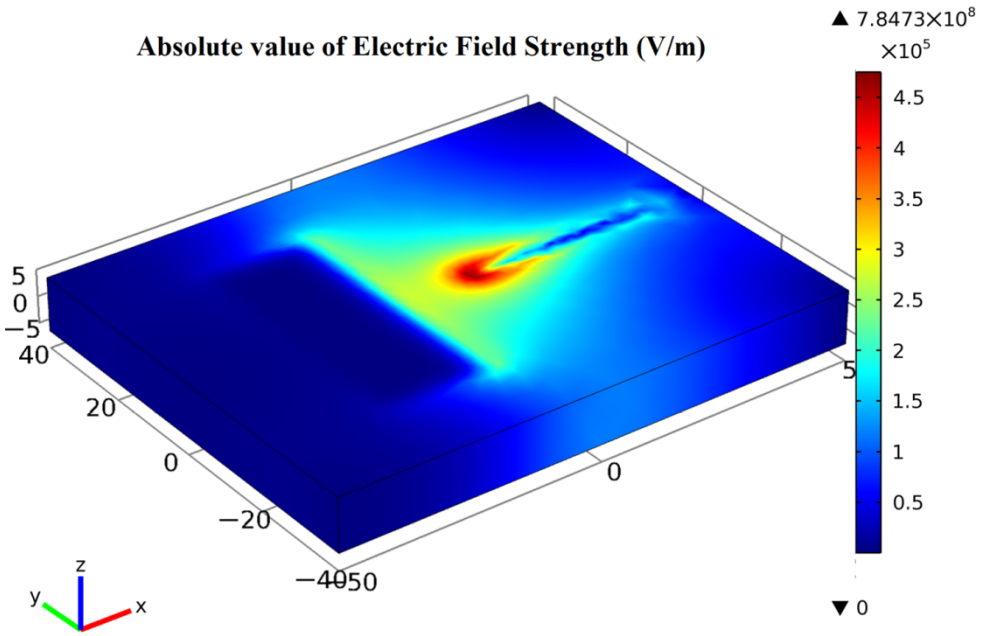

Figure 2.5: Electric field simulation on the specimen surface at 12 kV_{peak} (test setup A)

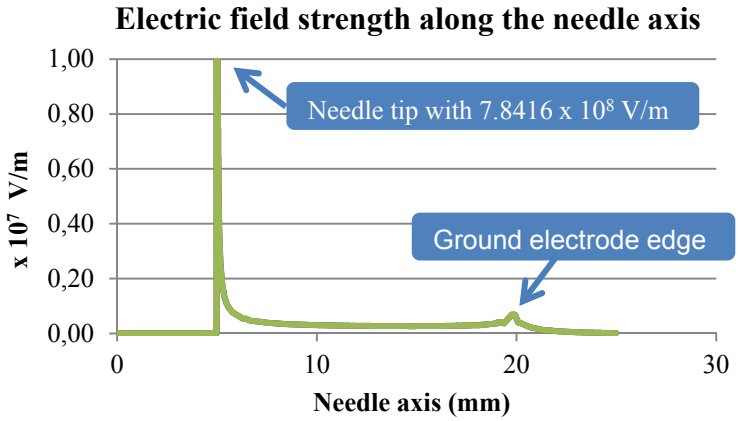

Figure 2.6: Absolute value of electric field strength along the needle axis towards the electrode against at 12 kV_{peak} calculated with static field

2.1.4. Electrode Arrangement for Separation of UV Radiation Stress (Test Setup B)

In order to study the effect of induced UV radiation on material surface erosion, suitable electrode arrangement was applied in order to examine the effect of UV radiation associated with electrical discharge. Test setup B exposes the specimen surface to UV stresses; whereas electrical stresses are limited. Both electrodes were placed on the main specimen surface; which empty the space above the test setup. A secondary specimen was inserted in parallel to the main one with 4 mm normal distance in between as shown in figure 2.7. In this way, direct influence of discharge on the secondary specimen surface was limited. Therefore, the damage resulting in the secondary specimen was considered as a direct effect of UV radiation.

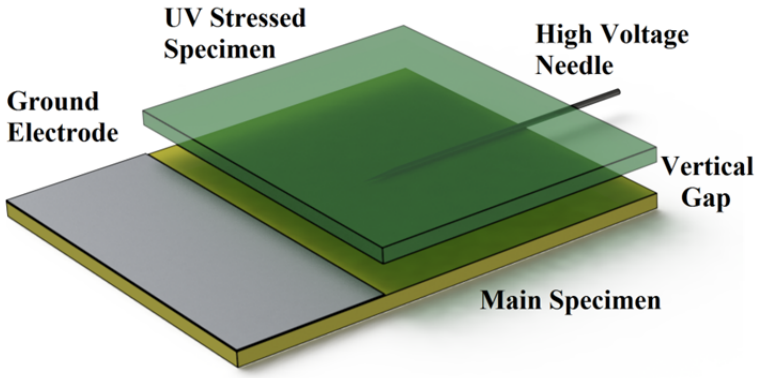

Figure 2.7: Test setup B for investigating the impact of UV radiation associated with electrical discharge on material surface

In order to prove that the impact on the lower surface of the secondary specimen is due to UV radiation and no charges are involved; the following procedures were performed. First, the electrical field simulation of the applied test setup B identifies whether the tangential field on the lower surface of the secondary specimen is sufficient to initiate an electrical discharge or not. Figure 2.8 (a) shows the electric field distribution on the lower surface of the secondary sample. The electric field is obviously weak (with maximum of 3.8 kV/cm) to result in discharge on the surface of the secondary sample. It can be also seen from figure 2.8 (b) that the region of high electric field strength is far from the lower surface of the secondary specimen. Therefore, it could be assumed that the space charges are limited in the direction towards the secondary specimen.

Nevertheless, this procedure cannot be regarded sufficient to deny the bombardment of any charged particle on the surface of the specimen of concern. The reason for that is the space charge, which could exist in discharge zone and in turn changes the distribution of the electric field. Another procedure was performed to validate the test setup B; in which the spread of UV radiation is imaged. This procedure assumes that the spread of UV radiation is governed by charged particles distribution in discharge zone.

Figure 2.9 shows a side view of the test setup and the resulting UV radiation under 12 kV_{peak} and 500 Hz. It can be seen that the extension of UV radiation in z-direction was up to 0.7 mm above the main specimen surface along the needle electrode as well as in the direction to ground electrode. The maximum spread of UV in z-direction is 1.2 mm in front of the needle tip. It can be assumed that charged particle impact extended only to a small distance above the main specimen surface (i.e. 1.2 mm). Therefore, the selected position of the secondary specimen was well isolated from charged particles, which could bombard on material surface. From the investigations made above, the applied test setup expresses efficiently the impact of UV on material surface with the isolation of charged particles. The modified test setup was applied under different values of test voltage magnitudes and frequencies in order to study the effect of electrical factors on induced UV radiation.

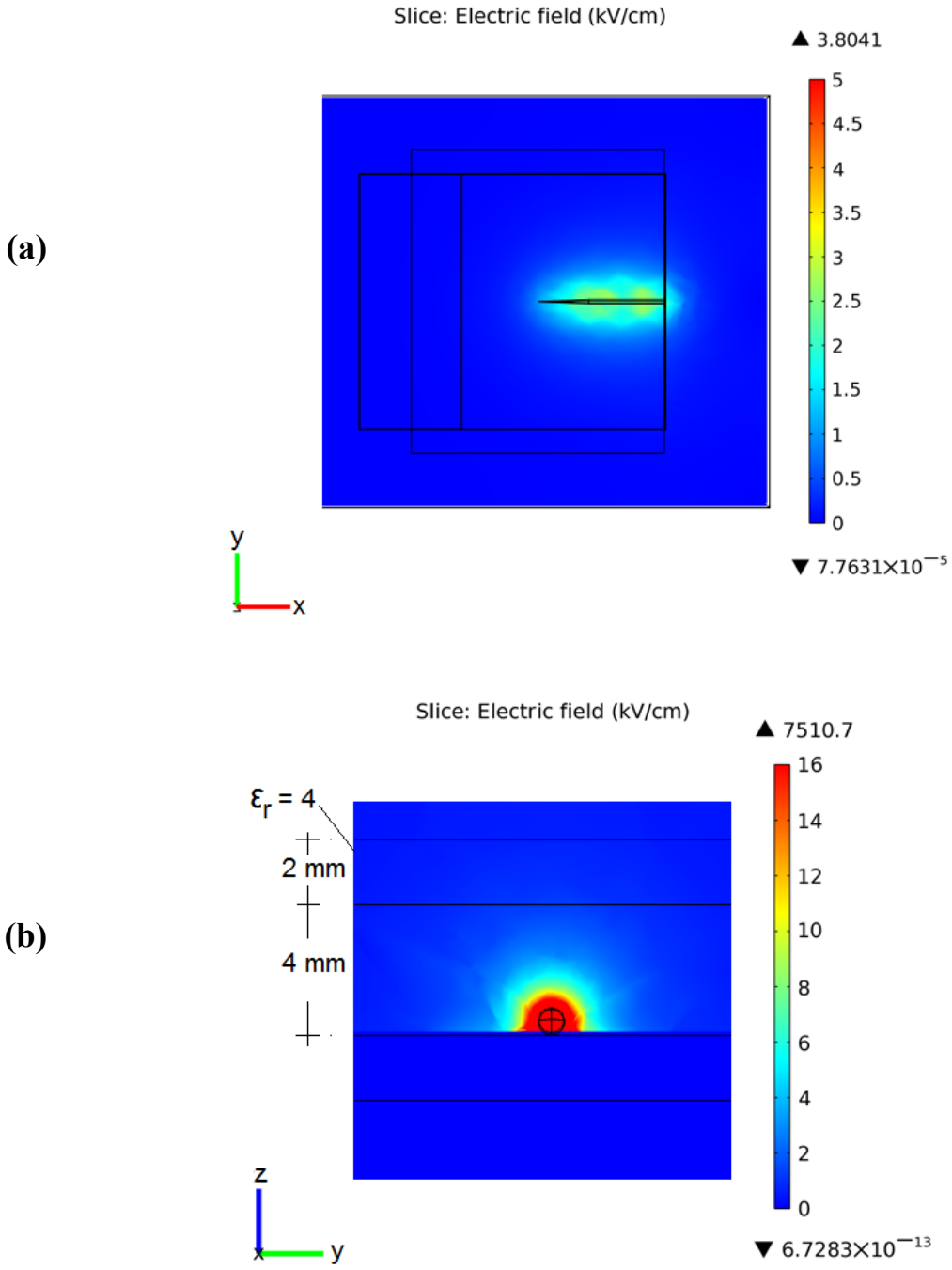

Figure 2.8: Electric field distribution at 12 kV_{peak}; (a) on the lower surface of the secondary specimen, (b) in the gap between the two specimens at x=5, i.e. in front of needle tip

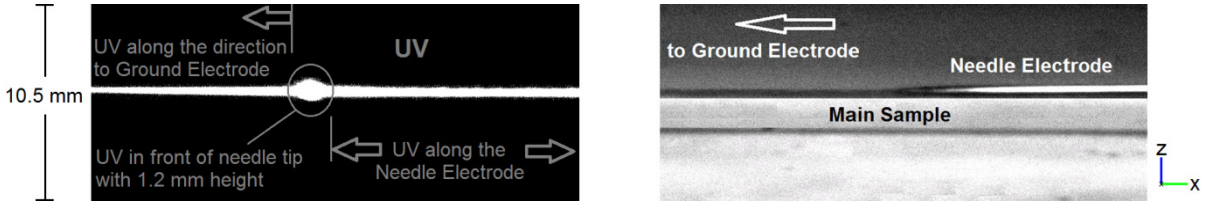

Figure 2.9: UV radiation imaging under 12 kV_{peak} and 500 Hz; left: UV radiation, right: electrode arrangement of test setup A

2.2. Test Voltage Generation and Measurement

The test voltages were generated primarily using a signal generator (Agilent 33220A), used to provide a sinusoidal waveform of adjusted amplitude up to 10 V_{peak}. The output of the signal generator was then passed through a high voltage amplifier (Trek 20/20C) with output voltage up to 20 kV_{peak} and output current up to 20 mA_{peak}. The output voltage magnitude of the function generator was adjusted in accordance with the amplifier gain (2000). The output of the amplifier was then connected to the needle electrode via a double-insulated cable which helps to prevent high frequency AC currents from flowing through extraneous coupling paths to other devices. In this way no noise or distortion are introduced to the supplied currents. If the current drawn by the test setup exceeds the trip limit (20 mA), the high voltage output is automatically disabled.

The amplitude of the test voltage was measured through a voltage monitor signal supplied by the high voltage amplifier. This has been verified by direct measurement of the voltage at the specimen by using a high voltage probe. The monitor signal is a representation of the low voltage to the amplifier output; where its magnitude equals to $1/2000^{th}$ of the output high voltage. Actually this is a feedback signal which was connected to a monitoring device (i.e. oscilloscope) to measure test voltage magnitude.

The current measurement was performed indirectly via 10 W, 50 Ω ± 2% resistor, which was connected in series with the plane electrode in its ground path. All the used cables are short shielded ones in order to limit the influence of the inductance. Moreover, the used resistor [ZAE-64], [ZAE-77] is specially designed high voltage to eliminate the inductive effect in the circuit by using parallel resistors. In such a way the resulting magnetic field from each resistor is neutralized by that of the neighboring.

Then, the voltage across the resistor was measured with aid of the oscilloscope, from which the current can be calculated. All the signals to be measured from the high voltage region were transmitted over BNC cables to the oscilloscope in the control area. In order to avoid any damage in the control area caused by an overvoltage, each signal was first passed through an over voltage protection circuit. In case of overvoltage, it introduces an alternative path (i.e. ground) for the signal to be dissipated and not to reach the oscilloscope.

The data acquisition was performed via a real-time oscilloscope (Agilent DS05014A) with four independent channels. The measurement bandwidth is 100 MHz; so that high frequencies such as those occurring at partial discharge can be detected. The record length is 10^6 samples per each channel. The oscilloscope with input impedance is 50 Ω was connected to a computer via the RS-232 port to support the communication interface in between. The software used for the storage and analysis of the measured signals is *Matlab Instrument Control* Toolbox. The whole schematic circuit diagram of the test setup including the measurement system is illustrated in figure 2.10.

Due to the fact that the discharge currents of all specimens stressed under the same conditions are not exactly the same, the current is measured for each specimen (three current signals). Current signals in addition to the test voltage signal are automatically measured and

stored in sequence via the oscilloscope channels as shown in figure 2.10; where each channel carries one of the signals to be stored. In order to understand the storage process of the discharge current signals, it has to be assumed that the proposed electrode arrangement (figure 2.2) guarantees nearly constant mean discharge parameters after the first three hours of stress as shown in figure 2.3. This means that there is no need to get all the discharge current cycles during the 96 hours and it is acceptable to have a certain pause time period between successive storages.

The storage is performed in sequence through the oscilloscope channels (from 1 to 4). The signals are acquired with a length of one complete cycle according to the frequency of test voltage. There is no externally applied pause time interval between two successive storage processes in order to store as much as possible from the discharge current during the whole test period. In this way, the elapsed time in the storage process, during which no signals are detected, is consumed only in acquiring the signals' dataset from the oscilloscope to PC. Following these procedures, using the oscilloscope Agilent DS05014A, results in 30,000 stored cycles for each signal along the whole stress period of 96 hours and independent of the test frequency. This means that storage is performed with cycling frequency of 5.2 cycles per minute.

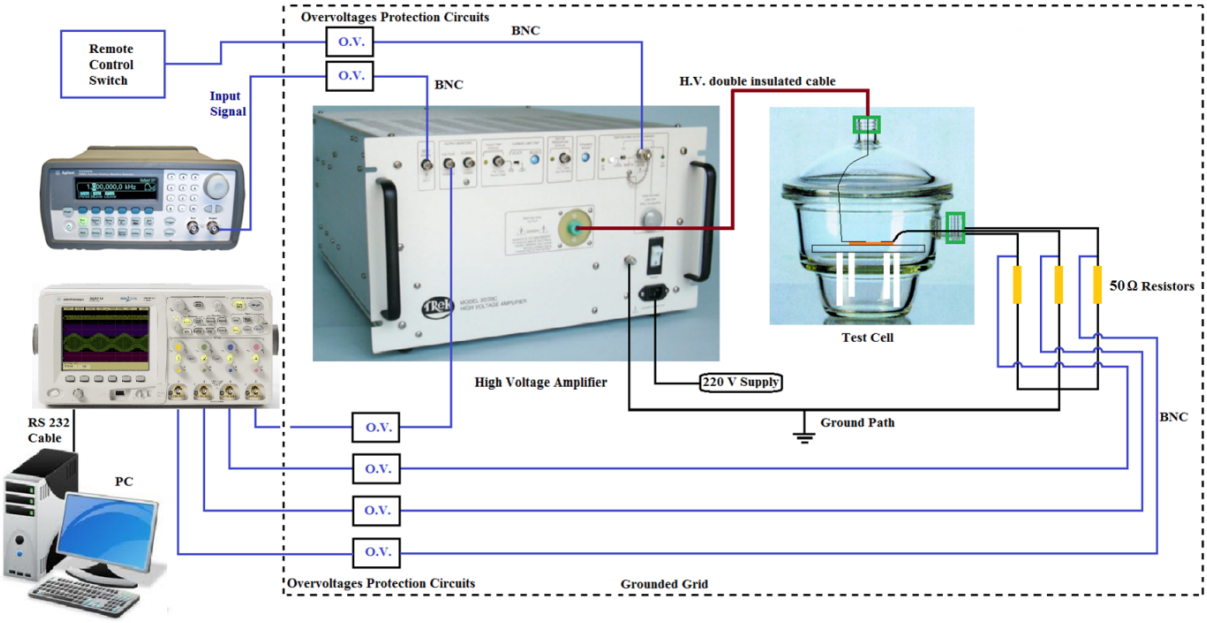

Figure 2.10: Schematic diagram of the whole experimental setup

2.3. Temperature Control

Temperature of the test cell was raised using two (300 mm x 120 mm x 0.4 mm) thermo self-adhesive heating foils attached to the inner surface of the test cell. The power requirement for each foil is 65 W at 230 V and surface temperature range is up to 90°C. Heating foils temperature was adjusted such that it generates heat energy sufficient to reach the desired surface temperature of the specimens. The difference between the heat energy generated and that arrived at material surface is the amount of energy lost to surroundings, and the capacity of the selected heating foils is capable of reaching the required temperatures.

The inner surface temperature could be adjusted through using an on/off temperature control circuit connected to the heating foils. The circuit activates the heating foils through the temperature switch, when the measured temperature via the temperature sensor (NTC 5 kΩ at 25°C) is lower than a pre-set temperature. The sensor was mounted inside the vessel on the PLEXI plate, i.e. near the stressed specimens. When the temperature reaches the desired level, the heater is switched off again. The relay responds even to slight temperature variations. This control algorithm was done with the aid of PIC12F683 programmed microcontroller.

2.4. Humidity Control

The water vapor concentration, and therefore the relative humidity over a salt aqueous solution is less than that over pure water. This is because water is present in both the gas and the liquid phase, whereas the scarcely volatile salt molecules are only present in the liquid. They dilute the water and hinder escape of water molecules into the air. With the aid of the above mechanism of saturated salt aqueous solutions the relative humidity inside the vessel was controlled. A certain amount of the saturated solution was introduced in the closed vessel after placing the samples and electrodes. After 12 hours the system hence adjusted to equilibrium and then the test voltage could be applied at the desired relative humidity. In each test series a data logger (Voltcraft DL-140TH) was placed inside the vessel to record both temperature and relative humidity during treatment. The fabrication of the saturated solutions was performed according to ISO 483 (see table 2.2).

Table 2.2: Saturated solutions for control of relative humidity inside test cell according to ISO 483

Saturated solutions	%RH @ 25°C	Solubility (g/ml)
Lithium Chloride (LiCl)	11	200 ml H_2O + 200 g LiCl
Magnesium Chloride ($MgCl_2.6H_2O$)	33	100 ml H_2O + 400 g $MgCl_2$
Magnesium Nitrate ($Mg(NO_3)_2.6H_2O$)	53	100 ml H_2O + 400 g $Mg(NO_3)_2$
Sodium Chloride (NaCl)	75	100 ml H_2O + 200 g NaCl
Distilled Water	100	

2.5. UV Radiation Imaging Technique

A PCO UV sensitive digital camera was used to capture images in UV range in addition to visible region of electromagnetic spectrum. With this UV camera very low intensities of light could even be recorded. The range of the electromagnetic spectrum, in which the camera is sensitive, is 190 nm $\leq \lambda \leq$ 1100 nm. In order to use the camera to record in the UV range a UV lens (Nikon UV-105 mm F4.5) was mounted on the PCO camera. This lens with a sensitivity spectrum 200 nm $\leq \lambda \leq$ 900 nm of is highly effective for capturing images in the ultraviolet range. Once focused in the visible light, it does not require to be refocused in order to capture the images in the UV light.

Since visible light is also detectable with the camera system, a UV bandpass filter, with a sensitivity spectrum 250 nm $\leq \lambda \leq$ 380 nm, is mounted on the lens in order to confirm the complete darkness in the surroundings of the discharge zone. Thus it can be assumed that the captured photos are exactly representing the induced UV radiation from the corona discharge on the specimen surface as illustrated in figure 2.11. The data transmission takes place after each shot via fiber optic cable from the camera to the PC that also handles the camera control.

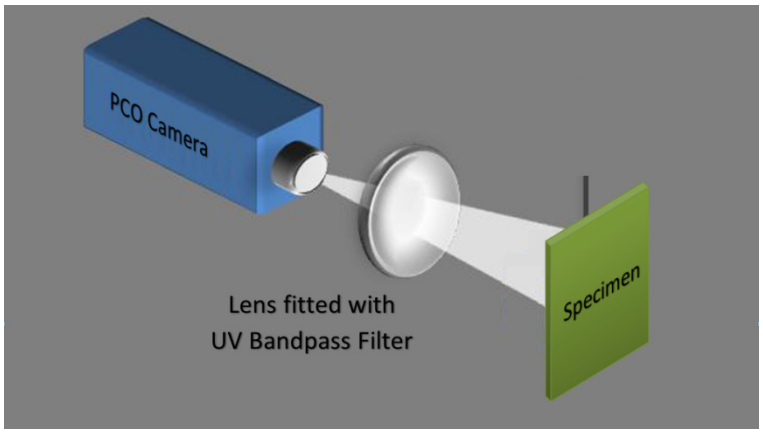

Figure 2.11: Schematic diagram of the imaging system for UV on specimen surface in test setup A

3. Evaluation Methods

All the data resulted after finishing all the test series, voltages, currents as well as the scan of the laser profilometer were evaluated. For a better understanding of the techniques used in this evaluation phase a detailed description will be introduced to the following points:

- Erosion quantification
- Evaluation of electrical discharge
- Analysis and processing of UV images
- X-ray Photo Electron Spectroscopy (XPS)
- Statistical methods

3.1. Erosion Quantification

During the specimen treatment the insulating material was affected by the electrical discharge resulting in some morphological changes in the surface in the form of erosion. The amount and the shape of that erosion were measured with high resolution using a laser profilometer.

3.1.1. Laser Profilometer and µscan Software

In the calculation procedures of the erosion parameters, three parameters were used for identifying the erosion severity on the insulator surface; surface eroded area, maximum erosion depth and eroded volume. Before proceeding in the calculation of these parameters in the *Matlab* software, we should first illustrate the preparation procedure of the scanning data through the µscan software used for the surface analysis. The preparation steps using the laser profilometer and its associated µscan software are as follows:

- Scanning resolution of the profilometer is adjusted to 5 µm on both x and y directions on scanned area of 40 mm x 40 mm. The normal distance between the measuring sensor and the scanned specimen is 100 µm with minimum reflection limit of 20%.
- *Interpolation:* After finishing the scanning process defect points which are far from reality were excluded using the Gauss low pass filter and then calculated with an interpolation algorithm of the data points of the neighbor area.
- *Levelling:* From the fact that there is no 100% flat surface in reality; any inclination or curvature in the measured surface was removed using the levelling tool. To determine the new reference plane, it is necessary to scan the specimen surface with large area, that even undamaged areas outside of the erosion were captured. In this process the new reference plane was calculated and subtracted from the data points and the surface was as close as possible to be flat (see figure 3.1). Resulting matrix contains the height information (Z coordinate) of the surface points with a number of points dependent on the scanning step, which was adjusted to 5 µm in this work.

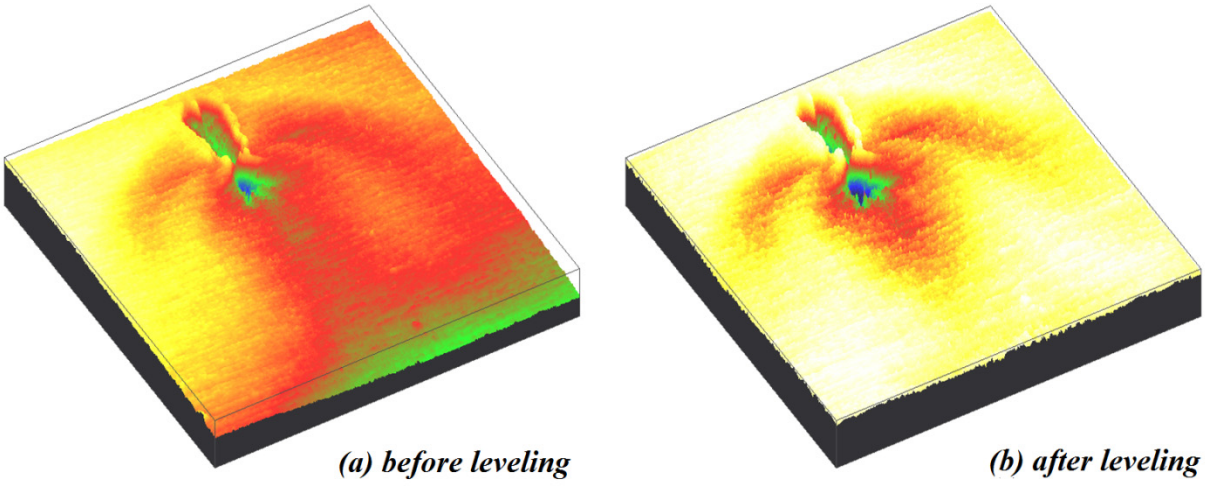

Figure 3.1: Levelling of eroded surface using polynomial approximation fitting in µscan Software

3.1.2. Matlab Algorithm

The data points collected from the µscan software were then analyzed via *MATLAB*. The resulting data points were divided into number of infinitesimal elements in form of triangular prism in order to calculate the surface eroded area and the total eroded volume. Figure 3.2 presents the triangular prism representing the infinitesimal element with surface area A_i bounded by the vertices of (X_{i1},Y_{i1}), (X_{i2},Y_{i2}) and (X_{i3},Y_{i3}). The depths of those vertices, i.e. Z_{i1}, Z_{i2} and Z_{i3}, represent the measured erosion depths at those data points. Once the surface triangles were obtained for the scanned data points, the eroded area could be easily calculated from the summation of the triangles' areas as followed in equation [3.1]. Hence the eroded volume could be determined with the aid of the vertices of each triangle (Z coordinates) and the calculated infinitesimal areas as in equation [3.2].

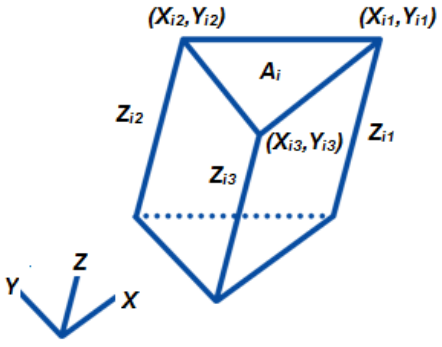

Figure 3.2: Triangular prism representing the infinitesimal element in calculating the total eroded volume and surface eroded area

$$Total\ Eroded\ Area = \sum_{i=1}^{n} A_i \qquad [3.1]$$

$$Total\ Eroded\ Volume = \sum_{i=1}^{n} Vol_i = \sum_{i=1}^{n} A_i \cdot \frac{(Z_{i1} + Z_{i2} + Z_{i3})}{3} \qquad [3.2]$$

This method gives a better picture of the actual slope of the insulating surfaces and hence a better representation of the erosion profile. The short time elapsed to analyze the scanned data points as well as to calculate the required erosion parameters is an advantage. Saving time comes from the tool used for surface levelling that applies polynomial approximation fitting with polynomial order from 1 to 3 depending on the degree of surface inclination. Additionally, the algorithm applied to determine the erosion parameters from the obtained data points depending on the summation of finite elements leads indeed to a precise quantification of the erosion.

3.2. Evaluation of Electrical Discharge

3.2.1. Discharge Parameters

In order to describe the characteristics of a discharge, three discharge parameters can be introduced. The discharge parameters are total discharge energy $\boldsymbol{E_{total}}$, cumulative charge $\boldsymbol{Q_{cum}}$ over the whole test period and the average number of pulses per cycle $\boldsymbol{N_{cycle}}$. The total discharge energy $\boldsymbol{E_{total}}$ is determined from the sum of all discharge pulses energies. The pulse energy is calculated by multiplying the discharge magnitude $\boldsymbol{Q_i}$ by the instantaneous value of the test voltage $\boldsymbol{V_i}$ at which the discharge occurs as followed in equation [3.3]. Similarly, cumulative charge $\boldsymbol{Q_{cum}}$ is calculated from the sum of charge magnitudes for all pulses as followed in equation [3.4]. The main aim behind calculating all the above discharge parameters is to find an exact description of discharge process during the whole material stressing period.

$$Q_{cum} = \sum_{i=1}^{n} Q_i \qquad [3.3]$$

$$E_{total} = \sum_{i=1}^{n} V_i . Q_i \qquad [3.4]$$

3.2.2. Discharge Pulses Extraction Technique

Extraction of PD pulses from the measured voltage signals displayed by the oscilloscope is considered the basic requirement for the evaluation of corona discharge process on polymeric materials. The PD pulses were detected through the measured voltage across the resistor connected in the ground path of the ground electrode. Therefore, the main function in extracting these PD pulses is to extract the discharge current from this measured signal (see figure 3.3) by removing the capacitive current waveform. Filtering is a primary challenge [SHI-00] as the oscilloscope displays not only capacitive current waveform and measurement noise but also PD pulses of interest. An ideal discharge current waveform is shown in figure 3.4 in order to illustrate the shape of the individual components.

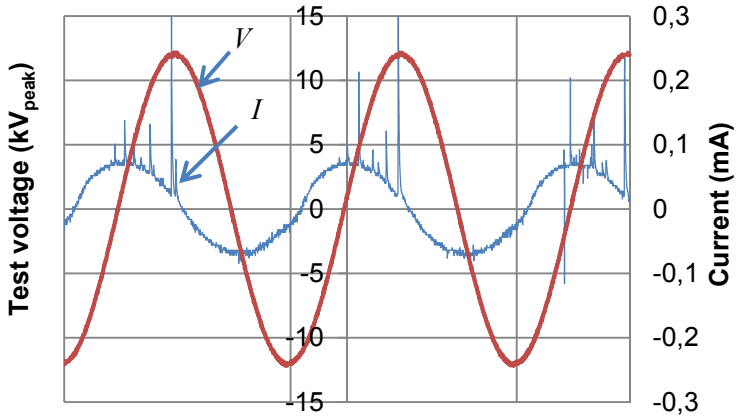

Figure 3.3: Stored current (mA) and test voltage (kV$_{peak}$) signals

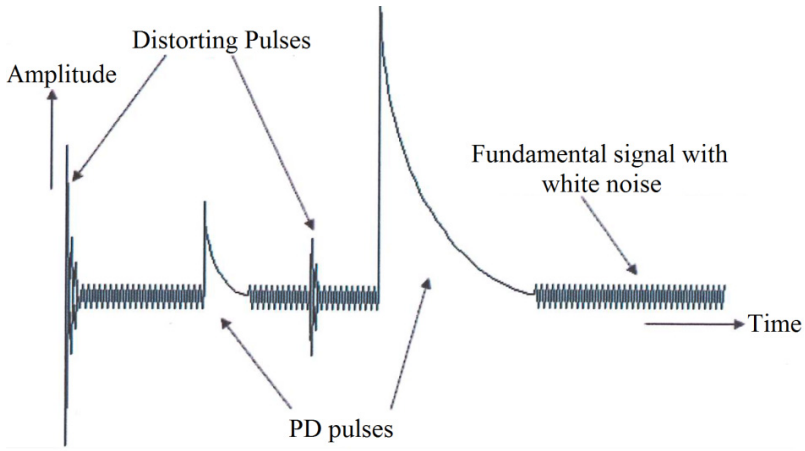

Figure 3.4: Ideal representation of the PD pulses, distorting pulses and white noise superimposed on the fundamental current signal

Here the distorting pulses can be distinguished from the PD pulses, because PD pulses have only positive or negative instantaneous values and no zero-crossings as in case of the distorting pulses. The distorting pulses are bipolar with reference to the current waveform; whereas the PD pulse shows the same polarity of the current waveform in the half cycle at which it took place. Another discriminating criterion is the pulse width (i.e. frequency), which is very effective because the width of a distorting pulse is much shorter than a PD pulse. In other words the distorting pulses exhibit higher frequency components, when analyzed be frequency analysis tool, compared to the PD pulses. A filter can be constructed with the explained distinguishing characteristics between PD pulses and the other distorting pulses. In order to obtain the PD pulses using this filter; the other components (i.e. the fundamental waveform, the distorting pulses and the white noise) will be masked from the recorded signal. The filtering process is performed in two main individual steps:

1. **Calculating fundamental signal and eliminating some distortions**

The fundamental waveform is obtained from averaging the received signal and removing all the superimposed pulses. Then, the distorting pulses which show lower values than that of the fundamental waveform are eliminated. This is achieved considering that

the distortion pulses differ from the PD pulses in such that, the former ones are bipolar referred to the fundamental waveform. Hence any pulses below the fundamental signal in the positive half cycle or above it in the negative half cycle will be eliminated. Finally the remaining pulses are determined by subtracting the calculated fundamental waveform from the measured signal as shown in figure 3.5.

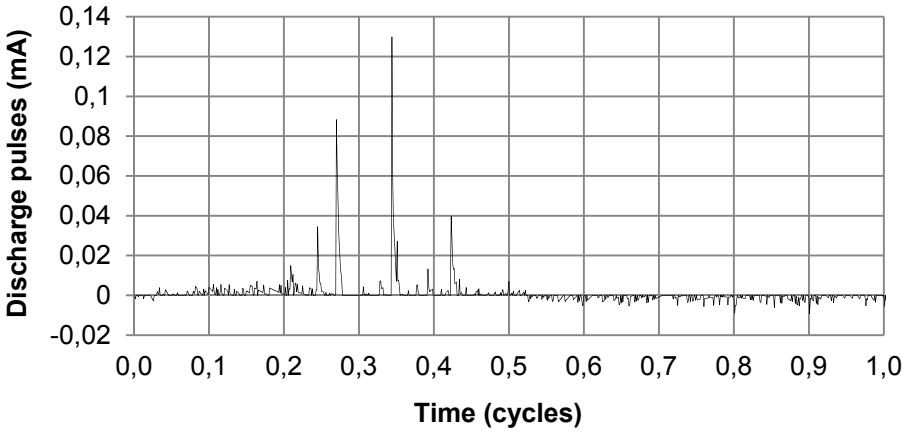

Figure 3.5: remaining pulses for one cycle before filtering

2. Filtering using Discrete Wavelet Transform

Taking in to consideration the difference in pulse width and in turn in frequency components between distorting pulses and PD pulses, a frequency analysis tool is necessary for discrimination. Traditionally, the techniques used for signal processing are realized in either the time or frequency domain to analyze and extract PD pulses [MA-02]. Fourier Transform (FT) is a perfect tool for analyzing periodic stationary signals, but not for non-stationary signals (i.e. PD pulses). It only gives a qualitative overview about frequency components in the signal while the time information for these components is lost, i.e. it is impossible to determine what frequency bands exist at certain time interval.

With regard to the PD pulse structure, there always exist non-periodic and fast transient features in the PD signals detected, which tend to be ignored and cannot be revealed efficiently and explicitly by this kind of conventional transform. For these reasons, when the Fourier transform is applied to partial discharge analysis, it has serious limitations. To overcome this deficiency, a modified method, *Short Time Fourier Transform* (STFT) allows to represent the signal in both time and frequency domain through time windowing function [SHI-01]. The window length determines a constant time and frequency resolution. However, this narrow time windowing used in order to capture the transient behavior of a signal results in a poor frequency resolution.

The nature of the real PD signals is non-periodic; such signals cannot easily be analyzed by conventional transforms. It was then essential to find another technique that preserves time information of the signal while avoiding frequency resolution problems associated with STFT. *Discrete Wavelet Transform* (DWT) is a multi-resolution signal analysis technique that overcomes the limitations of FT by employing analyzing functions that are localized in both time and frequency [ADD-02]. The wavelet transform decomposes the signal into different

scales with different levels of resolution by dilating a single prototype function, the mother wavelet [ADD-02]. Furthermore, a mother wavelet has to satisfy that it has a zero net area, which suggests that the transformation kernel of the wavelet transform is a compact support function, thereby offering the potential to capture the PD pulses which normally occur in a short time period [TSA-02], [MA-02]. Another important advantage of such wavelet-based de-noising is that it works well not only for signals which are smooth, but also for signals with abrupt jumps, sharp spikes and other irregularities [SHI-00].

The wavelet decomposition results in levels of approximated and detailed coefficients. The algorithm of wavelet signal decomposition is illustrated in figure 3.6. Reconstruction of the signal from the wavelet transform and post processing, the algorithm is shown in figure 3.7. This multi-resolution analysis enables us to analyze the signal in different frequency bands; therefore, we could observe any transient in time domain as well as in frequency domain.

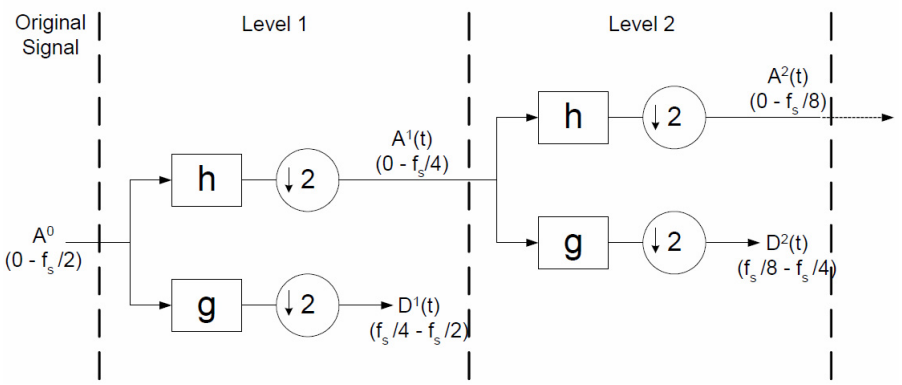

Figure 3.6: Multi-resolution wavelet decomposition, h = low-pass decomposition filter; g = high-pass decomposition filter; ↓ 2= down-sampling operation. $A^1(t)$, $A^2(t)$ are the approximated coefficient of the original signal at levels 1, 2 etc. $D^1(t)$, $D^2(t)$ are the detailed coefficient at levels 1,2. [TSA-02]

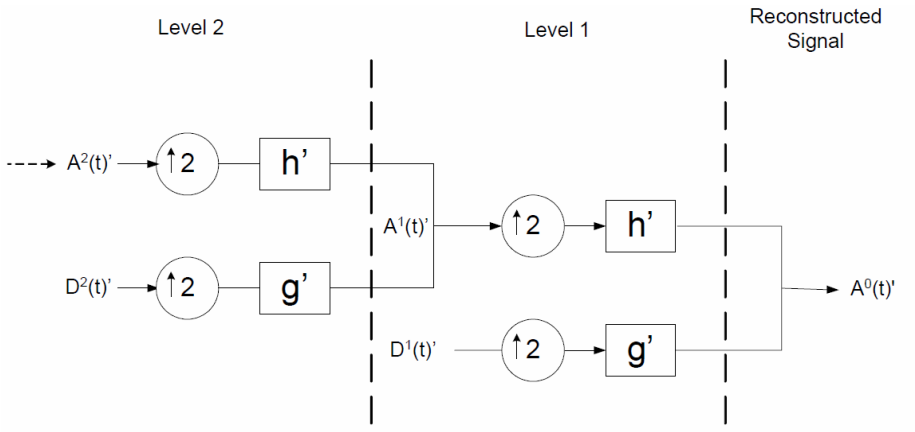

Figure 3.7: Multi-resolution wavelet reconstruction, h' = low pass reconstruction filter; g' = high-pass reconstruction filter; 2 = up-sampling operation. $A^1(t)'$, $A^2(t)'$ are the processed or non-processed approximated coefficient of the original signal at levels 1, 2 etc. $D^1(t)'$, $D^2(t)'$ are the processed or non-processed detailed coefficient at levels 1,2. [TSA-02]

The general wavelet denoising procedure is as follows:

- ***Decomposition:*** This step involves choosing a mother wavelet and a maximum decomposition level with which we can properly distinguish the PD occurrence and then computing the decomposition coefficients at each level.
- ***Thresholding:*** This step involves selecting appropriate threshold limit at each level and threshold method (hard or soft thresholding) and applying threshold to the coefficients at each level to best remove the noises.
- ***Reconstruction:*** In this step, signal reconstruction with the modified coefficients through inverse wavelet transform is carried out to obtain a denoised signal.

To best characterize the PD pulses in a noisy signal, received from the oscilloscope, we should select our "mother wavelet" carefully to better approximate and capture the transient pulses of the original signal. "Mother wavelet" will not only determine how well we estimate the original signal in terms of the shape of the PD pulses, but also, it will affect the frequency spectrum of the denoised signal. The selected mother wavelet is Db2 (i.e. Daubechies 2), which leads to the best representation of the PD pulses [TSA-02], [SHI-01], [MA-02]. This is referred to the transient characteristics of the Db2, which is quite similar to that of PD pulses [KUM-12].

From the previous section, we have known that the wavelet transform is constituted by different levels. The maximum level to apply the wavelet transform depends on how many data points are contained in a data set, since there is an operation of down-sampling by 2 from one level to the next one. In our experience, one factor that affects the number of level we can reach to achieve the satisfactory noise removal results is the signal-to-noise ratio (SNR) in the original signal. So as to remove almost all noise from the analyzed signals, we could only go up to 5 levels otherwise we would remove also the PD signal.

Two rules are generally used for thresholding the wavelet coefficients; soft or hard thresholding. Hard thresholding can be described as the process of setting to zero the elements whose absolute values are lower than the threshold. Soft thresholding is called shrink or kill which is an extension of hard thresholding. It is based on setting the elements with absolute values lower than the threshold to zero, and then shrinking the other coefficients. Soft and hard thresholding can be defined by equations [3.5] and [3.6] respectively [KUM-12].

$$\widehat{w} = \begin{cases} \text{sign}(w).(|w| - \lambda), & |w| \geq \lambda \\ 0, & \text{otherwise} \end{cases} \quad [3.5]$$

$$\widehat{w} = \begin{cases} w, & |w| \geq \lambda \\ 0, & \text{otherwise} \end{cases} \quad [3.6]$$

Where, w is the wavelet coefficient value and λ is the threshold level. In this study, we adopt the soft thresholding method. Donoho et al. developed a universal thresholding rule [DON-94] which can effectively remove the Gaussian random noise. The universal thresholding rule is as follows:

$$\lambda = \sigma\sqrt{2\log N} \qquad [3.7]$$

Where, N is the length of the coefficients, σ is the standard deviation of noise which equals to $MAD/0.6745$, MAD represents median absolute deviation of the coefficients, and λ denotes the threshold [KUM-12]. Discrete Wavelet Toolbox (DWT) in *Matlab* is used to decompose the examined signal into several frequency components. Then, a certain denoising threshold is applied to distinguish the noise level to be avoided. Finally the signal is reconstructed via inverse DWT process with the desired discharge pulses and no distorting pulses anymore exist (see figure 3.8). Then, PD pulse can be used to calculate the discharge characteristics mentioned in 3.2.1.

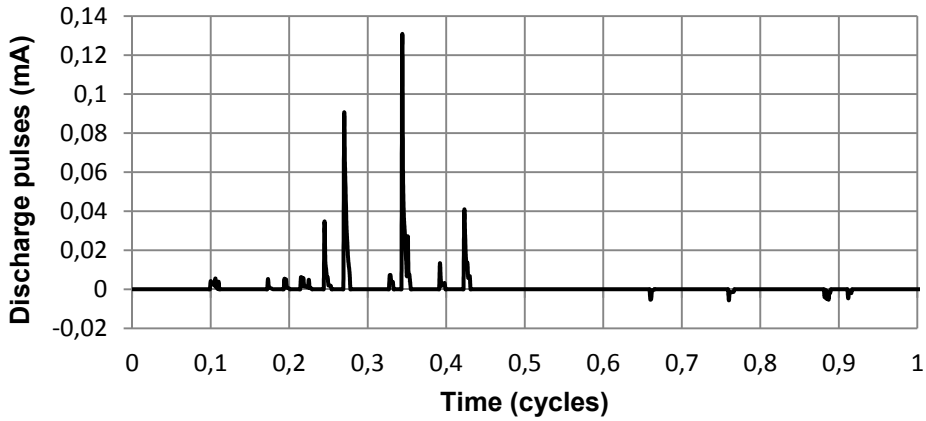

Figure 3.8: Resulting pulses for one cycle.

3.3. Analysis and Processing of UV Images

UV irradiation on specimen surface can be divided into two zones, intensive and weak UV regions. Intensive UV region exists near the needle electrode vicinity; whereas weak UV region represents the zone of low UV intensities existing far from the needle electrode. The difference between intensive and weak UV regions is clarified by the separation of the two ranges of intensities (see figure 3.9). The captured image was stored in the PC as a matrix of pixels in a JPG file. The image file represents the radiation intensity levels at different locations of the image matrix. By using a *MATLAB* program, the pixels' intensities (represented by the elements of the image matrix) were summed up to obtain the cumulative intensity [PIN-02], [PIN-05].

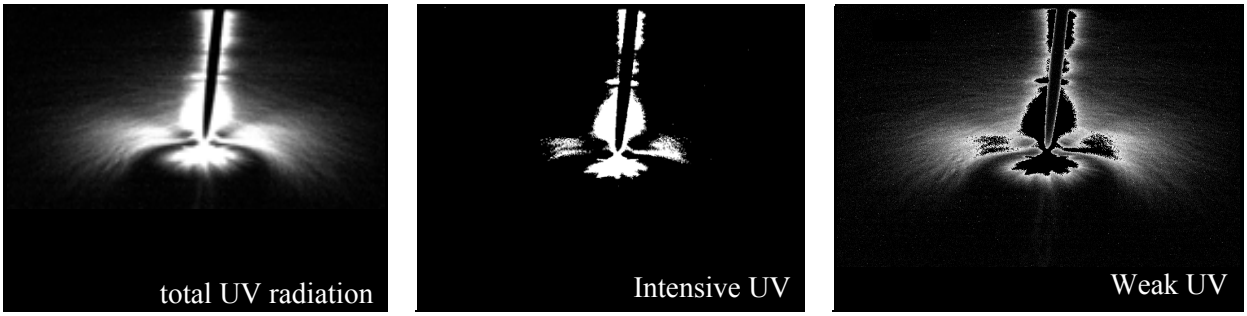

Figure 3.9: The difference between the intensive and weak UV radiation on the specimen surface

The noise level in the obtained image is defined as the threshold intensity above which UV intensities are clearly separated from the background image. In the resulting UV image, pixels that have intensities higher than the noise level are considered illuminated. UV radiation parameters are illuminated area, A_{UV} (mm^2) and cumulative UV intensity, I_{UV} (a.u.) (i.e. arbitrary units). UV parameters are calculated as follows:

a. *Irradiated area, A_{UV}:* The area is calculated by calculating the number of pixels that are part of UV radiation spectrum as in equation [3.8]. Where the number of illuminated pixels is N_{UV} and A_{UV} is the whole illuminated area of the image. The area A_{UV} is calculated from dividing N_{UV} by the square of image resolution (i.e. 72 pixels per inch). Then it is calculated in mm^2 and divided by the square of lens magnification ratio, which is 5 times the size in reality.

$$A_{UV} = \frac{N_{UV}}{(Resolution, pixels/inch)^2} \times \frac{(25.4, \frac{mm}{inch})^2}{(magnification\ ratio)^2} \quad [3.8]$$

b. *Cumulative UV Intensity, I_{UV}:* UV intensity is calculated by performing weighted sum of all pixels that are part of UV emission spectrum. The pixel intensity is measured relative to I_{noise} the base noise threshold level as followed in equation [3.9].

$$I_{UV} = \sum_{n=1}^{N_{UV}} (I_{pixel}(n) - I_{noise}) \quad [3.9]$$

3.4. X-ray Photoelectron Spectroscopy (XPS)

XPS (X-ray Photoelectron Spectroscopy), also known as ESCA (Electron Spectroscopy Chemical Analysis), has been found useful for investigating the aging behavior of insulating materials [GUB-92], [HIL-98], [KUM-03], [MA-11]. XPS is a powerful tool for monitoring the changes in the surface chemistry of many materials. XPS is considered one of the most applied electron spectroscopy techniques in the area of polymeric material testing. The strength of XPS lies in the availability of a large amount of data of core level electron binding energies for several elements in diverse chemical structures. The most distinguishing feature is the quantitative analysis of material compositions. Therefore, the degree of damage can be determined quantitatively and qualitatively.

The working principle of this technique is based on the photoelectric effect [LEN-08]. Each atom in the surface has core electron with the characteristic binding energy that is conceptually, not strictly, equal to the ionization energy of that electron. When an X-ray beam directs to material surface, the energy of the X-ray photon is adsorbed completely by the core electron of an atom. If the photon energy, $\boldsymbol{h\nu}$, is large enough, the core electron will then escape from the atom and emit out of the surface. The emitted electron with the kinetic energy of $\boldsymbol{E_k}$ is referred to as the photoelectron (see figure 3.10). The binding energy $\boldsymbol{E_b}$ of the core electron is given by the Einstein relationship:

$$\boldsymbol{E_b = h\nu - E_k - \emptyset} \quad [3.10]$$

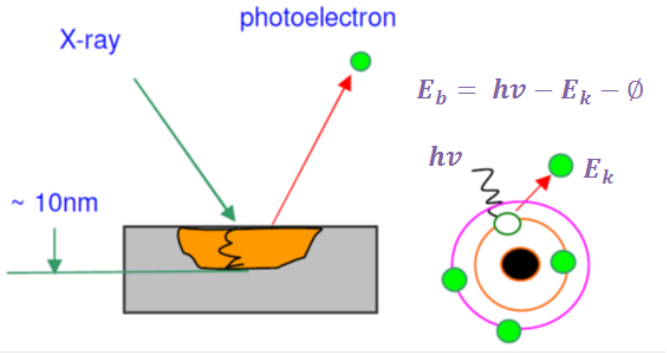

Figure 3.10: Theory of X-ray photoelectron spectroscopy [WU-07]

Where $\boldsymbol{hv}$ is the X-ray photon energy (for filament Al Kα, $\boldsymbol{hv}$ =1486.6 eV); $\boldsymbol{E_k}$ is the kinetic energy of the photoelectron, which can be measured by the energy analyzer; and ∅ is the work function induced by the analyzer, about 4~5 eV. This term is an adjustable instrumental correction factor that accounts for the few eV of kinetic energy induced by the photoelectron as it is absorbed by the instrument's detector. Since the work function ∅ can be artificially compensated, it is eliminated, giving the binding energy as follows:

$$\boldsymbol{E_b = hv - E_k} \qquad [3.11]$$

All XPS measurements were performed with a Leybold Heraeus photoelectron spectrometer type LHS 10 [HEB-99]. Experiments were conducted with non-monochromatic Al Kα x-ray source was operated at 120 W (high voltage = 12 kV_{rms}, emission current = 10 mA). The energy scale was calibrated with reference to the Cu 2p3/2 and Ag 3d5/2 peaks at binding energies of 932.7 eV and 368.3 eV. The analysis area for the high-resolution spectra was 8 mm x 8 mm. This rectangular area was cut from the specimen with a center point under the needle tip. The O 1s, C 1s, and Si 2p spectra were acquired at pass energy of 20 eV and the number of scans per element is 30. Binding energy peaks were determined by referencing to the adventitious C 1s photoelectron peak at 285.0 eV. Quantitative XPS analysis was performed with CasaXPS V.12 software. The atomic concentrations were calculated from the photoelectron peak areas by subtracting a linear background. C 1s peak deconvolution was done using mixed 70% Gaussian / 30% Lorentzian components.

3.5. Statistical Models

A statistical test is a method which checks whether an assumption about an unknown probability distribution is consistent, or whether the assumed distribution of the actual distribution deviates significantly. The assumption hence is a statistical hypothesis, whose formulation is defined by the null hypothesis H_0 [HAU-92]. The result of a statistical test is a numeric value, by which it is decided to determine, whether the null hypothesis H_0 is rejected in favor of the alternative hypothesis H_A or not. The two hypotheses are statements about the data to be tested, which are mutually exclusive. The definition of hypotheses depends on the statistical test. The significance level α represents the probability that the null hypothesis is rejected [HAU-92].

3.5.1. Significance Value

In order to interpret the results of each test, a decision between the null and alternative hypotheses is taken based on the result of the applicable distribution and the selected significance level. In computer based statistical programs, the significance value (p-value) is usually calculated while performing a statistical test. Using this value, a decision between null and alternative hypothesis is achieved by comparing the p-value with α. If the resulting p-value is less than α, then the null hypothesis is rejected in favor of the alternative hypothesis. If the p-value is greater than α, however the null hypothesis cannot be rejected.

3.5.2. Experimental Design

There are many experimental designs available to researchers working on electrical insulation. Since each experimental design has its inherently unique advantages and disadvantages, it is very important to select an appropriate design which matches the objective of an experiment. There are many available references available to assist researchers in selection phase of experimental design [DAN-76], [DAV-76]. One experimental design in common use is well suited to finding factors and interactions which are causing a change in a property of interest. Since it is one of the most useful experimental designs and supports the identification of erosion mechanism, *factorial design* is applied.

Traditional experimental design is one in which all known factors (variables) under analysis are kept constant except one. The single factor is varied over a range of values and its effect on the property of concern is studied. An example of this type of design is that in which the amount of fillers in an insulating material is varied while the remainder of the involved variables are held constant to determine the effect of filler amount on aging.

In contrast to traditional design, a factorial design is one in which several factors are varied simultaneously within one experiment. The main advantages in using this more complex design are that more information is obtained and synergistic (interactive) effects can be identified if they exist. Analysis of a factorial experiment usually consists of an *Analysis of Variance* (*ANOVA*), which reveals the degree of significance of each factor or interaction at the specified confidence level. This analysis is performed with aid of Minitab 16 software.

In working with factorial designs a specific terminology is usually used to enable efficient discussion of the test arrangement. This terminology is listed in the following points:

- The variables are called factors.
- Typical factors are voltage, frequency, pressure, humidity, and so on.
- Each factor is evaluated at two or more levels. For example, voltage is evaluated at levels of 10, 12, and 14 kV_{peak} and temperature is evaluated at 20, 40, and 60°C.
- In a factorial design, the total number of experimental trials (runs) is equal to the product of the number of levels of both factors. In the above example, it will be 3 x 3 different experimental combinations. When using the same number of levels for all factors, the following formula can be applied.

$$\text{No. of experimental combinations} = (No.\ of\ levels)^{No.of\ factors} \quad [3.12]$$

3.5.3. Building Generalized Linear Model in ANOVA Test

In this study specimen size of each measurement is 5 samples for the same test conditions. Because the response (dependent) variable (i.e. eroded volume, eroded area, etc.) were found to be normally distributed, the data may be analyzed using a *General Linear Model (GLM)* including an interaction term between independent variables of interest (i.e. voltage, frequency, etc.). An interaction is needed when two variables (quantitative or factors) act together to influence the response. For example, as mentioned earlier, in erosion evolution it is required to know how voltage and frequency affect erosion levels. Then, the analyzed model includes a term for voltage, a term for frequency, and also the interaction between these two factors, which is added to the model as their product, thus voltage × frequency.

Adding covariates can greatly improve the accuracy of the model and may significantly affect the final analysis results. In a general linear model, a covariate is any continuous predictor, which may or may not be controllable. The failure to incorporate a covariate can produce misleading analysis results; it could result in misjudgment of factor significance on a certain response. Before performing the general linear model analysis with the selected covariates, it must be first verified that the covariates and response are linearly related. The model construction is performed as follows:

1. All covariates linearly related to the studied response are included in the model.
2. After the first run of the model, all covariates which have no significance on the examined response (as their p-values exceed 0.05) are eliminated.
3. The refitted model is run with the remaining covariates and the stressing factors.
4. If there is no evidence that the investigated factors have interaction in terms of the analyzed response, the model should therefore be refitted without the interaction term (which otherwise complicates the interpretation of the model's parameter estimate), and then inspect the significance of the individual variables.
5. If the interaction was found to be significant, but for example one of the factors was not, then we cannot remove it from the model as it is clearly still important, but in the form of an interaction with the other one.

4. Test Setup Validation

In this chapter the applied test setup was validated in terms of getting representative results on the level of both erosion characteristics and discharge parameters. Four stressing factors were analyzed in independent test series in terms of both discharge intensity and erosion characteristics of the specimen surface. Each influencing stress was controlled to be studied separately without any interaction with any other stresses in order to be able to quantify its effect. While investigating a certain stress (highlighted in yellow in table 4.1) the settings for the other stresses were kept constant. Therefore, it would be possible to make a correlation between that stress and the changes in the sample.

4.1. Examined Test Series

a) Test Series 1: Magnitude of Test Voltage

Impact of the applied test voltage magnitude as a stressing factor was studied in this test series. Different magnitudes of AC voltage are applied; 8, 9.5, 10, 11, 11.5, and 12 kV_{peak}. The frequency of the applied voltage was adjusted at 500 Hz in order to save the test time and reach the expected erosion. Table 4.1 describes the parameters setting for this test series referred to the stressing factor under study. The chamber was ventilated during this test series to limit the effect of Ozone as well as other gaseous decomposition byproducts (N_xO_y, HNO_x ...). The air flow system consists of a pressurized clean air supply equipped with a pressure regulator and a flow meter adjusted at a continuous rate of 10 liter per minute. The temperature inside the desiccator was held constant at 25°C and the relative humidity was less than 5 %RH to maintain normal operating conditions.

b) Test Series 2: Frequency of Test Voltage

The influence of test voltage frequency was examined in this test series. The chosen values for test voltage frequency are 100, 200, 300, 400 and 500 Hz at a voltage magnitude of 12 kV_{peak}. In this test series the test cell was also ventilated during the treatment to limit the effect of gaseous decomposition byproducts (O_3, N_xO_y, HNO_x ...). The air flow control system was the same used for the test voltage magnitude in test series 1.

c) Test Series 3: Humidity

In this test series the effect of humidity on erosion behavior of material surface was studied. Therefore, no dry air flow was supplied and the desiccator was sealed. All parameters are kept constant except the air humidity inside the vessel. Five values are chosen to be applied for the relative humidity starting from dry air until 100 %RH.

d) Test Series 4: Temperature

The influence of temperature on the erosion severity on the dielectric material surface was analyzed in this test series. So for each test series the ambient conditions are adjusted at certain extent, so that the desiccator was sealed and no dry clean air flow was supplied. When

studying the effect of temperature, the humidity was held constant at (33 ± 4) %RH and the change in temperature becomes the parameter to be tested.

Table 4.1: Test parameters setting for each test series on epoxy resin 60% by weight silica micro-filled specimens

Test Series	Voltage (kV_{peak})	Frequency (Hz)	Humidity (%RH)	Temperature (°C)	Test duration (hours)
1	8, 9.5, 10, 11, 11.5, 12	500	5	25	96
2	12	100, 200, 300, 400, 500	5	25	96
3	8	500	11, 33, 53, 70, 100	25	96
4	10	500	33 ± 4	25, 30, 40, 50, 60	96

4.2. Nature of Discharge Pulses

For the used test setup, the discharge pattern can be explained as follows: As the voltage is slightly increased, streamers will occur in the positive half-cycles (burst pulses), whereas Trichel pulses of small magnitude with higher repetition rate take place during the negative portion of the voltage cycle [NAS-71]. It can be observed that the stored current signal follow this pattern with discharge activity almost in the positive half-cycles beside tiny pulses on the negative part of the cycles as shown in figure 3.3. The location of the pulses with respect to the voltage waveform is governed not only by the applied electric field but also influenced by the space charges existing in the discharge region. The space charge influence alters the shape of electric field on the specimen surface between electrodes [PAT-00], [PAT-99]. In such a way, the location of the PD pulses with respect to the applied test voltage signal is shifted from the expected location.

4.3. Discharge Parameters

a) Test Series 1: Test Voltage Magnitude

Regarding the discharge parameters, three quantities for each test series are considered; i.e. total discharge energy, cumulative charge and average number of pulses per cycle. It was found as shown in figure 4.1 that increasing the voltage magnitude from 8 kV_{peak} up to 12 kV_{peak} results in a certain increase in all discharge parameters under analysis. In other words, the partial discharge intensity is dependent on the magnitude of the test voltage and reaches significant levels at higher voltages. This observation can be expected from the equations used to calculate these quantities; where energy is dependent on the test voltage. It can be also seen that the number of pulses per cycle increased with the rise of test voltage magnitude.

b) Test Series 2: Test Voltage Frequency

The increase of the applied frequency has a certain impact on discharge parameters as can be seen from figure 4.2. The number of pulses per cycle was nearly constant over the examined frequency range. This could be referred to the same discharge inception and extinction voltages and the same potential difference across the discharge path. Hence, the total number of pulses within the whole stress period (i.e. 96 hours) will be proportional to the supply frequency. In other words, the higher the supply frequency, the higher the discharge intensity on specimen surface.

c) Test Series 3: Humidity

In this test series all the stressing factors affecting discharge intensity were kept fixed except the humidity of the air inside the vessel. Therefore, any change in discharge parameters would be attributed to the change in humidity degree. It can be observed from figure 4.3 that most of discharge parameters can be regarded as not affected by the humidity increase within the lower degrees. On the other hand at higher degrees of humidity the parameters are affected to a small extent by humidity increase in inverse proportional relationship. The rate of decrease in discharge parameters magnitudes is very small compared to that rate of humidity increase. This can be attributed to the scattering and absorption of UV under humid conditions leading to a reduced percentage of UV which reaches the surface [PIN-05].

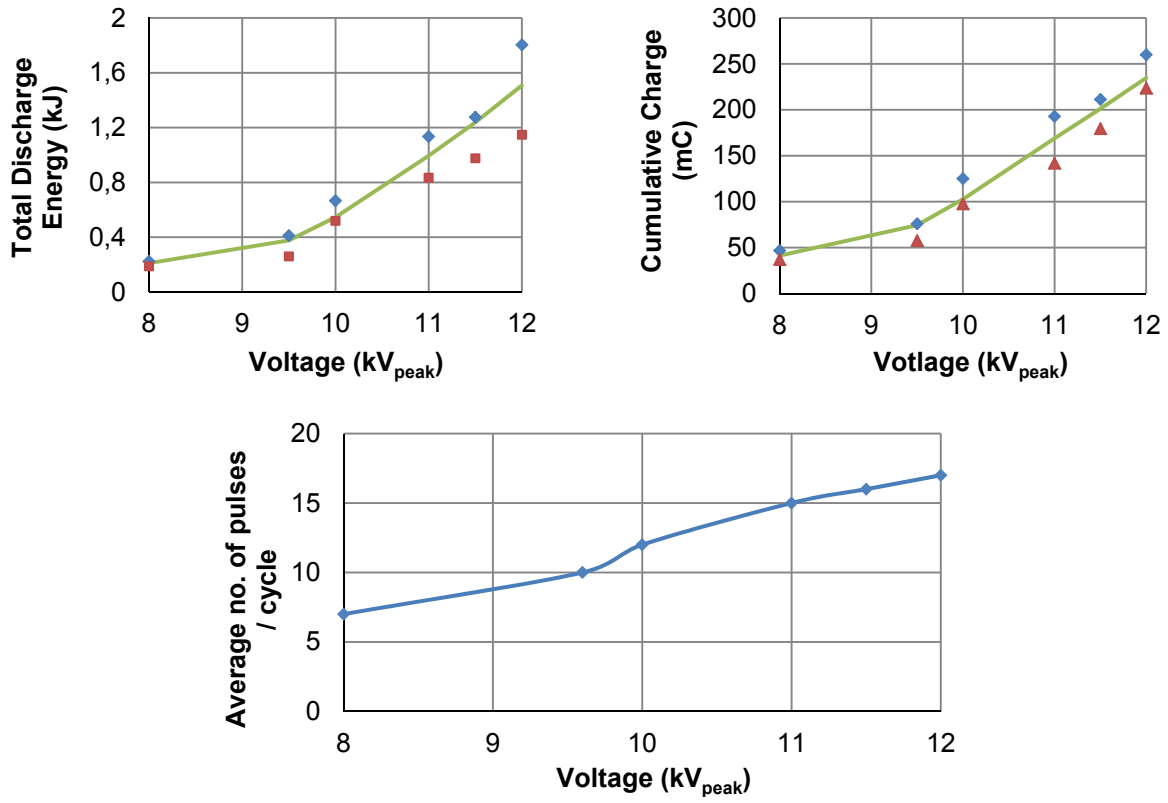

Figure 4.1: Discharge parameters (median, span of 3 samples) for test series 1, other parameter settings see table 4.1

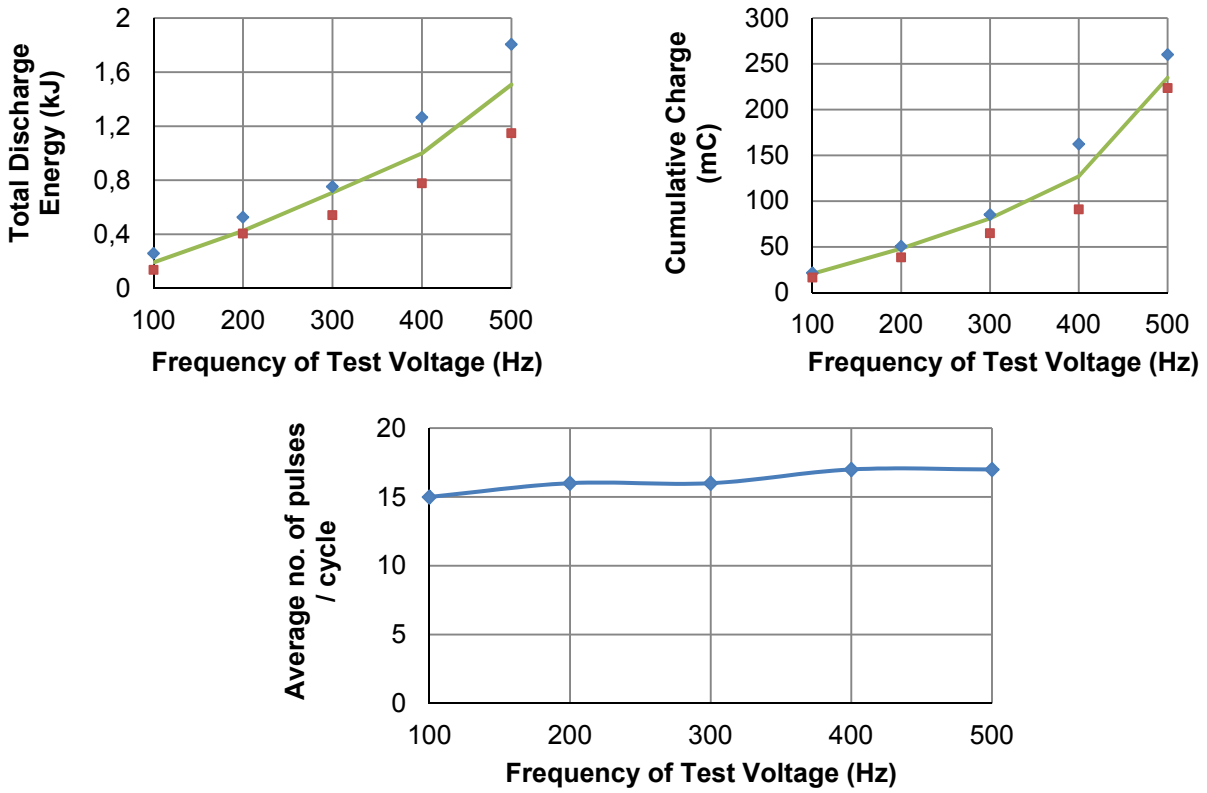

Figure 4.2: Discharge parameters (median, span of 3 samples) for test series 2, other parameter settings see table 4.1

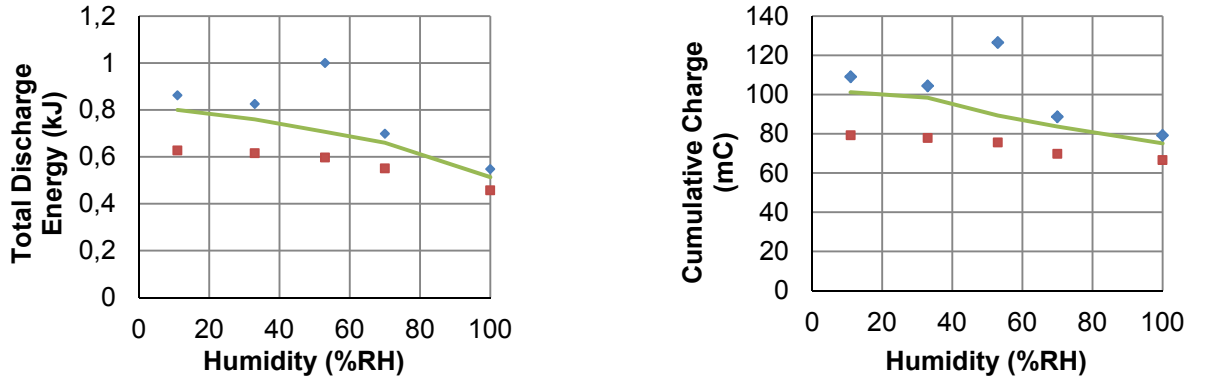

Figure 4.3: Discharge parameters (median, span of 3 samples) for test series 3, other parameter settings see table 4.1

d) Test Series 4: Temperature

The effect of temperature change on discharge intensity was studied and the response of each discharge parameter was calculated. The rise of charged particles temperature in the discharge zone results in higher kinetic energy and higher probability of generating more charged particles. Additionally, temperature rise in a constant volume discharge gas results in an increase in the pressure inside the test vessel according to the general gas law. At higher pressure charged particles make more collisions with gas molecules resulting in higher probability of ionization. It is clear from figure 4.4 that discharge parameters are directly proportional to temperature rise, but with a slow rate of change.

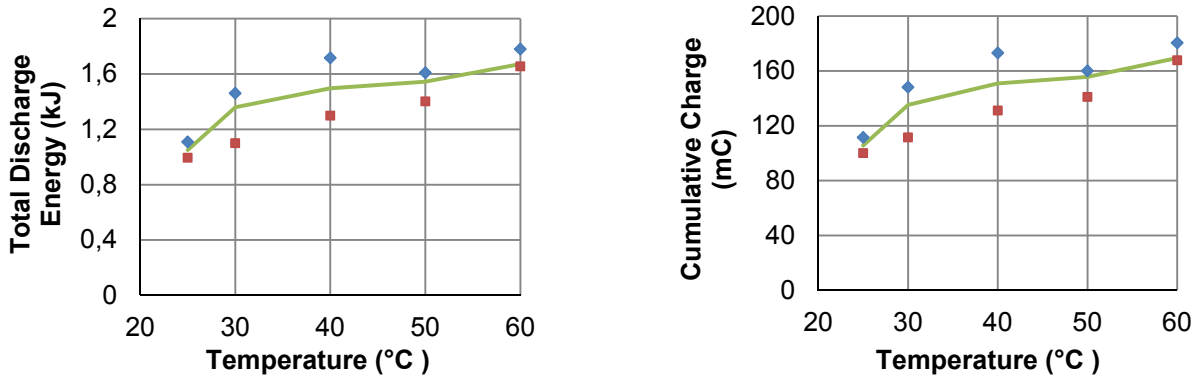

Figure 4.4: Discharge parameters (median, span of 3 samples) for test series 4, other parameter settings see table 4.1

4.4. Visual Observation and Specimen Appearance

The main focus is on the severity of the material surface erosion displayed by the specimen as well as the specimen appearance of the specimen before and after the test runs. The surface analysis of the surface using the laser profilometer showed the severest erosion depth in front of needle tip. It can be seen that there was a considerable erosion depth, but the erosion width was a little bit small because of the needle size. Figure 4.5 represents a 2-D image of stressed specimen surface, in which different degrees of erosion in discharge zones can be observed. It is clear that the erosion depth decreases in the other regions far from needle tip.

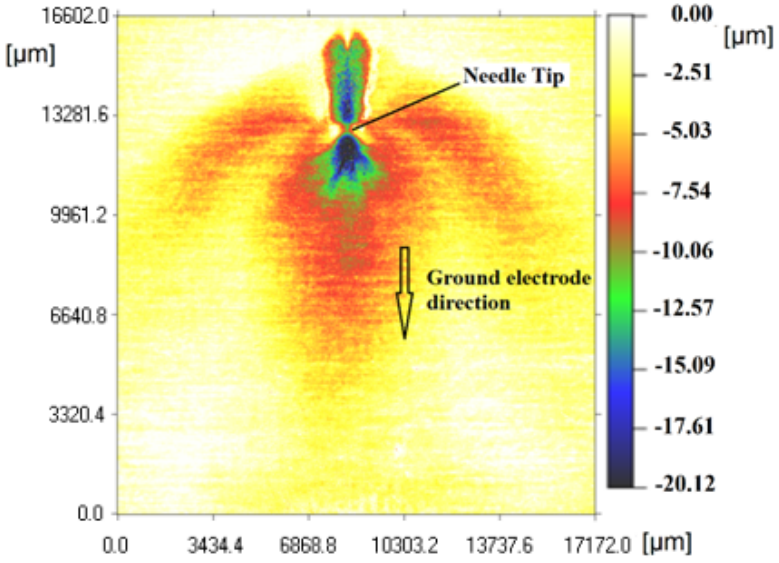

Figure 4.5: 2-D image of the eroded surface (12 kV peak, 500 Hz, 96 h, 25°C, 5 %RH)

Since the corona discharge was generated in front of the needle tip and diffused to the ground plate, the erosion was the severest at this location. The inhomogeneity of the applied electric field at the needle tip plays an important role in this erosion distribution. While the erosion depth decreases when getting apart from the needle tip. In the region between needle tip and the first needle-surface touch point (see figure 4.7), it can also be seen that there is considerable erosion. The next step is analyzing two different erosion profiles to

introduce a complete image of the eroded surface. Both of these profiles are normal to the specimen surface, while they are either perpendicular or parallel to the needle direction (see figure 4.6).

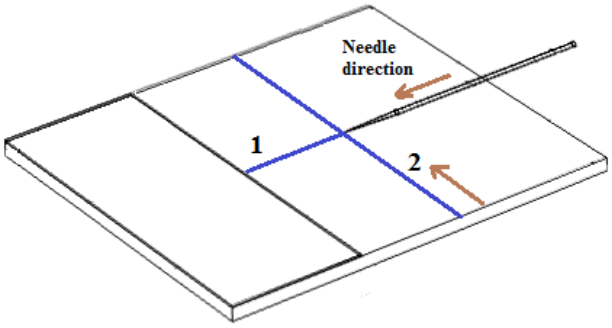

Figure 4.6: Erosion profile lines on the specimen surface

- **Profile 1**: This profile was taken along the needle direction and passing through the maximum erosion point. Here certain parameters can be calculated; the maximum erosion depth and the normal eroded area in the discharge region. There are two regions of erosion; the region between the needle tip and the ground electrode and that between the needle tip and the needle touch point (see figure 4.7).

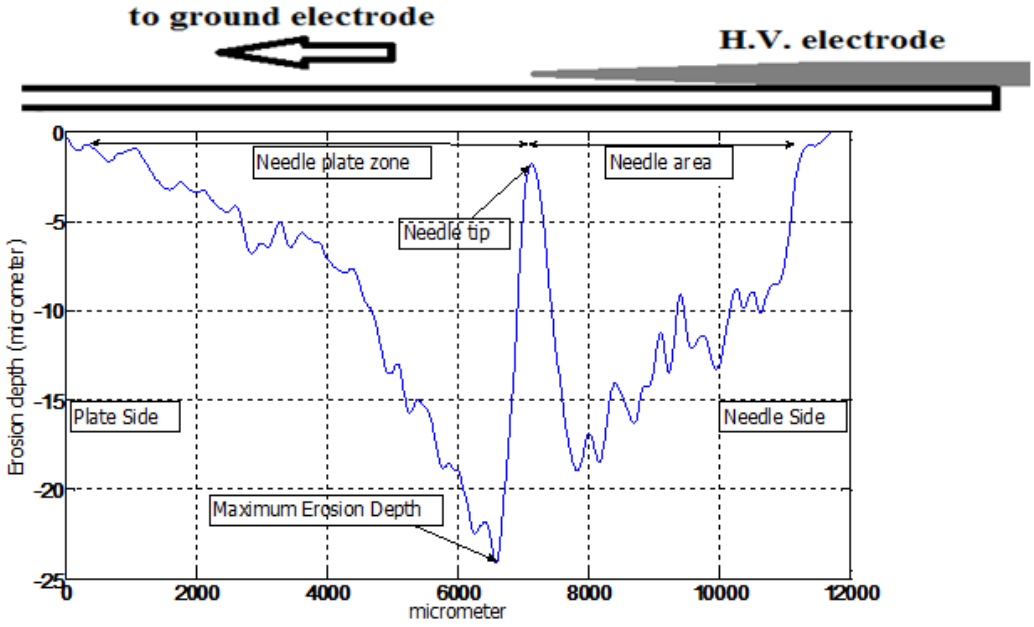

Figure 4.7: Erosion profile normal to the specimen surface and along the needle direction (12 kV_{peak}, 500 Hz, 96 h, 25°C and dry air)

- **Profile 2**: This profile was perpendicular to the needle direction and passing through the maximum erosion point. This case introduces a complete picture of the central region and the regions in its both sides. It can be noticed that this profile can be divided into different regions with different degrees of erosions. The highest affected region was the narrow region in front of the needle tip. Then, two local peaks can be observed which divides the eroded area into three zones; the central region and two lateral zones on both sides of the axis of symmetry (see figure 4.8).

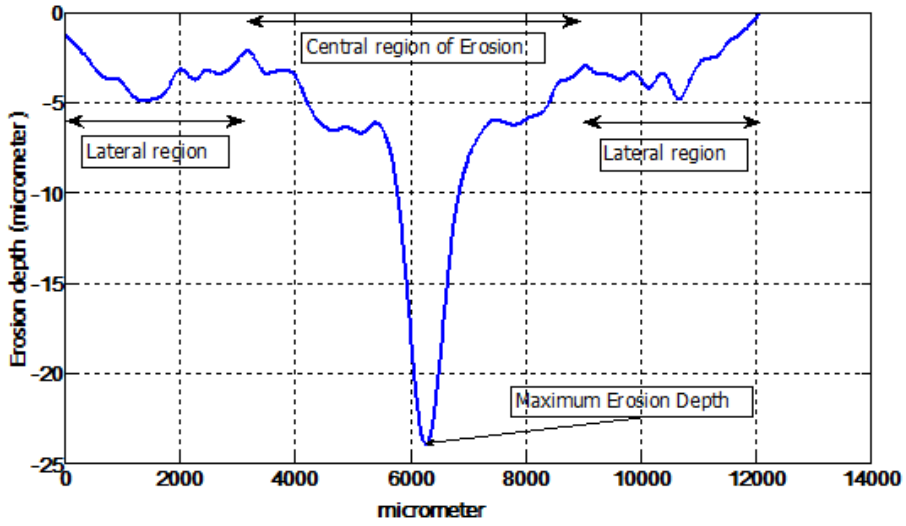

Figure 4.8: Erosion profile normal to the specimen surface and perpendicular to the needle direction (12 kV_{peak}, 500 Hz, 96 h, 25°C and dry air)

4.5. Erosion Characteristics

a) Test Series 1: Test Voltage Magnitude

Three characteristics were evaluated for each sample; maximum erosion depth, eroded surface area and eroded volume. It is obvious from figure 4.9 that maximum erosion depth is dependent on the test voltage magnitude. That is nearly correlated to the discharge behavior under the influence of increasing test voltage magnitude. Surface erosion severity (represented by maximum erosion depth) is significantly dependent on corona discharge intensity. Eroded surface area as well as total eroded volume exhibits a nonlinear behavior to the increase of the test voltage. The rate of change of both characteristics is almost constant until test voltage reaches a value of 11 kV_{peak}, above which erosion severity increases rapidly.

b) Test Series 2: Test Voltage Frequency

It is obvious from figure 4.10 that erosion characteristics are dependent on the magnitude of the applied frequency. Erosion degree increases with the frequency due to increase in the number of pulses per second, pulse repetition rate and discharge current magnitude. From the erosion characteristics and the results of the discharge parameters (in section 4.2) the situation is unclear concerning the correlation between the erosion severity and discharge intensity under the influence of test frequency change. In particular, the increase in eroded volume and area corresponding to the frequency change from 400 Hz to 500 Hz shows some correlation to discharge parameters, i.e. energy and cumulative charge.

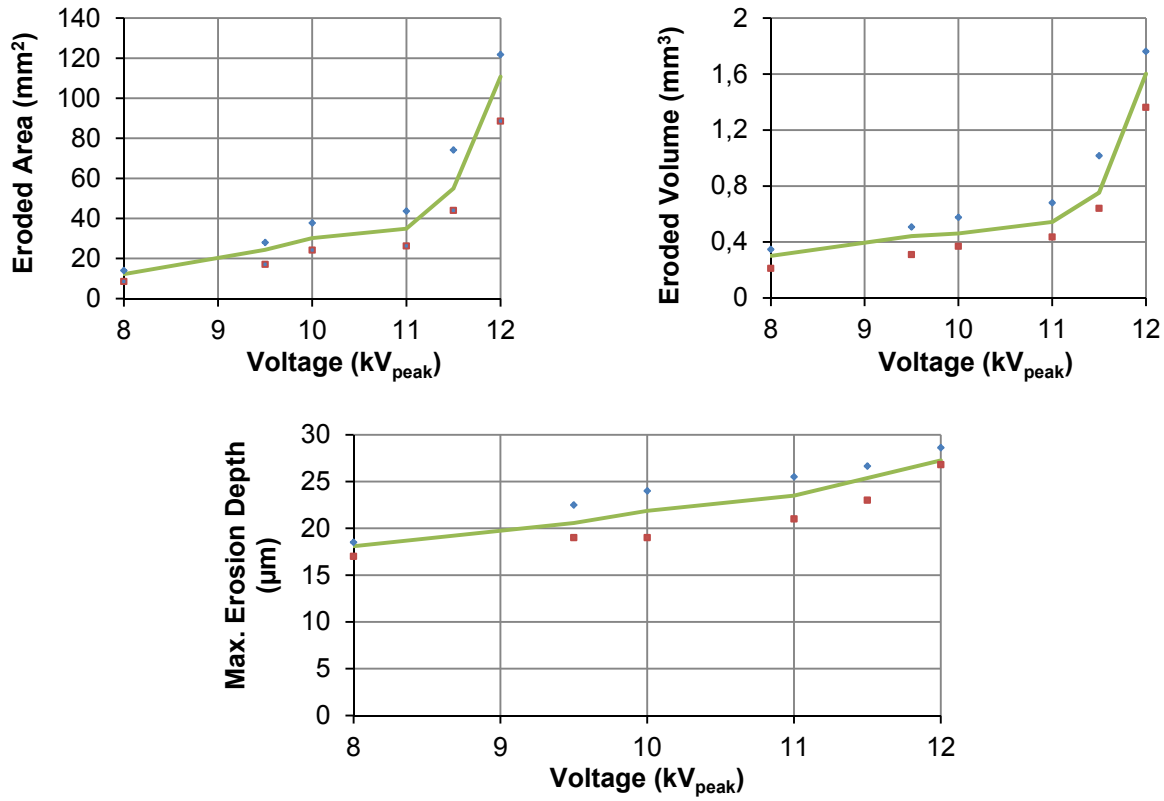

Figure 4.9: Erosion characteristics (median, span of 3 samples) for test series 1, other parameter settings see table 4.1

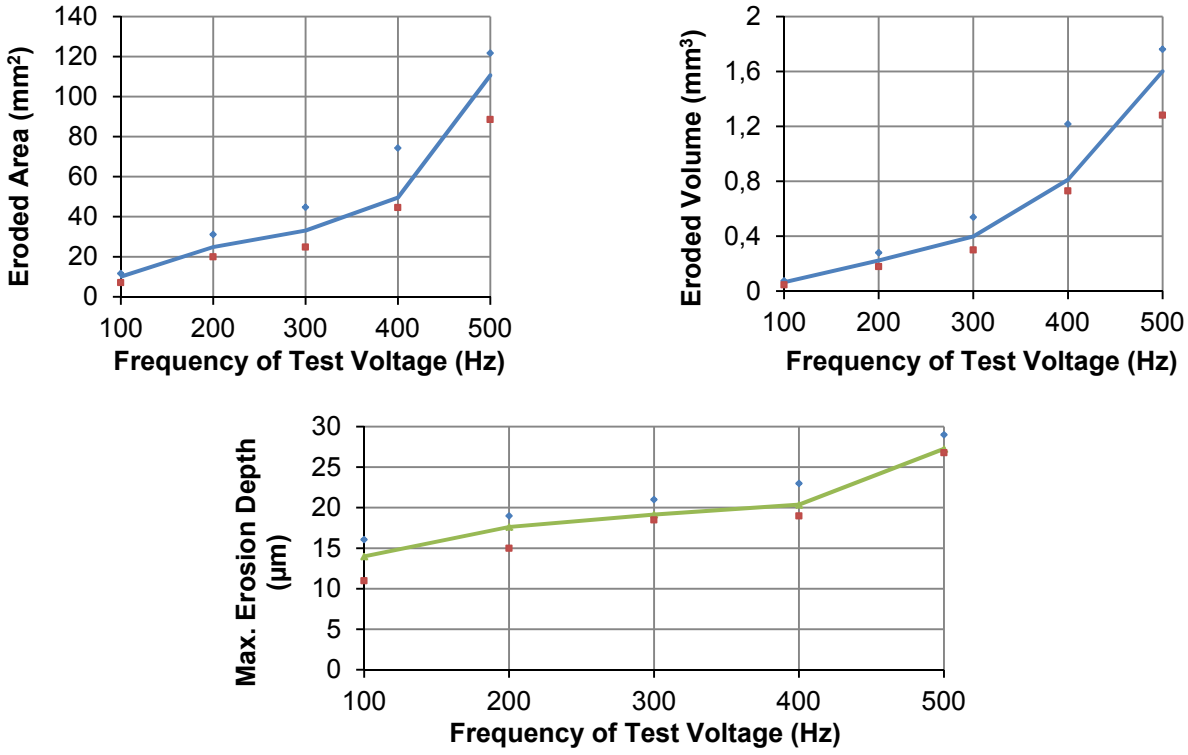

Figure 4.10: Erosion characteristics (median, span of 3 samples) for test series 2, other parameter settings see table 4.1

c) Test Series 3: Humidity

The magnitudes of erosion characteristics were analyzed versus the humidity of the discharge medium. It can be seen from figure 4.11 that maximum erosion depth is nearly constant with humidity variation from 11 up to 100 %RH. This behavior matches the response of discharge parameters which show a small decrease with humidity increase (figure 4.3). Therefore, it can be stated that maximum erosion depth is not humidity dependent; however it depends much more on discharge intensity. This proves that erosion in the high electric field region in front of needle tip (maximum erosion depth location) is mainly guided by discharge. While getting far from the needle tip, the less intensive discharges receive support from environmental influencing factors in the evolution of surface erosion. On the other hand it can be inferred from figure 4.11 that surface eroded area and total eroded volume increase with a high rate of change versus the humidity increase. Therefore, the increase of erosion in this phase, considering constant discharge activity, is mainly due to humidity.

d) Test Series 4: Temperature

At the beginning of analyzing the effect of temperature on the erosion characteristics, an important detail should be mentioned. Here the acceleration of erosion process is expected to be governed by the degree of temperature rise and the enhancement of discharge intensity. It can be observed from figure 4.12 that erosion characteristics increase directly with temperature rise exhibiting a nonlinear behavior.

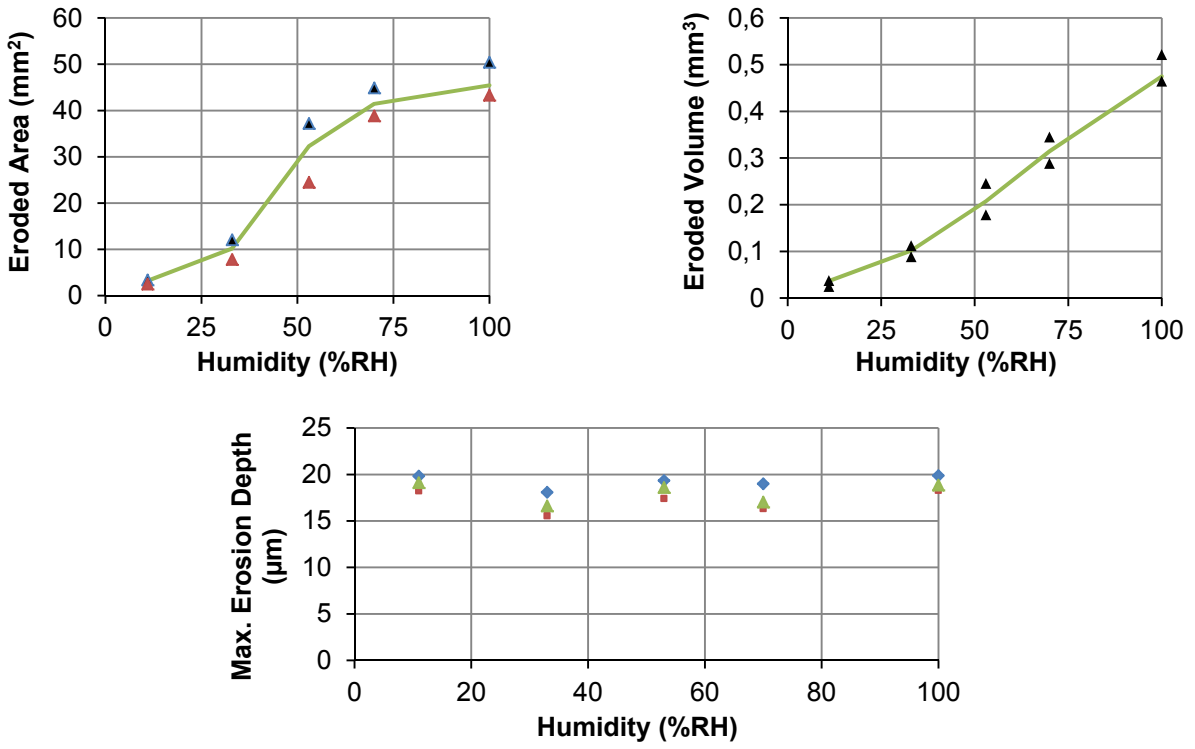

Figure 4.11: Erosion characteristics (median, span of 3 samples) for test series 3, other parameter settings see table 4.1

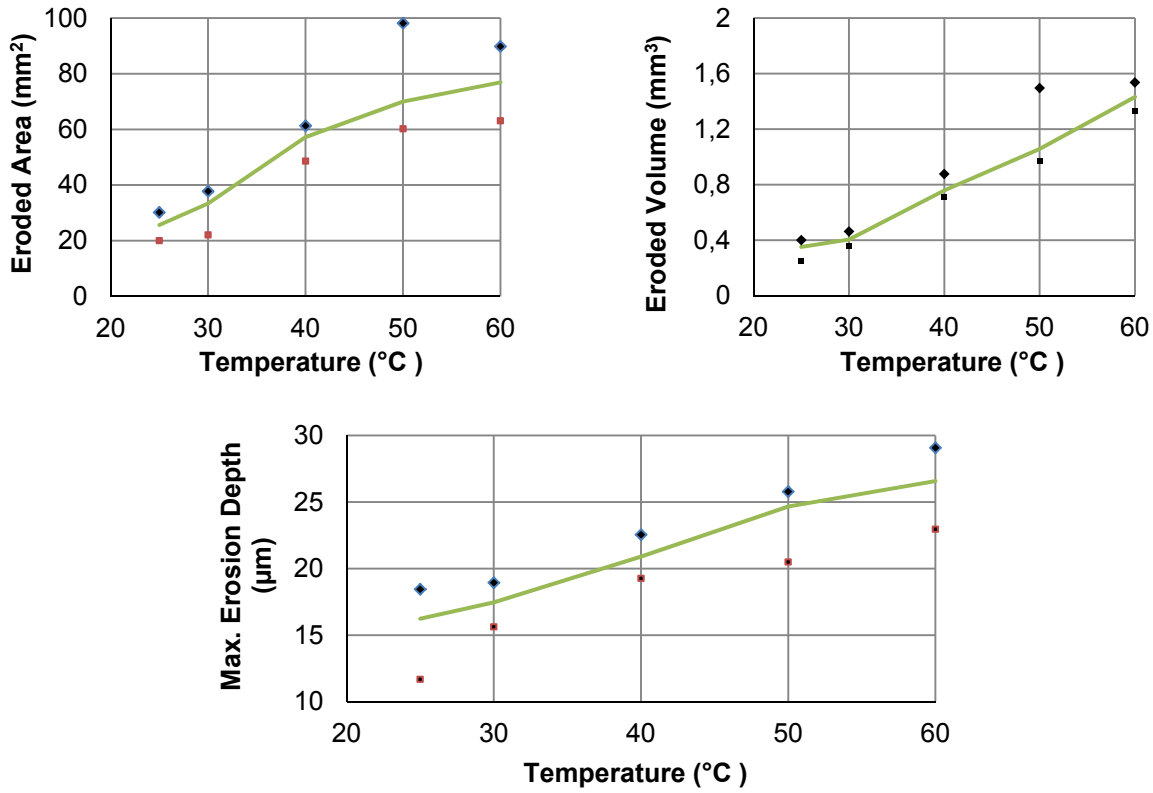

Figure 4.12: Erosion characteristics (median, span of 3 samples) for test series 4, other parameter settings see table 4.1

4.6. Conclusions

- The applied test setup is capable of producing measurable erosion and enables the control of different stressing factors. Hence this test setup will be used in the next chapters regarding that the range of adjusted values for the electrical stresses (voltage magnitude and frequency) depends mainly on material under stress. Where, the upper limit of the range is governed by the value that leads to the occurrence of flashover, whereas the lower limit is controlled be the minimum level of stress at which the resulting erosion can be significantly distinguished.
- Discharge intensity (i.e. total discharge energy and cumulative charge) is positively correlated to all factors of influence except for humidity; where discharge intensity is negatively correlated.
- All influencing factors proved to have impact on all erosion characteristics, whereas humidity change has almost no influence on maximum erosion depth. This reflects the dominating influence of electrical discharges on erosion mechanism in the regions of high electric field.
- Surface erosion phenomenon is significantly dependent on discharge intensity on specimen surface.
- In most of the obtained results, both discharge intensity and erosion severity introduces a nonlinear behavior at higher stress magnitudes.

- The test needs to be performed under a combination of all parameters to check whether the factors are already accelerating each other. Hereafter statistical models will be constructed to verify the influence of each stressing factor as well as the significance of their interaction if exists.
- In order to obtain a deeper view of the examined phenomena it is mandatory to have a larger number of specimens in each test series, which supports the statistical studies performed on the obtained results.

5. Influencing factors

In this chapter, the influence of all stressing factors on material surface in terms of erosion characteristics was examined. Additionally, the affected discharge parameters under the impact of those stresses were analyzed. From the results on both levels, i.e. erosion and electrical discharge, a reasonable quantification can be introduced to the influence of stressing factors on insulating polymers. Interaction study was also held to examine, whether the stresses lead to synergism in between.

5.1. Epoxy Resin Under Analysis

The material used for investigation in this study is used for indoor electrical insulators for medium and high voltage, such as switch and apparatus components, bushings, instrument transformers and dry type transformers. The epoxy resin used in this work is modified, solvent-free, medium viscous bisphenol A (Araldite CY 225 with 100 parts per weight). HY 225 with 80 ppw is used as liquid, modified, pre-accelerated anhydride curing agent and silica flour is used as filler (270 ppw). The advantages of Araldite casting resin system are the high resistance to mechanical and electrical stresses, high resistance to thermal shock and excellent long term behavior in relation to breakdown strength.

5.2. Electrical Stressing Factors

5.2.1. Testing Procedure

Factorial analysis was performed in terms of discharge parameters and erosion severity of the specimens' surface. This analysis was performed between voltage magnitude and frequency of test voltage. While investigating a certain test series, the settings for the other factors of influence were kept constant as shown in table 5.1. Therefore, it is possible to make a correlation between the factors of influence under study and the resulting damage, and to quantify the interaction between the factors.

Table 5.1: Test parameters setting for each test series

Test Series	Voltage (kV_{peak})	Frequency (Hz)	Temperature (°C)	Humidity (%RH)
1, 2	10, 12, and 14	50, 250, and 500	20	33

The value of test voltage magnitude was taken via a voltage monitor signal supplied by the high voltage amplifier. The current measurement was performed indirectly via a 50 Ω series high voltage resistor connected in series with the plane electrode in its ground path. The number of specimens used for each test series is five, for which statistical analysis was performed. Hence all the signals to be measured were transferred in sequence via 8 channel relay to an oscilloscope. The oscilloscope was connected to a computer via RS-232 port to support communication interface in between. The whole schematic circuit diagram of the test setup and measurement system is shown in figure 5.1.

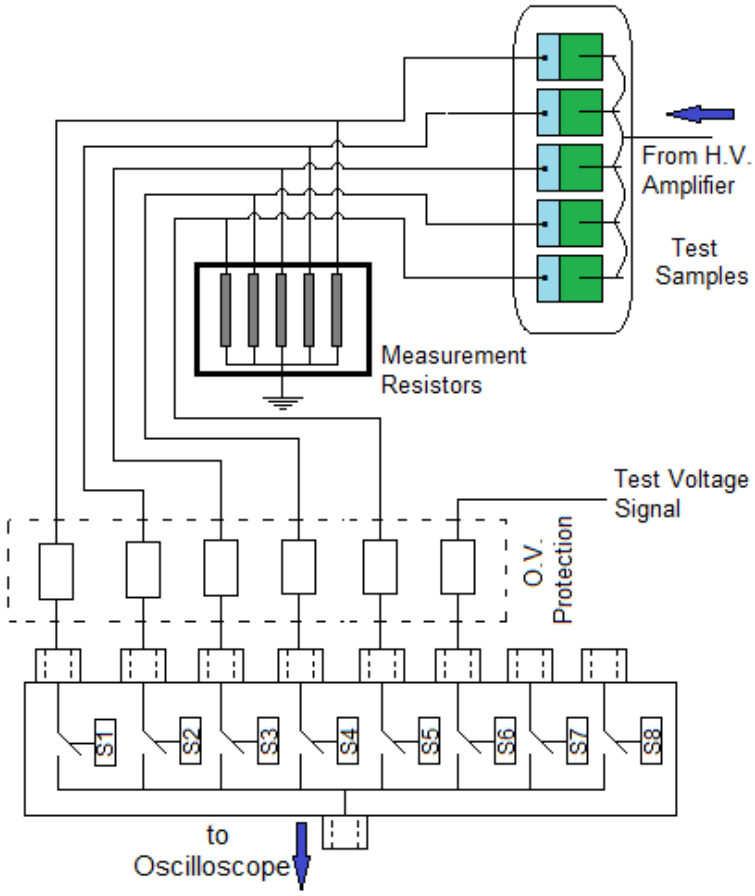

Figure 5.1: Test setup with the measurement system for discharge currents

5.2.2. Discharge Parameters

The influence of electrical stressing factors on discharge parameters is presented in figure 5.2. It was found that increasing either of the magnitude or the frequency of test voltage results in a certain increase in discharge parameters under analysis. It can be also seen that at lower values of either of those factors, the increase in discharge parameters with the other factor is almost linear. However, any enhancement in either of those factors introduces nonlinearity in the discharge parameters change with the other factor. There is a synergism between electrical factors in terms of discharge parameters.

The influence of test voltage magnitude on discharge intensity is consistent with the results of [ANG-08], [ANG-12]. Anglhuber et al have proven that the higher the level of the test voltage magnitude, the higher the discharge intensity as well as the resulting material damage, i.e. erosion degree. These results confirm that needle-to-plate electrode arrangement used in this work leads to the same results similar to the IEC 60343 used in all the previous work in erosion resistance tests. However, this is only observed on the level of test voltage magnitude and not test frequency. On the other hand, the influence of the test frequency on discharge intensity agrees with the investigations performed by [NYA-11], who studied partial discharge in solid polymeric insulating materials. However, the discharge intensity in [NYA-11] was characterized by the spread and intensity of UV radiation associated with the discharge and not by discharge parameters.

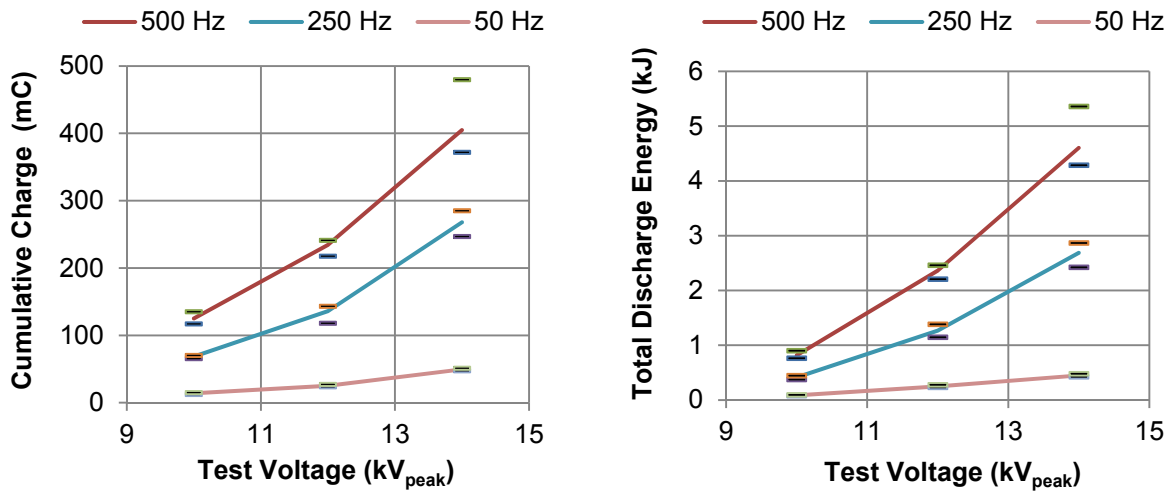

Figure 5.2: Discharge parameters (median, span of 5 samples each), other settings see table 5.1

5.2.3. Erosion Characteristics

From figure 5.3, it can be noticed that erosion severity is dependent on the magnitude as well as frequency of test voltage. That is nearly correlated to discharge behavior under the effect of increasing electrical stresses. Surface erosion severity is hence significantly dependent on surface discharge parameters. The interaction between magnitude and frequency of test voltage can be also observed in terms of the resulting surface damage. For example, the rate of change in erosion characteristics with respect to voltage magnitude increases at higher values of test frequency. This confirms the fact that there is an interaction between both stresses in terms of erosion characteristics. Nonlinear regression on the obtained erosion characteristics yields equations [5.1] to [5.3], whereby eroded volume $\boldsymbol{Vol}$ is in mm^3, eroded area $\boldsymbol{A}$ is in mm^2, maximum erosion depth $\boldsymbol{D_{max}}$ is in µm, the test frequency $\boldsymbol{f}$ is in Hz and the voltage $\boldsymbol{V}$ is in volts. From these equations, it could be concluded that the rate of increase of $\boldsymbol{Vol}$ and $\boldsymbol{A}$ with respect to both electrical influencing factors is much higher than that of $\boldsymbol{D_{max}}$. Additionally, the minimum influence of test frequency is detected in the eroded area.

$$\boldsymbol{Vol[mm^3] = 7 \times 10^{-4} \cdot \left[\frac{f\,[1/s]}{50\ 1/s}\right]^{0{,}887} \cdot \left[\frac{V}{kV_{peak}}\right]^{3}} \quad [5.1]$$

$$\boldsymbol{A[mm^2] = 9{,}6 \times 10^{-3} \cdot \left[\frac{f\,[1/s]}{50\ 1/s}\right]^{0{,}472} \cdot \left[\frac{V}{kV_{peak}}\right]^{4}} \quad [5.2]$$

$$\boldsymbol{D_{max}[\mu m] = 0{,}292 \cdot \left[\frac{f\,[1/s]}{50\ 1/s}\right]^{0{,}717} \cdot \left[\frac{V}{kV_{peak}}\right]^{1{,}1}} \quad [5.3]$$

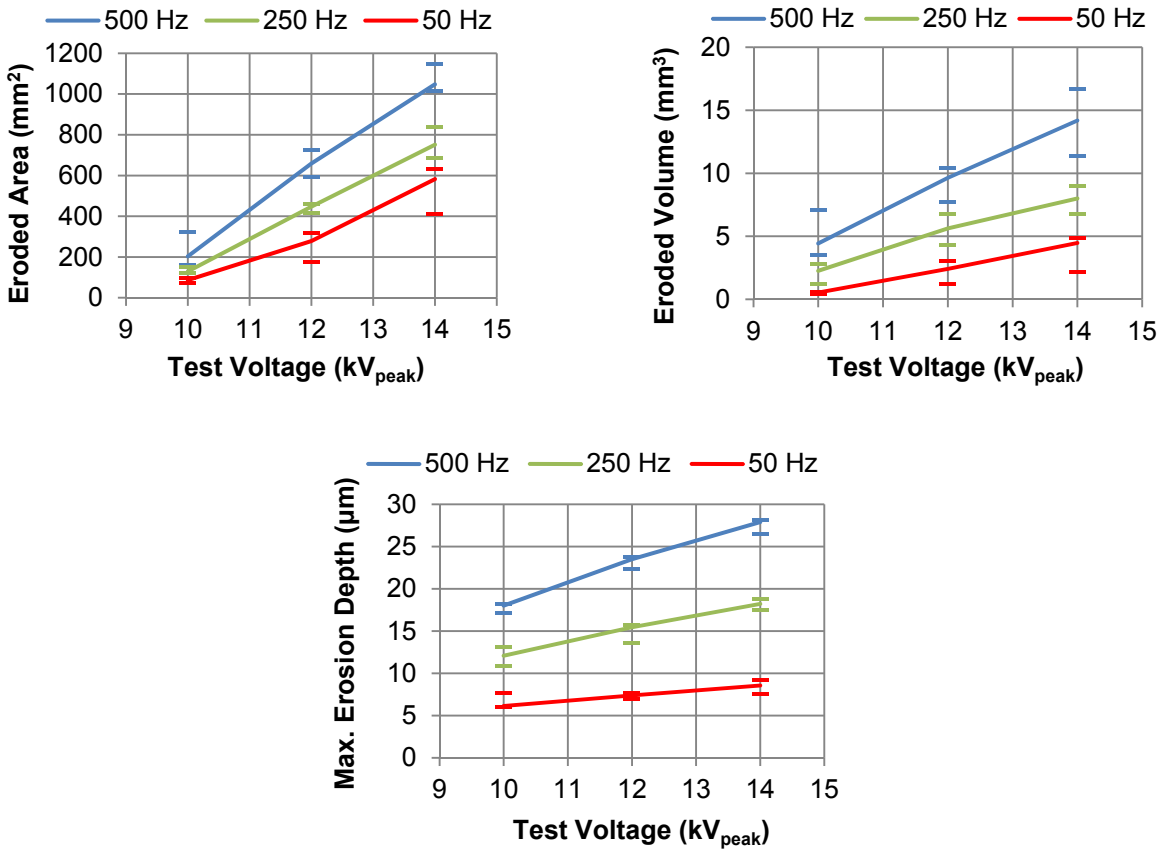

Figure 5.3: Erosion characteristics (median, span of 5 samples), other settings see table 5.1

The influence of the test voltage magnitude on material erosion is in accordance with the results of [ANG-08], [ANG-12]. Concerning the impact of test frequency, Tanaka et al [TAN-07], [TAN-08a] have examined the acceleration of material aging under the impact of test frequency at the same 60 Hz equivalent time. This means that the analysis has been performed for constant number of cycles and not for the same stress time duration.

Many studies in literature apply only one characteristic for representing surface erosion, i.e. maximum erosion depth, which represents one point on the damaged surface exposed to electric field enhancement [KOZ-05a, 05b], [TAN-06, 08a, 08b], [CAV-07], [MOR-99, 00, 01a and 01b]. Nevertheless, Anglhuber et al [ANG-08], [ANG-12] involved, in addition to the 95% erosion depth, the total eroded volume as an important characteristic in the quantification of surface erosion. In this way the quantified erosion using only maximum erosion depth is irrelevant to the whole eroded zone of the material surface. Therefore, the erosion degree is fully quantified by three characteristics, i.e. eroded area, volume and maximum erosion depth, which is a powerful tool in the quantification of erosion degree. Thus, better understanding to the influence of the examined factors and the main stresses involved in erosion phenomena is achieved.

5.2.4. XPS Results

The erosion of polymer surface can be analyzed by XPS, and the experimental settings that are used in this study are explained in chapter 3. The main peaks found in the full spectrum range are C 1s, O 1s, O 2s, Si 2p and Si 2s (both silicone peaks are due to the silica filler in the material composition). The core level XPS spectra for a virgin epoxy resin specimen are shown in figure 5.4. The basic information such as the area of those peaks shows how the chemical structure of the polymer surface is changed as a result for the imposed stresses.

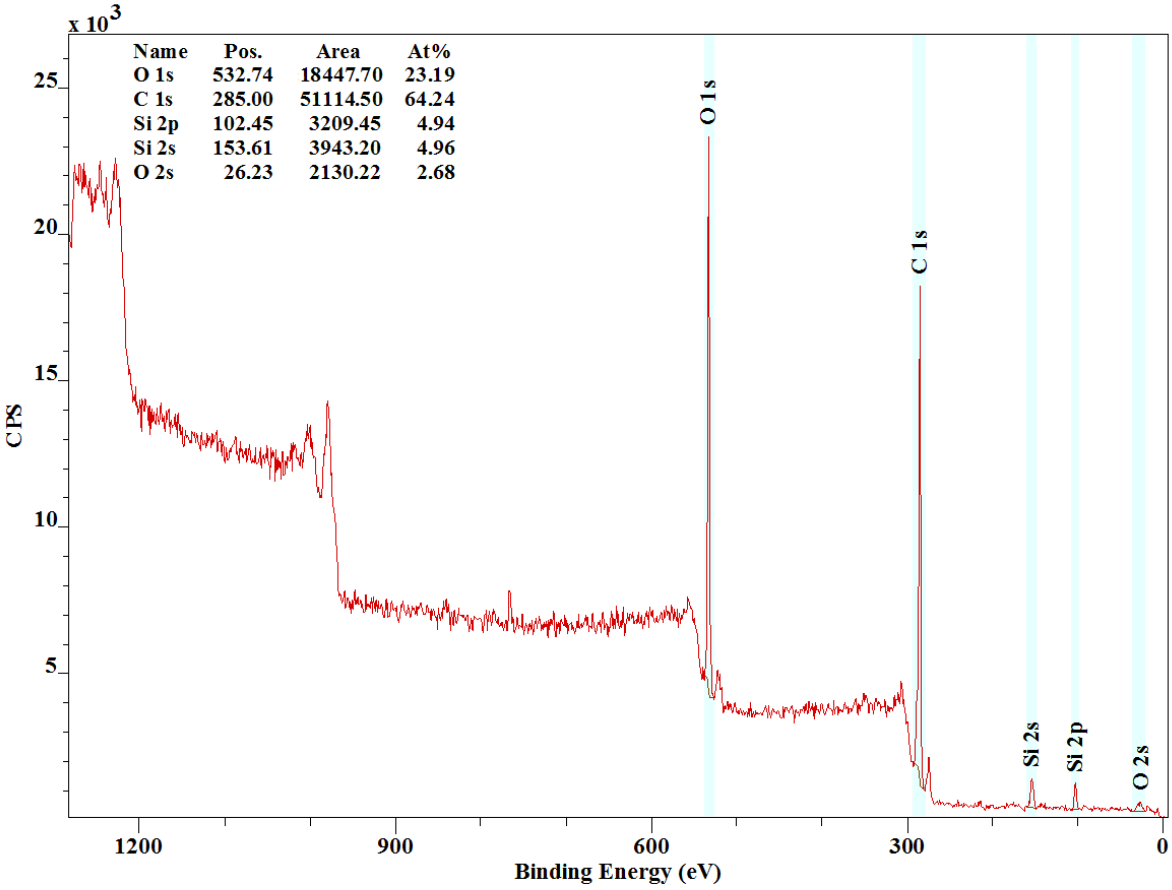

Figure 5.4: Core XPS spectra of a virgin epoxy resin specimen

Deconvolution of the XPS core level bands gives the average binding energies for different products in detail. The deconvolution model of C 1s peak of a virgin epoxy resin specimen is shown in figure 5.5. C 1s has main strong peak at 285 eV due to the C–H, C–C bonds in the polymer. Beside this peak there are three shifted ones due to functional groups arisen from oxygen bonds with carbon atoms. The three peaks are C–OH, C=O and O=C–OH (or shortly COOH) at binding energy of 286.5 eV, 287.5 eV and 289 eV respectively. As a rule of thumb, the chemical shift in the binding energy of C 1s peak is about +1.5 eV per oxygen atom linked to the carbon atom [BOU-11]. The main oxygen peak is seen as O 1s signal around 532-533 eV, which intensifies with the newly produced C–Ox species in the C 1s peak.

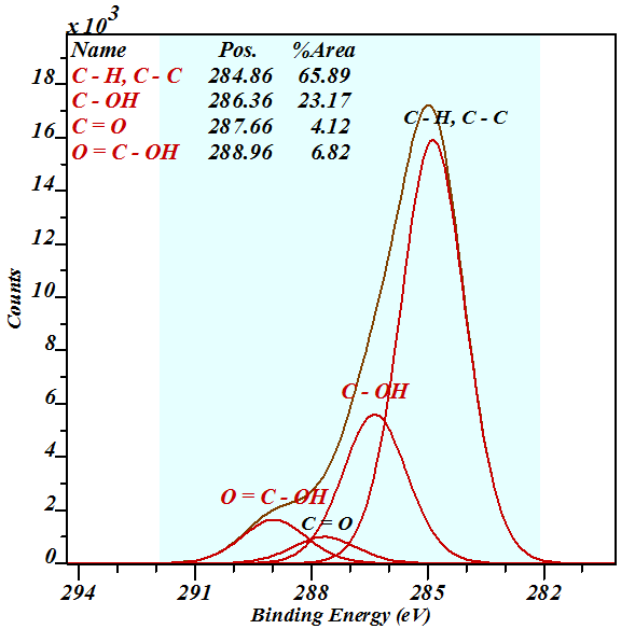

Figure 5.5: Deconvolution model of C 1s peak of a virgin epoxy resin specimen

The influence of corona discharges on material surface is studied in terms of material composition. The stresses under study are the electrical influencing factors, i.e. test voltage magnitude and frequency. Deconvolution of C 1s peak of stressed epoxy resin specimens facilitates the study of the variation in every peak area. This study is performed as a function of both stresses, which are examined on the levels of 50 Hz and 250 Hz for frequency and 10 kV, 12 kV and 14 kV for voltage.

When stresses increase the intensity of C–H, C–C peak is decreased due to the increase of bond dissociation of such groups (i.e. chain scission) under stress to react with oxygen and produce more oxygen bonds [RAM-12] as listed in table 5.2. This is clearly detected from the oxygen containing hydroxyl groups in the form of alcohols (C–OH), which is increased with electrical stresses. The increase in oxygen containing functional groups is seen as a direct effect of material degradation due to electrical discharges. The other oxygen containing groups, C=O and O=C–O, are only influenced by frequency increase, whereas voltage magnitude has no clear impact.

The other oxygen containing groups are directly proportional to the test frequency. This behavior of such oxygen containing groups with respect to test frequency stress could be attributed to material deterioration through the thermal stimulation processes within the surface layers of polymeric materials [NIA-14]. Although such phenomenon is not likely to dominate in epoxy resin insulating material (in which concentration of free electrons is too low), it is possible for an insulating material which possesses traps below the conduction band [DIS-92]. Therefore, the excited electrons may be trapped in these energy bands (traps) by losing their energy and as a consequence trapped charges may be generated. This process is known as thermal stimulation of insulating materials. Generated trapped charges within the insulating material result in electrical field enhancement within the insulating material. This impact leads an acceleration of material surface deterioration and in turn results in higher erosion severities.

Table 5.2: Area change in C 1s deconvolution peaks (with respect to the whole envelope area of C 1s peak) and O 1s peak (normalized to that of virgin material specimens) of discharge stressed specimens, 20°C, 33 %RH, 96 hours

Analyzed specimens	***Stress parameters***		***C 1s deconvolution***				***relative O 1s peak***
	V kV_{peak}	***f*** Hz	***C – H, C – C*** *%*	***C – OH*** *%*	***C = O*** *%*	***O = C – OH*** *%*	$\frac{O\ 1s}{(O\ 1s)_{virgin}}$
Virgin			65.89	23.17	4.12	6.82	1
Stressed	10	50	61.49	25.90	4.82	7.79	1.658
	10	250	57.05	27.92	6.85	8.18	2.177
	14	50	59.13	29.66	3.90	7.31	1.920
	14	250	51.84	35.08	5.20	7.88	2.257

It can be also seen from figure 5.6 that the amount of O 1s / C 1s ratio is higher for discharge stressed samples compared to the unstressed one. This confirms the influence of electrical discharge on enhancing the intensity of oxygen bonds. As it can be seen, the test voltage magnitude has no impact on the value of this ratio. Another way to identify the oxygen concentration under different electrical stresses is to compare the O 1s peaks obtained with high resolution of 0.1 eV. The area of different O 1s peaks is normalized with respect to that of virgin material (see table 5.2). It is found that the area of O 1s peaks for stressed specimen is much larger than that for the virgin specimen. It is also noted that both electrical stress parameters are directly correlated to oxygen concentration in material surface, even if the rate of increase in the peak area with respect to electrical stresses is not high.

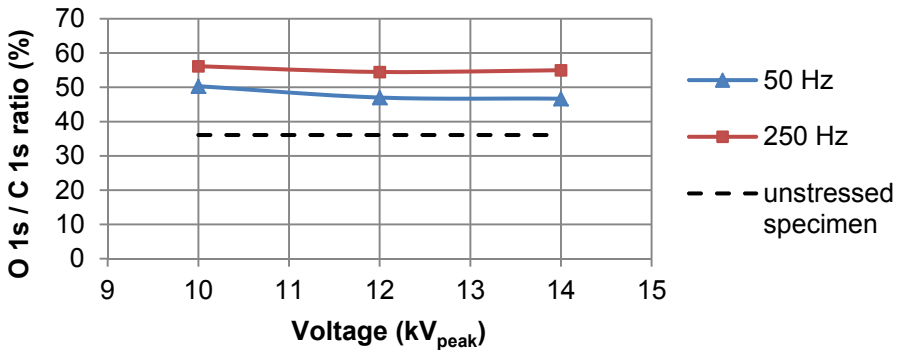

Figure 5.6: Influence of corona discharge on material composition, 20°C, 33 %RH, 96 h

High resolution spectra of Si 2p orbital peaks were further analyzed to examine the changes in chemical surface composition. Deconvolution model of virgin specimen is shown in figure 5.7 exhibiting two peaks at binding energies of 103.4 ± 0.2 and 101.9 ± 0.2 eV. The peaks are referred to inorganic silica compounds SiOx, i.e. Si atoms bonded to one or two oxygen atoms. The amount of silica in epoxy composition is attributed to the amorphous reinforcing filler added to the polymer. Discharge stressed specimens at normal temperature and humidity conditions exhibit no change in the percentage area of the two peaks. Therefore, there is no influence of discharge stress on material composition in terms of oxidation of silica peaks.

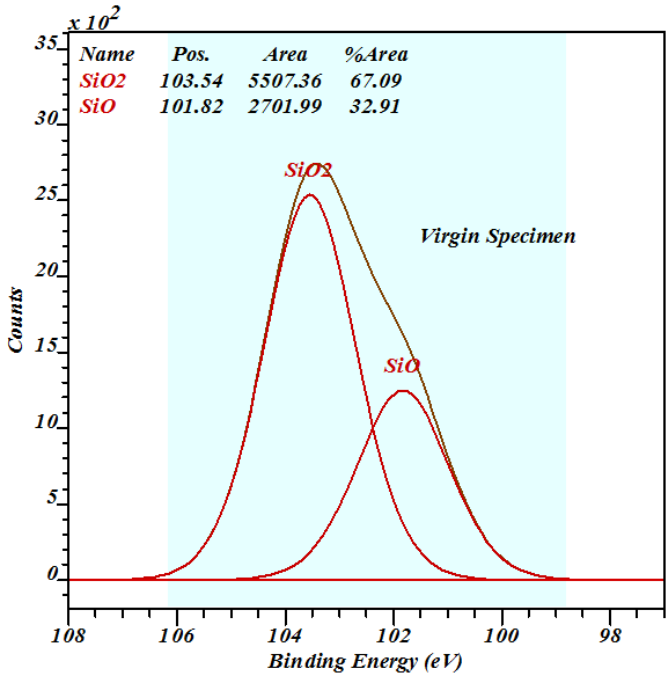

Figure 5.7: Deconvolution model of Si 2p peak for virgin material specimen

5.2.5. Statistical models

Five statistical models were analyzed for the sake of investigating all property variables influenced by electrical factors. Each factor was examined in three levels; 10, 12, and 14 kV_{peak} for voltage magnitude and 50, 250, and 500 Hz for frequency. The selected confidence level is 95% and the adjusted significance level for the hypothesis test is 0.05. The different variables under analysis are: eroded volume (***Vol***), erode area (***A***), maximum erosion depth ($\boldsymbol{D_{max}}$), total discharge energy ($\boldsymbol{E_T}$), cumulative charge ($\boldsymbol{Q_{cum}}$), UV Intensity ($\boldsymbol{I_{UV}}$) and UV illuminated area ($\boldsymbol{A_{UV}}$). The model construction is performed as follows:

1. All covariates linearly related to the examined response were included in the model.
2. After the first run of the model, all covariates which had no significance on the examined response (as their p-values exceed 0.05) were eliminated.
3. The refitted model was run with the remaining covariates and the stressing factors of concern.

All the five examined models are summarized in table 5.3 to explain the main factors of influence on the studied response in each model. The results for each model in the table determine the effective covariates for the examined response. Additionally, the influence of the both stressing factors as well as their interaction is verified.

One of the examined models is illustrated in detail and the results are then taken from the optimum refitted model. Figure 5.8 presents the analysis of variance for eroded volume characteristic. From the model it can be interpreted that test voltage magnitude and frequency as well as their interaction have a significant influence on eroded material volume, which is confirmed by their p-values (less than 0.05). It is also concluded that total discharge energy and cumulative charge as covariates have a certain impact on eroded volume.

Table 5.3: Summary of the statistical models and the correlation coefficients for all variables

Model	1	2	3	4	5
Response	Eroded Volume	Eroded Area	Max. Erosion Depth	Total Discharge Energy	Cumulative Charge
Covariates	**E_T & Q_{cum}** • p-values: 0.012 & 0.00 • CCs: 0.919 & 0.925	**Vol & A_{UV}** • p-values: 0.00 & 0.034 • CCs: 0.931 & 0.925	**Q_{cum}** • p-value: 0.00 • CC: 0.950	**Q_{cum} & I_{UV}** • p-values: 0.00 & 0.00 • CCs: 0.981 & 0.955	**E_T** • p-value: 0.00 • CC: 0.981
Impact of voltage	significant • p-value: 0.0 • CC = 0.544	significant • p-value: 0.00 • CC: 0.786	significant • p-value: 0.00 • CC: 0.298	significant • p-value: 0.001 • CC: 0.488	significant • p-value: 0.00 • CC: 0.407
Impact of frequency	significant • p-value: 0.00 • CC: 0.707	significant • p-value: 0.001 • CC: 0.452	significant • p-value: 0.00 • CC: 0.914	significant • p-value: 0.001 • CC: 0.691	significant • p-value: 0.00 • CC: 0.812
Interaction	significant • p-value: 0.004	significant • p-value: 0.00	significant • p-value: 0.002	significant • p-value: 0.002	significant • p-value: 0.00

Tukey's test provides grouping information and two sets of multiple comparison intervals; one group for voltage magnitude levels and the other for voltage frequency. In the grouping table, factor levels within the same group are significantly different from each other. Therefore, all level means have significantly different eroded volume degree. The first 95% confidence interval in the first set (voltage magnitude) of the Tukey's output is 2.235 to 5.136. That is, the mean eroded volume resulting from 12 kV_{peak} minus that from10 kV_{peak} is somewhere between 2.235 to 5.136 mm^3. This means that the resulting eroded volume is larger for higher voltage magnitude. The other intervals in both sets are interpreted in the same way. The impact of all stresses differs significantly because all of the confidence intervals exclude zero. Therefore, all stresses have significantly different average impact on eroded volume.

The role of the constructed statistical models is first to confirm the conclusions drawn from the results in terms of the influence of stressing factors on discharge intensity as well as erosion severity. Second, the dominating parameters controlling the discharge and erosion characteristics are identified (for example, whether total discharge energy or cumulative charge is governing the erosion process). From the examined models above concerned with erosion characteristics and discharge parameters, the following can be concluded:

- Discharge parameters exhibit covariance in between. Both discharge parameters, energy and charge, have a direct influence on eroded volume with correlation coefficients (CCs) of 0.919 and 0.925 respectively.
- Total discharge energy and UV intensity show a covariance in between with correlation coefficient of 0.955; however there is no evidence on correlation between UV intensity and cumulative charge.
- Eroded area is mainly governed by UV illuminated area with a correlation coefficient of 0.925; which reflects that the spread of electric discharge on the surface controls how much from the total exposed surface area is eroded.

General Linear Model: Eroded Volume versus Voltage; Frequency

```
Factor     Type   Levels  Values
Voltage    fixed       3  10; 12; 14
Frequency  fixed       3  50; 250; 500

Analysis of Variance for Eroded Volume, using Sequential SS for Tests

Source             DF   Seq SS  Adj SS   Seq MS       F      P
Cumulative Charge   1  668,874   2,026  668,874  488,25  0,000
Total Energy        1    9,776  16,611    9,776    7,14  0,012
Voltage             2   22,070  11,106   11,035    8,06  0,001
Frequency           2   39,945   3,062   19,972   14,58  0,000
Voltage*Frequency   4   25,812  25,812    6,453    4,71  0,004
Error              33   45,208  45,208    1,370
Total              43  811,686

S = 1,17045   R-Sq = 94,43%   R-Sq(adj) = 92,74%

Grouping Information Using Tukey Method and 95,0% Confidence
Voltage   N  Mean  Grouping
14       14   8,7  A
12       15   6,2    B
10       15   2,5      C
Means that do not share a letter are significantly different.

Tukey 95,0% Simultaneous Confidence Intervals
Response Variable Eroded Volume
All Pairwise Comparisons among Levels of Voltage
Voltage = 10  subtracted from:
Voltage  Lower  Center  Upper  -----+---------+---------+---------+-
12       2,235   3,685  5,136        (------*-------)
14       4,654   6,134  7,615                  (-------*------)
                              -----+---------+---------+---------+-
                                 2,0       4,0       6,0       8,0
Voltage = 12  subtracted from:
Voltage   Lower  Center  Upper  -----+---------+---------+---------+-
14       0,9686   2,449  3,929  (------*-------)
                              -----+---------+---------+---------+-
                                 2,0       4,0       6,0       8,0

Grouping Information Using Tukey Method and 95,0% Confidence
Frequency   N  Mean  Grouping
500        14  10,0  A
250        15   5,2    B
 50        15   2,2      C
Means that do not share a letter are significantly different.

Tukey 95,0% Simultaneous Confidence Intervals
Response Variable Eroded Volume
All Pairwise Comparisons among Levels of Frequency
Frequency =  50  subtracted from:
Frequency  Lower  Center  Upper  ----+---------+---------+---------+--
250        1,526   2,977  4,428  (-----*-----)
500        6,279   7,759  9,240                (-----*-----)
                              ----+---------+---------+---------+--
                                2,5       5,0       7,5      10,0

Frequency = 250  subtracted from:
Frequency  Lower  Center  Upper  ----+---------+---------+---------+--
500        3,302   4,782  6,263        (-----*-----)
                              ----+---------+---------+---------+--
                                2,5       5,0       7,5      10,0
```

Figure 5.8: The optimum refitted general linear model for eroded volume (Model 1), from Minitab

- Cumulative charge exhibits a direct impact on maximum erosion depth with a correlation coefficient of 0.95.
- Electrical stressing factors are strongly affecting the erosion process and an interaction exists between both factors significantly in terms of erosion characteristics as well as discharge parameters.

Cumulative charge has proven to be the discharge parameter which controls the maximum erosion depth. This indicates that the amount of charge carried by the charged particles impinging on the surface at a certain point is the factor that determines how deep the erosion is. On the other hand the eroded volume, which represents the whole amount of material removed from the material surface, is controlled by two factors total discharge energy and cumulative charge.

5.3. Environmental Factors

5.3.1. Testing Procedure

Factorial analysis was performed on two test series in terms of discharge parameters and erosion severity of specimen surface. The analysis was performed between temperature and humidity of discharge medium. The settings for the electrical factors of influence were kept constant as shown in table 5.4. Therefore, it was possible to make a correlation between the factors of influence under study and the resulting damage. It is also possible to perform an interaction analysis between those factors. In the listed table below temperature is examined at 3 levels, 20, 40, and 60°C, while humidity is studied at 4 levels from dry to humid air i.e. 11, 33, 53, and 70 %RH.

Table 5.4: Test conditions for environmental factors of influence

Test Series	Voltage (kV_{peak})	Frequency (Hz)	Temperature (°C)	Humidity (%RH)
3, 4	12	500	20, 40, and 60	11, 33, 53, and 70

5.3.2. Discharge Parameters

The effects of environmental factors on discharge parameters were studied and the response of each discharge parameter was calculated. It can be seen from figure 5.9 that discharge parameters are slightly affected by humidity change in inverse proportional relationship. This could be attributed to the fact that, under humid conditions scattering and absorption of UV results in a reduced percentage of UV reaching specimen surface. This interpretation could be proven by investigating the influence of humidity by applying different electrical stresses under two test conditions; dry (11 %RH) and humid conditions (70 %RH). Each colored region in figure 5.10 represents how far UV characteristics are influenced by humidity change. Boundaries of the colored regions are given by median values. The upper boundary represents UV characteristic value at 11 %RH; whereas the lower boundary is for 70 %RH. UV characteristics are influenced by humidity increase to a certain extent independent

from magnitude and frequency of the test voltage. Those results are consistent with those conclusions from [PIN-05].

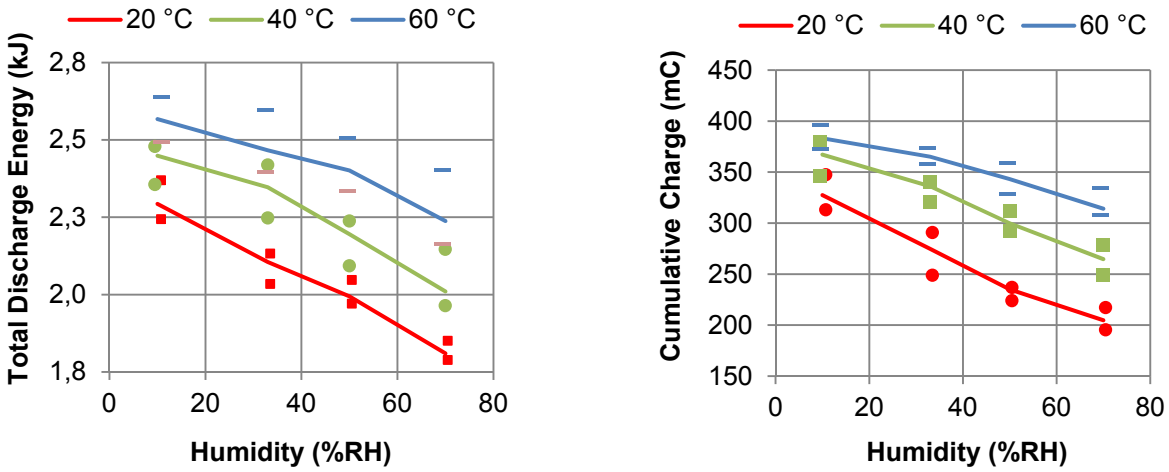

Figure 5.9: Discharge parameters (median, span of 5 samples), other settings see table 5.4

The rate of decrease in discharge parameters with humidity increase is higher at lower temperature degrees (figure 5.9). This referred to interaction between environmental factors in terms of discharge parameters. This interaction occurs because each factor is compensating the impact of the other one; where the impact of each on discharge parameters is the opposite of the other. On the other hand, It is clear from figure 5.9 that temperature rise increase discharge parameters but with a slow rate of change.

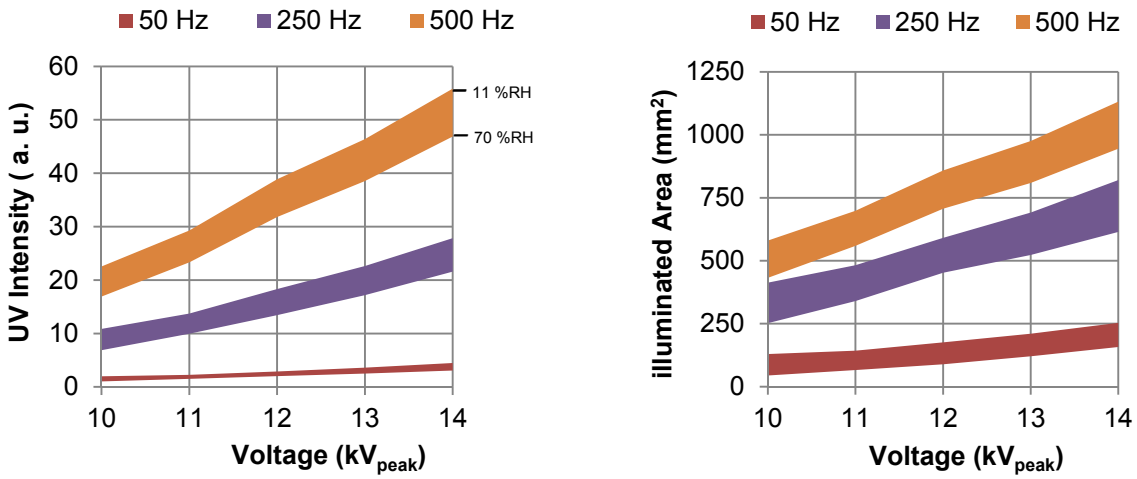

Figure 5.10: Humidity impact on UV characteristics

The influence of the temperature of discharge zone has not been widely examined. Nevertheless, a physical explanation could be introduced to illustrate these results. Temperature rise in a constant pressure environment results in gas expansion according to the general gas equation [5.4]; where **p** is gas pressure, **V** is volume, **N** is the number of moles, **R** is the universal gas constant (8.3144 j/mole-K), and **T** is the absolute temperature.

$$\mathbf{pV = NRT} \quad [5.4]$$

$$\bar{\lambda} = \frac{1}{4\sqrt{2}\pi r^2 n} \quad [5.5]$$

The mean free path $\bar{\lambda}$ is calculated from equation [5.5], where it depends on both the radius of colliding molecules r as well as gas molecular density n [NAS-71]. Gas expansion results in a decrease in the gas density and in turn an increase in the mean free path. With longer mean free path length, the electrons can, in collision with a neutral molecule, gain kinetic energy sufficient for ionization at smaller values of field strength. Therefore, the ionization boundary (x_0, E_0) in figure 5.11 is shifted from point (a) to (b) resulting in an extended discharge area.

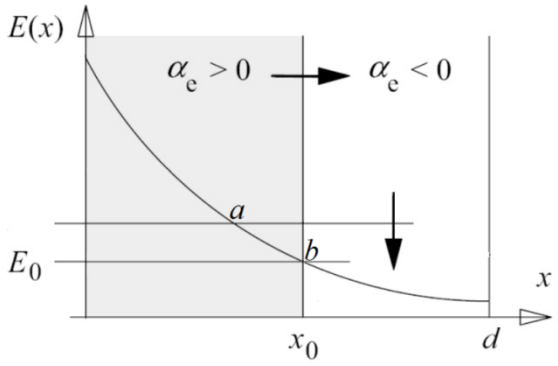

Figure 5.11: Influence of temperature rise on ionization boundary

5.3.3. Erosion Characteristics

The environmental factors of influence were found to be directly correlated to material erosion as shown in figure 5.12. The rate of change in eroded area and volume is nearly constant with respect to the change in the involved influencing factor. On the other hand, maximum erosion depth is nearly constant with humidity increase at low temperature degrees. Therefore, it can be stated that maximum erosion depth is not humidity dependent at room temperature; however it depends much more on discharge intensity (see section 5.2.2). At high temperature it exhibits a decreasing trend with humidity increase. It is referred to the impact of humid conditions on discharge parameters.

The above results elucidate that erosion in the high electric field region in front of the needle tip (maximum erosion depth location) is mainly guided by discharge. However, getting far from the needle tip incorporates environmental factors as factors assisting the less intensive discharges far from needle tip in the evolution of surface erosion. The independence of maximum erosion depth with respect to humidity increase is consistent with the results obtained by [MOR-00], [MOR-01a], where the humidity has an influence only when mechanical bending stresses are applied.

Nonlinear regression on the obtained erosion characteristics yields equations [5.6] to [5.8], whereby eroded volume Vol is in mm^3, eroded area A is in mm^2, maximum erosion depth D_{max} is in µm, temperature of discharge medium ϑ is in ℃ and the humidity H is in %RH.

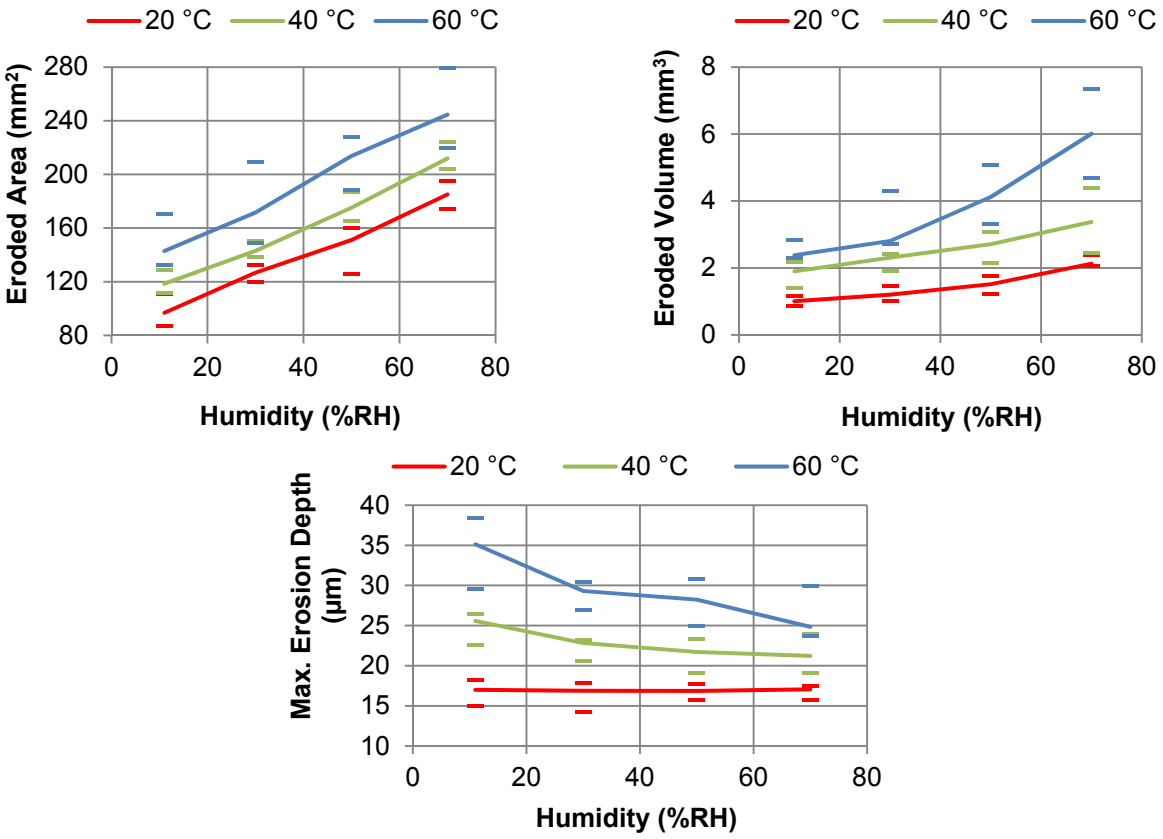

Figure 5.12: Erosion area and volume (median, span of 5 samples), other settings see table 5.4

$$\boldsymbol{Vol}[\boldsymbol{mm^3}] = \mathbf{0.040} + \mathbf{0.043} \cdot [\boldsymbol{\vartheta}[°\mathrm{C}]] + \mathbf{2{,}277} \times \mathbf{10^{-3}} \cdot [\boldsymbol{\vartheta}[°\mathrm{C}]]^{\mathbf{0{,}840}} \cdot \left[\frac{\boldsymbol{H}[\%\boldsymbol{RH}]}{\mathbf{11}\ \%\boldsymbol{RH}}\right]^{\mathbf{2}} \quad [5.6]$$

$$\boldsymbol{A}[\boldsymbol{mm^2}] = \mathbf{45.813} + \mathbf{1.393} \cdot [\boldsymbol{\vartheta}[°\mathrm{C}]] + \mathbf{17} \cdot \left[\frac{\boldsymbol{H}[\%\boldsymbol{RH}]}{\mathbf{11}\ \%\boldsymbol{RH}}\right] \quad [5.7]$$

$$\boldsymbol{D_{max}}[\boldsymbol{\mu m}] = \mathbf{7.37} + \mathbf{0{,}45} \cdot [\boldsymbol{\vartheta}[°\mathrm{C}]] - \mathbf{0.035} \cdot [\boldsymbol{\vartheta}[°\mathrm{C}]] \cdot \left[\frac{\boldsymbol{H}[\%\boldsymbol{RH}]}{\mathbf{11}\ \%\boldsymbol{RH}}\right] + \mathbf{0.68} \cdot \left[\frac{\boldsymbol{H}[\%\boldsymbol{RH}]}{\mathbf{11}\ \%\boldsymbol{RH}}\right] \quad [5.8]$$

From the above equations, it could be concluded that both $\boldsymbol{Vol}$ and $\boldsymbol{A}$ are dependent on the influencing factors. However, the interaction between both factors could be proven in terms of eroded volume and not in eroded area. Regarding maximum erosion depth $\boldsymbol{D_{max}}$, however the humidity term appears in equation [5.8], it could be assumed that the two terms including humidity at 20°C are very small (-0.02 to -0.13 µm for the investigated humidity range) compared to the other terms (16.37 µm). Therefore, it can be stated that $\boldsymbol{D_{max}}$ is humidity independent at room temperature; whereas it exhibits a strong dependence on the temperature of discharge zone. The impact of temperature on erosion severity is both in direct and indirect way. Erosion severity increase was observed as an impact of temperature as shown in figure 5.12. The indirect influence is the enhancement of discharge intensity with temperature rise figure 5.9, which in turn has a direct influence on surface erosion. In this way the surface characteristics during corona stresses are clearly influenced by temperature.

5.3.4. XPS Results

The influence of ambient conditions on material surface stressed with constant corona discharge was studied in terms of material composition through the XPS analysis. The impact of both temperature and humidity of discharge medium can be identified, through the analysis of peaks area variation. This study was performed as a function of humidity and temperature, which were examined on two levels of 11 %RH and 70 %RH for humidity and 20°C and 60°C for temperature. Deconvolution models of C 1s peak of stressed specimens under different ambient conditions are analyzed as listed in table 5.5.

Table 5.5: Area change in C 1s deconvolution peaks (with respect to the whole envelope area of C 1s peak) and O 1s peak (normalized to that of virgin material specimens) of stressed specimens under different ambient conditions, 12 kV_{peak}, 500 Hz, 96 hours

Analyzed specimens	***Stress parameters***		***C 1s deconvolution***				***relative O 1s peak***
	ϑ °C	***RH %***	***C – H, C – C %***	***C – OH %***	***C = O %***	***O = C – OH %***	$\frac{O\ 1s}{(O\ 1s)_{virgin}}$
Virgin			65.89	23.17	4.12	6.82	1
Stressed	20	11	55.53	29.05	5.31	10.11	1.47
	20	70	52.20	31.10	6.82	9.88	1.09
	60	11	52.25	32.35	6.17	9.23	1.27
	60	70	47.76	35.06	6.10	11.08	1.73

When both environmental stresses increase, the concentration of C–H, C–C peak is decreased due to the increase of bond dissociation of such groups under stress to produce more oxygen bonds. Additionally, the area under the peak of oxygen containing hydroxyl groups (C–OH) exhibits an increase with the stress imposed from environmental factors. At low temperature degrees the humidity of discharge medium enlarges the concentration of C=O peak, present in ketones [–C=O] or aldehydes [–CH=O]. At high temperature degrees, the humidity of discharge medium enlarges the concentration of O=C–O bonds due to esters [O=C–O–C] and carboxylic acids [COOH].

It can be also seen in figure 5.13 that the amount of O 1s / C 1s ratio is larger for environmentally stressed specimens compared to the unstressed one. This confirms the influence of both temperature and humidity on enhancing the concentration of oxygen bonds. Additionally, it is noted that at higher temperature degrees (i.e. 60°C), the O 1s / C 1s ratio exhibits an increasing trend with humidity increase. However, at lower temperature degrees (i.e. 20°C) humidity increase results in a slight decrease in the O 1s / C 1s.

The area of O 1s peak with respect to that of the virgin specimen obtained with high resolution of 0.1 eV is listed in table 5.5. It can be seen that the amount of O 1s is larger for environmentally stressed specimens compared to the unstressed ones. This confirms the effect of both factors on enhancing O_2 concentration. Moreover, it is noted that at higher temperature degrees (i.e. 60°C), O 1s ratio exhibits an increasing trend with humidity increase. At low temperature degrees (i.e. 20°C), humidity increase leads to a decrease in the area of O 1s peak.

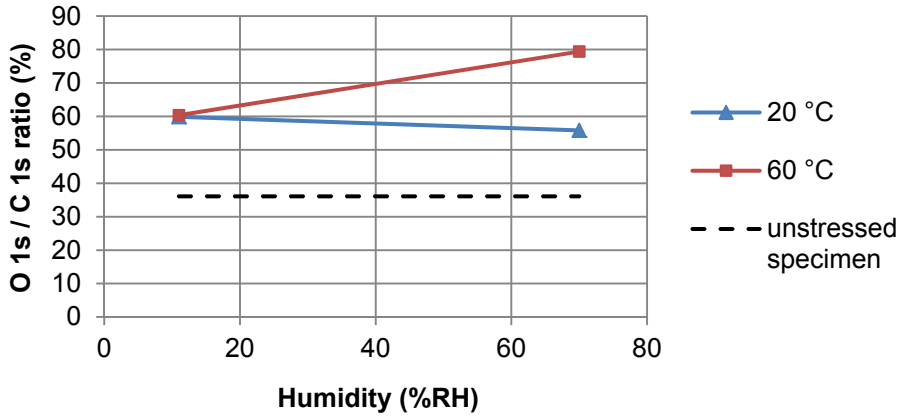

Figure 5.13: Influence of environmental factors on material composition (12 kV_{peak}, 500 Hz, 96 h)

Table 5.6 illustrates the Si 2p deconvolution models of the stressed specimens, which result in further explanation of the material response to different stresses. The influence of humidity increase on the percentage area of the silica peaks. Here the humidity of discharge medium has no influence on the silica peaks either at high or low temperature degrees. It was found that temperature introduces a dominant factor of influence on the Si 2p deconvolution peaks. Rising temperature from 20°C to 60°C results in an increase in the area of double bonded silica peak from ~67% to ~74%. Considering the results in 5.2.4, there is no influence of discharge stress on material composition in terms of oxidation of silica peaks. Therefore, the resulting increase in the oxidation degree of material surface could be referred to the influence of temperature rise. Although these results in the surface composition influenced by ambient conditions under discharge stresses have no comparable investigations in the literature, it is physically interpretable and can be regarded as leading results in this point.

Table 5.6: Area change in Si 2p deconvolution peaks (with respect to the whole envelope area of Si 2p peak) of stressed specimens under different ambient conditions, 12 kV_{peak}, 500 Hz, 96 hours

Stress Parameters		***Si 2p deconvolution***	
ϑ °C	***RH %***	***SiO_2 %***	***SiO %***
20	11	67.22	32.78
20	70	67.32	32.68
60	11	73.70	26.30
60	70	73.66	26.34

5.3.5. Statistical Models

In this section the influence of environmental factors was studied for all the properties of concern. Temperature was examined in three levels; 20, 40, and 60°C, whereas 4 levels are applied for humidity; 11, 33, 50, and 70 %RH. The confidence level is 95% and the adjusted significance level for the hypothesis test is 0.05. The different variables under analysis are: eroded volume (***Vol***), erode area (***A***), maximum erosion depth (D_{max}), total discharge energy (E_T), cumulative charge (Q_{cum}), UV Intensity (I_{UV}) and UV illuminated area (A_{UV}). All the five examined models are summarized in table 5.7 to explain the main factors of influence on the studied response in each mode.

Table 5.7: Summary of the statistical models and the correlation coefficients for all variables

Model	1	2	3	4	5
Response	Eroded Volume	Eroded Area	Max. Erosion Depth	Total Discharge Energy	Cumulative Charge
Covariates	**A** • p-value: 0.00 • CC: 0.896	**Vol** • p-value: 0.00 • CC: 0.896	---	---	**E_T** • p-value: 0.00 • CC: 0.978
Impact of Temperature	significant • p-value: 0.004 • CC: 0.537	insignificant • p-value: 0.16 • CC: 0.734	significant • p-value: 0.00 • CC: 0.888	significant • p-value: 0.00 • CC: 0.690	significant • p-value: 0.00 • CC: 0.741
Impact of Humidity	significant • p-value: 0.00 • CC: 0.782	significant • p-value: 0.00 • CC: 0.487	significant • p-value: 0.00 • CC: -0.236	significant • p-value: 0.00 • CC: -0.651	significant • p-value: 0.00 • CC: -0.621
Interaction	significant • p-value: 0.00	significant • p-value: 0.00	significant • p-value: 0.005	significant p-value: 0.032	significant • p-value: 0.00

The results for each model in the table determine the effective covariates for the examined response. Additionally, the influence of the both stressing factors as well as their interaction is verified. One of the examined models is illustrated in detail and the results are then taken from the optimum refitted model. After eliminating covariates, which have no significance on the examined response in each model, the refitted model is run to obtain the final results (see figure 5.14). The optimum refitted model presents the analysis of variance for eroded volume. It could be inferred that temperature and humidity as well as their interaction have a significant influence on eroded material volume.

Tukey's test provides grouping information and two sets of multiple comparison intervals; one group for temperature levels and the other for humidity. In the grouping table of the temperature set, factor levels within the same group are significantly different from each other. Therefore, all levels means have significantly different eroded volume degree. Humidity levels within the same group are significantly different from each other except for the last two levels, 11 %RH and 33 %RH, as they share the same group. Therefore, both means of those levels have quite similar impact in terms of eroded volume degree. The first 95% confidence interval in the first set (temperature) of the Tukey's output is 0.5153 to 1.396. That is, the mean eroded volume resulting from 40°C minus that from 20°C is somewhere between 0.5153 to 1.396 mm^3. This means that the resulting eroded volume is larger for higher temperature. The other intervals in both sets are interpreted in the same way. The impact of all stresses differs significantly because all of the confidence intervals exclude zero. Therefore, all stresses have significantly different average impact on eroded volume.

From the examined models concerned with erosion characteristics and discharge parameters, the following can be concluded:

- Eroded volume and eroded area exhibit covariance in between and direct correlation of 0.896. Although temperature is directly correlated to the eroded area with 0.734, it could not be proven that it has a significant influence on this erosion characteristic. Temperature cannot be removed from the model as it is clearly still important, but in the form of an interaction with humidity. Interaction between both factors significantly exists in terms of all erosion characteristics.

General Linear Model: Eroded Volume versus Temperature; Humidity

```
Factor       Type   Levels  Values
Temperature  fixed       3  20; 40; 60
Humidity     fixed       4  11; 33; 53; 70
Analysis of Variance for Eroded Volume, using Adjusted SS for Tests
Source                DF   Seq SS  Adj SS  Adj MS       F      P
Eroded Area            1  101,351  12,199  12,199  154,49  0,000
Temperature            2   12,185   0,995   0,497    6,30  0,004
Humidity               3    3,975   3,699   1,233   15,61  0,000
Temperature*Humidity   6    4,982   4,982   0,830   10,51  0,000
Error                 47    3,711   3,711   0,079
Total                 59  126,204
S = 0,281011   R-Sq = 97,06%   R-Sq(adj) = 96,31%
Grouping Information Using Tukey Method and 95,0% Confidence
Temperature   N  Mean  Grouping
60           20   4,1  A
40           20   2,4    B
20           20   1,5      C
Means that do not share a letter are significantly different.
Tukey 95,0% Simultaneous Confidence Intervals
Response Variable Eroded Volume
All Pairwise Comparisons among Levels of Temperature
Temperature = 20  subtracted from:
Temperature   Lower  Center  Upper  ---+---------+---------+---------+---
40           0,5153  0,9556  1,396  (------*-----)
60           2,1661  2,6064  3,047                          (-----*------)
                                    ---+---------+---------+---------+---
                                     0,70      1,40      2,10      2,80
Temperature = 40  subtracted from:
Temperature  Lower  Center  Upper  ---+---------+---------+---------+---
60           1,210   1,651  2,091           (------*-----)
                                   ---+---------+---------+---------+---
                                    0,70      1,40      2,10      2,80
Grouping Information Using Tukey Method and 95,0% Confidence
Humidity   N  Mean  Grouping
70        15   3,9  A
53        15   2,8    B
33        15   2,1      C
11        15   1,9      C
Means that do not share a letter are significantly different.
Tukey 95,0% Simultaneous Confidence Intervals
Response Variable Eroded Volume
All Pairwise Comparisons among Levels of Humidity
Humidity = 11  subtracted from:
Humidity    Lower  Center   Upper  -----+---------+---------+---------+-
33        -0,3838  0,1751  0,7340  (------*------)
53         0,2568  0,8157  1,3747         (------*------)
70         1,3770  1,9359  2,4949                (------*------)
                                   -----+---------+---------+---------+-
                                      0,00      0,80      1,60      2,40
Humidity = 33  subtracted from:
Humidity    Lower  Center  Upper  -----+---------+---------+---------+-
53        0,08167  0,6406  1,200        (------*------)
70        1,20187  1,7608  2,320                (------*------)
                                  -----+---------+---------+---------+-
                                     0,00      0,80      1,60      2,40
Humidity = 53  subtracted from:
Humidity   Lower  Center  Upper  -----+---------+---------+---------+-
70        0,5613   1,120  1,679           (------*------)
                                 -----+---------+---------+---------+-
                                    0,00      0,80      1,60      2,40
```

Figure 5.14: The optimum refitted model for eroded volume (Model 1)

- Temperature proved to have an influence on total discharge energy and cumulative charge in the form of direct correlation of 0.690 and 0.741, respectively. Interaction between both factors significantly affects discharge parameters.
- From model 4, humidity has an influence on total discharge energy and cumulative charge in the form of inverse correlation of - 0.651 and - 0.621, respectively.
- Model 3 proved the influence of humidity on maximum erosion depth, which are inversely correlated with a correlation coefficient of - 0.236 (weakly correlated).
- The week correlation between humidity and maximum erosion depth leads to the fact that erosion in the high electric field region in front of needle tip (maximum erosion depth location) is mainly guided by electrical stressing factors.

5.4. Interaction between Voltage Magnitude and Humidity

As a matter of fact the polymeric insulating materials are subjected in service to several aging stress factors which are mainly environmental, electrical and mechanical. Accelerated environmental stressing performed on EPDM and HTV SIR used for high voltage insulators did not reveal the same degradation observed in service [DE-90]. This could be explained by the fact that when several aging factors are simultaneously affecting a material, synergistic effects may occur. The influence of humidity on discharge parameters and UV characteristics were examined in section 5.2.2. It was shown that cumulative charge is negatively correlated to humidity change and UV characteristics are reduced with increasing humidity degree of discharge medium. Those results necessitate the investigation of interaction that could exist between electrical stresses and humidity.

5.4.1. Testing Procedure

Factorial analysis was performed on two factors in terms of discharge parameters and erosion severity of specimen surface. The analysis was performed between electrical stressing factor (magnitude of the test voltage) and humidity of discharge medium. The settings for the other factors of influence were kept constant as shown in table 5.8. It is now possible to hold a correlation between voltage and humidity in terms of the resulting damage. It is also possible to perform an interaction analysis between both factors. In the listed table below the test voltage is examined at 3 levels, 10, 12, and 14 kV_{peak}, while humidity is studied at 3 levels 11, 33, and 70 %RH.

Table 5.8: Test conditions for studying the interaction between test voltage and humidity of discharge medium

Voltage (kV)	***Frequency (Hz)***	***Time (hours)***	***Temperature (°C)***	***Humidity (%RH)***
10, 12, and 14	*500*	*96*	20	*11, 33, and 70*

5.4.2. Discharge Parameters

After investigating the nine combinations of both factors, discharge parameters were calculated for each and displayed below in figure 5.15. In general, the behavior of both discharge characteristics is obviously influenced by both factors; exhibiting direct correlation with voltage and inverse trend with humidity. The influence of test voltage as well as humidity has been separately examined in the previous sections 5.2.2 and 5.3.2, respectively, which revealed the same results. This factorial analysis between test voltage and humidity is mandatory to check the interaction in between. However, the graphs are not sufficient to judge, whether there is an interaction between both factors or not. In order to answer the question, statistical model has to be constructed and analyzed.

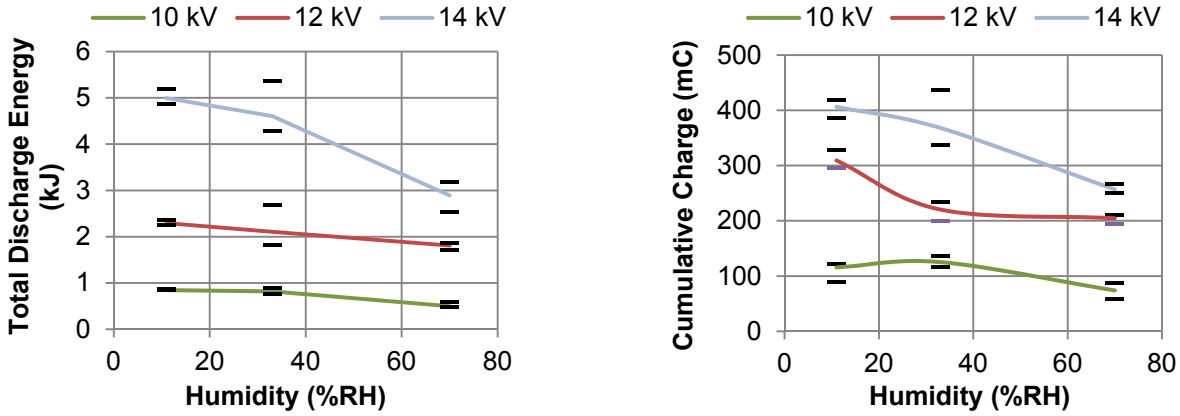

Figure 5.15: Discharge parameters (median, span of five samples each), other settings see table 5.8

5.4.3. Erosion Characteristics

Material erosion characteristics were found dependent on both factors of influence, voltage and humidity; where a direct correlation is clear as shown in figure 5.16. Maximum erosion depth is significantly dependent on test voltage magnitude. In contrast, humidity introduces no influence on maximum erosion depth regardless of test voltage level. The interaction between both factors in terms of erosion severity is not clear and needs further statistical analysis to examine, if exists.

5.4.4. Statistical Models

The influence of voltage magnitude as well as humidity was studied for all properties of concern. Test voltage magnitude was examined at three levels; 10, 12, and 14 kV_{peak}, while humidity is studied at three levels 11, 33, and 70 %RH. The selected confidence level is 95% and the adjusted significance level for the hypothesis test is 0.05. All the five examined models are summarized in table 5.9 to explain the main factors of influence on the studied response in each mode. The results for each model in the table determine the effective covariates for the examined response. Additionally, the influence of the both stressing factors as well as their interaction is checked.

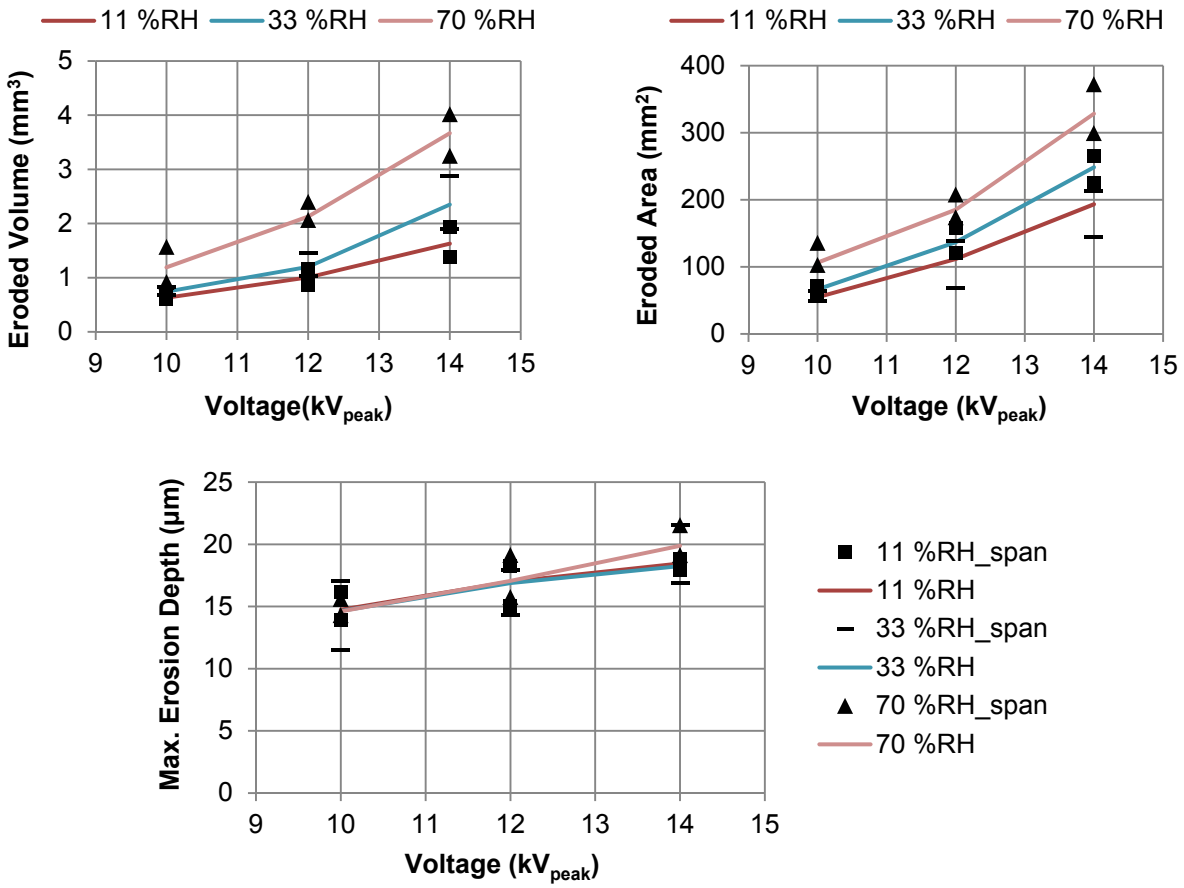

Figure 5.16: Erosion characteristics (median, span of five samples each), other settings see table 5.8

Table 5.9: Summary of the statistical models and the correlation coefficients for all variables

Model	1	2	3	4	5
Response	Eroded Volume	Eroded Area	Max. Erosion Depth	Total Discharge Energy	Cumulative Charge
Covariates	--	--	**A** • p-value: 0.00 • CC: 0.783	**Q_{cum}** • p-value: 0.00 • CC: 0.952	**E_T** • p-value: 0.00 • CC: 0.952
Impact of Voltage	significant • p-value: 0.00 • CC: 0.746	significant • p-value: 0.00 • CC: 0.836	significant • p-value: 0.029 • CC: 0.606	significant • p-value: 0.00 • CC: 0.914	significant • p-value: 0.00 • CC: 0.856
Impact of Humidity	significant • p-value: 0.00 • CC: 0.548	significant • p-value: 0.001 • CC: 0.428	insignificant • p-value: 0.141 • CC: 0.319	significant • p-value: 0.00 • CC: -0.274	significant • p-value: 0.00 • CC: -0.396
Interaction	significant • p-value: 0.00	insignificant • p-value: 0.087	insignificant • p-value: 0.193	significant • p-value: 0.00	significant • p-value: 0.00

One of the examined models is illustrated in detail and the results are then taken from the optimum refitted model. The optimum refitted model displayed in figure 5.17 presents the analysis of variance for maximum erosion depth. It could be inferred that voltage magnitude has a significant influence on maximum erosion depth. However, humidity as well as its interaction with voltage magnitude has no influence on this erosion property.

General Linear Model: Max. Erosion Depth versus Voltage; Humidity

```
Factor    Type   Levels  Values
Voltage   fixed       3  10; 12; 14
Humidity  fixed       3  11; 33; 70

Analysis of Variance for Max. Erosion Depth, using Sequential SS for Tests

Source            DF   Seq SS  Adj SS   Seq MS      F      P
Eroded Area        1  120,964  21,398  120,964  84,42  0,000
Voltage            2   11,212  10,359    5,606   3,91  0,029
Humidity           2    5,947   1,651    2,973   2,08  0,141
Voltage*Humidity   4    9,248   9,248    2,312   1,61  0,193
Error             35   50,154  50,154    1,433
Total             44  197,524

S = 1,19707   R-Sq = 74,61%   R-Sq(adj) = 68,08%

Grouping Information Using Tukey Method and 95,0% Confidence
Voltage   N  Mean  Grouping
14       15  17,8  A
12       15  16,9  A
10       15  14,7    B

Means that do not share a letter are significantly different.

Tukey 95,0% Simultaneous Confidence Intervals
Response Variable Max. Erosion Depth
All Pairwise Comparisons among Levels of Voltage
Voltage = 10  subtracted from:
Voltage   Lower  Center  Upper  --+---------+---------+---------+----
12       0,8544   2,114  3,373          (-------*-------)
14       1,8489   3,108  4,368                (--------*-------)
                             --+---------+---------+---------+----
                             0,0       1,5       3,0       4,5
Voltage = 12  subtracted from:
Voltage    Lower  Center  Upper  --+---------+---------+---------+----
14       -0,2650  0,9945  2,254  (--------*-------)
                                 --+---------+---------+---------+----
                                 0,0       1,5       3,0       4,5

Grouping Information Using Tukey Method and 95,0% Confidence
Humidity   N  Mean  Grouping
70        15  17,4  A
33        15  16,3  A B
11        15  15,8    B

Means that do not share a letter are significantly different.

Tukey 95,0% Simultaneous Confidence Intervals
Response Variable Max. Erosion Depth
All Pairwise Comparisons among Levels of Humidity
Humidity = 11  subtracted from:
Humidity    Lower  Center  Upper  -------+---------+---------+---------
33        -0,7418  0,5176  1,777  (-----------*-----------)
70         0,3476  1,6070  2,867            (-----------*-----------)
                                  -------+---------+---------+---------
                                       0,0       1,0       2,0
Humidity = 33  subtracted from:
Humidity    Lower  Center  Upper  -------+---------+---------+---------
70        -0,1701   1,089  2,349       (-----------*-----------)
                                  -------+---------+---------+---------
                                       0,0       1,0       2,0
```

Figure 5.17: The optimum refitted model for maximum erosion depth (Model 3)

Tukey's test provides grouping information and two sets of multiple comparison intervals; one group for voltage magnitude levels and the other for humidity. In the grouping table for the set of voltage magnitude, the first two levels, 14 kV_{peak} and 12 kV_{peak}, share the same group. Therefore, both means of those levels have quite similar impact in terms of the degree of maximum erosion depth. The levels of the second set concerned with humidity are overlapping in grouping details, which confirms the independence of maximum erosion depth with respect to humidity change.

All 95% confidence interval in the first set (voltage magnitude) of the Tukey's output exclude zero, which means that the impact of all stresses differs significantly. Therefore, all stresses have significantly different average impact on maximum erosion depth. However, all the means of all humidity stresses in the second set exhibit an overlap, which is referred to the ineffectual impact of humidity on the erosion depth.

From the five models examined above concerned with erosion characteristics associated with correlation coefficients of examined variables, the following is concluded:

- There is no interaction between examined factors; i.e. test voltage and humidity in terms of eroded area as well as maximum erosion depth. Nevertheless, an interaction exists between both factors in terms of eroded volume. This interaction assumes that for the same amount discharge on material surface the higher the humidity of discharge medium, the more powerful the charged particles in erosion evolution. This confirms the synergism between test voltage and humidity in terms of erosion severity.
- Voltage magnitude and humidity exhibit significant influence on both discharge parameters; beside their interaction which could also be proven. Total discharge energy and cumulative charge exhibit covariance in between and direct correlation of 0.952.
- Both discharge parameters are dependent on test voltage with CCs of 0.914 and 0.856; whereas humidity introduces negative correlation with CCs of -0.274 and -0.396. The higher correlation coefficients with respect to test voltage than humidity proves that test voltage is the dominant factor here controlling discharge parameters.

5.5. Oxygen-free Environment

Corona discharge erosion processes fall broadly into three categories: those initiated by ion bombardment, by chemical reactions or by photon bombardment (UV). In air, nitrogen is inert gas and causes damage by bombardment whereas oxygen is active and causes damage by all mechanisms. In order to limit the effect of chemical reactions and to consider only the combined effect of ion and photon bombardment, discharge medium will be pure nitrogen. Beside that the effect of humidity is also limited and there is no possibility of acid attacks.

5.5.1. Methodology

In order to obtain oxygen-free environment, in which we study the influence of electrical discharges on material erosion, the following procedures were performed.

A. Oxygen Absorbers

Oxygen absorbers reduce oxygen concentration within a sealed container creating a very low-oxygen environment. The used oxygen absorber (ATCO FTM 1000) enables oxygen concentrations to reach values below 0.1% within 48 hours at an ambient temperature (20°C). The rate of oxygen absorption is in fact dependent upon temperature of the medium. The higher it is, the quicker the reaction is between the absorber and oxygen. Oxygen absorber is used in the form of 30 g polypropylene sachet with dimensions of 80 mm x 80 mm x 12 mm, which contain a mix of mineral active matters iron- and iron oxide-based.

Five oxygen absorber sachets are placed in the bottom of the test vessel and distributed on the surface and not stacked. This flat distribution is to guarantee the highest performance of the absorber and as the stack will result in temperature rise between sachets. The maximum handling time elapsed between removing oxygen absorbers from the vacuum pack and sealing within the intended place of use is one hour at (20°C). The assigned number of sachets is chosen to absorb the volume of oxygen within vessel as well as the volume of oxygen probably permeating through the vessel during the duration of treatment.

B. Flushing Nitrogen

Connected test setup is placed inside the test vessel about 40 mm above the oxygen absorber sachets. Inside the test vessel a GGO 370 oxygen sensor is attached and connected to oxygen meter GMH 3691 to display oxygen concentration during treatment. This device is capable of measuring oxygen concentrations form 0 to 100% O_2 gaseous with 0.1% accuracy. Then, the vessel is sealed and flushed with nitrogen from nitrogen bottle feeding to the side opening of the vessel. In such a way a very low-oxygen condition of approximately 0.4% is guaranteed, especially when combined with O_2 absorbers. Flushing time in such a way is only one hour in order to reach the desired O_2 concentration. Additionally there is no need to repeat flushing during test thanks to the oxygen absorbers which keeps O_2 concentration below 1%.

Flushing with nitrogen without using oxygen absorbers reduces the oxygen content to approximately 4% which depends greatly on the purity of the used nitrogen. If flushing is to be carried out only by gas from nitrogen bottles the flushing time and frequency may have to be prolonged to reach the target value. In addition, residual oxygen must be checked several times during the treatment, and flushing must be frequently repeated which would significantly affect the discharge medium.

5.5.2. Testing Procedure

Factorial analysis was performed on two test series in terms of discharge parameters and erosion severity of specimen surface. The analysis was performed between electrical stressing factors, magnitude and frequency of the test voltage. The settings for environmental factors of influence were kept constant as shown in table 5.10. It is now possible to make a correlation between the electrical stresses under study and the resulting damage. It is also possible to perform an interaction analysis between both stresses. In the listed table below the test voltage is examined at three levels, 10, 12, and 14 kV_{peak}, while the frequency of test voltage is studied at two levels 250 and 500 Hz.

Table 5.10: Test conditions for oxygen-free environment

Voltage (kV)	*Frequency (Hz)*	*Temperature (°C)*	*Humidity (%RH)*	*O_2 Concentration*
10, 12 and 14	*250 and 500*	20	*33*	*< 1%*

5.5.3. Discharge Parameters

The effect of this different discharge medium, oxygen-free environment, on discharge parameters was studied under different electrical stressing condition. The response of each discharge parameter is calculated and displayed in figure 5.18. It is clear that both voltage and frequency exhibits a significant influence on discharge parameters in form of direct correlation. Significant interaction obviously exists between both stresses concerning the examined parameters. This behavior is quite similar to that of discharge parameters calculated for air discharge medium in section 5.2.2 on the level of both magnitudes and rates of change. The behavior of discharge intensity with respect to electrical stressing factors is consistent with the results introduced by [MAS-78]. Mason has proven that there is almost no difference between the behavior of discharge intensity along with electrical stressing factors in nitrogen and that occurring in air.

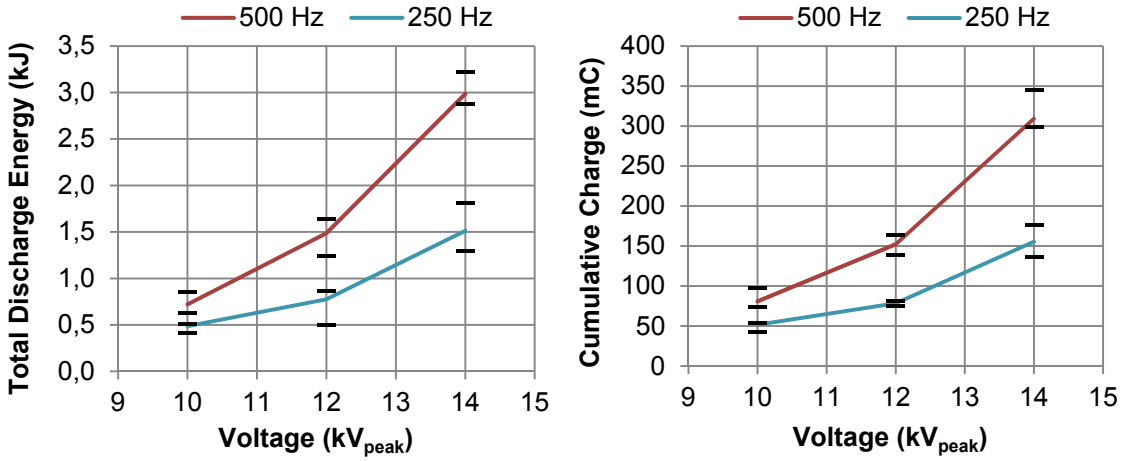

Figure 5.18: Discharge parameters (median, span of five samples each), other settings see table 5.10

5.5.4. Erosion Characteristics

Electrical stressing factors of influence were found to be directly correlated to material erosion characteristics, eroded area and volume, as shown in figure 5.19. There is also clear evidence on interaction between both stresses. On the other hand, maximum erosion depth introduces a slow rate of change with frequency increase; whereas it is comparatively dependent on test voltage magnitude with a higher rate of change. Additionally, there is no proof that interaction exists between both factors in terms of maximum erosion depth. In contrast to literature the erosion severity under discharge stresses in nitrogen medium has not been widely examined before.

Nonlinear regression on the obtained erosion characteristics yields the following equations from [5.9] to [5.11]. From the above equations, it could be concluded that the rate of increase of eroded area and eroded volume with respect to both electrical influencing factors is much higher than that of maximum erosion depth. In order to clarify the role of oxygen in discharge medium the results are compared to those obtained from discharge stressed specimens in air (see figure 5.3). It can be clearly observed that the erosion severity here does not exceed 30% compared to that in air under the same stress conditions. This could be referred to the role of oxygen in the erosion evolution either as an individual stress factor or via interaction with other stresses. Another point is the closed desiccator here that keeps the same gas molecules along the whole stress period; whereas an adequate air flow is applied to the discharge stressed specimens in air. This air flow supplies the discharge medium with new gas molecules that take part in the erosion process. Although the discharge intensity is quite close to that occurring in air, the different erosion mechanisms expected for both test environments.

$$Vol[mm^3] = 5 \times 10^{-6} \cdot \left[\frac{f[1/s]}{50\ 1/s}\right] \cdot \left[\frac{V}{kV_{peak}}\right]^4 \quad [5.9]$$

$$A[mm^2] = 2.6 \times 10^{-3} \cdot \left[\frac{f[1/s]}{50\ 1/s}\right]^{0,909} \cdot \left[\frac{V}{kV_{peak}}\right]^{3,5} \quad [5.10]$$

$$D_{max}[\mu m] = 0.078 \cdot \left[\frac{f[1/s]}{50\ 1/s}\right]^{0,21} \cdot \left[\frac{V}{kV_{peak}}\right]^{1,8} \quad [5.11]$$

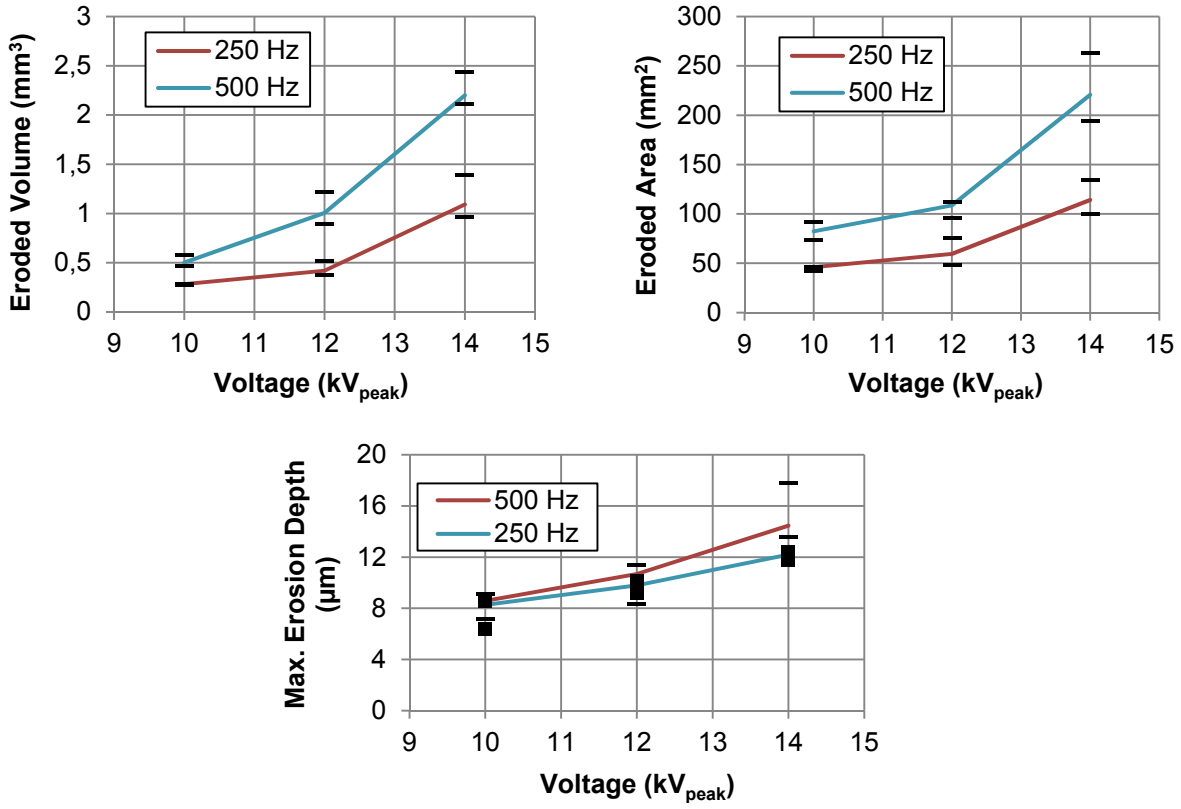

Figure 5.19: Erosion characteristics for oxygen-free (median, span of five samples each), other settings see table 5.10

5.5.5. XPS Results

In this section the influence of oxygen-free discharge medium on material surface in terms of material composition is studied by XPS analysis. The stresses under study are the electrical influencing factors; test voltage magnitude and frequency. This study is performed as a function of both stresses, which are examined on the levels of 500 Hz and 250 Hz for frequency and 10 kV and 14 kV for voltage magnitude. Deconvolution models for C 1s peaks are obtained for stressed specimens in oxygen free conditions under different electrical stresses as illustrated in table 5.11. Under stress impact, the concentration of C–H, C–C peak is decreased due to the increase of bond dissociation of such groups to react with oxygen and produce more oxygen bonds.

Moreover, the oxygen containing hydroxyl groups in the form of alcohols (C–OH) is increased with electrical stresses. The increase in oxygen containing functional groups is seen as a direct effect of material degradation due to electrical discharges. In contrast to the specimens stressed under the same conditions in is air, the behavior is quite similar in terms of oxidation degree which is clearly influenced by discharge activity.

Table 5.11: Area change in C 1s deconvolution peaks (with respect to the whole envelope area of C 1s peak) and O 1s peak (normalized to that of virgin material specimens) of discharge stressed specimens in oxygen-free environment, 20°C, 33 %RH, 96 hours

Analyzed specimens	***Stress parameters***		***C 1s deconvolution***				***relative O 1s peak***
	V kV_{peak}	f Hz	***C – H, C – C %***	***C – OH %***	***C = O %***	***O = C – OH %***	$\frac{O\ 1s}{(O\ 1s)_{virgin}}$
Virgin			65.89	23.17	4.12	6.82	1
Stressed	10	250	57.97	26.18	7.39	8.46	1.59
	10	500	57.57	28.37	5.58	8.48	1.38
	14	250	55.53	28.53	7.20	8.74	2.37
	14	500	55.98	29.90	6.42	7.70	1.68

Finally, the amount of O 1s / C 1s ratio is observed to be higher for the stressed specimens compared to the unstressed ones as shown in figure 5.20. Therefore, the influence of electrical discharges on accelerating oxidation process is ensured. Additionally there is no clear effect of electrical stresses on the variation of this ratio. Those results need to be confirmed by comparing O 1s peaks obtained with high resolution of 0.1 eV.

Area of O 1s peaks obtained with high resolution of 0.1 eV under different stresses is listed in table 5.11. Here the oxygen amount of material composition increases with the rise of test voltage magnitude; whereas applying higher test frequency results in a slight decrease in the area under the O 1s peak. Therefore, it can be stated that the change in the magnitude of the electrical stresses has a significant influence on the oxidation occurring on material surface under stress.

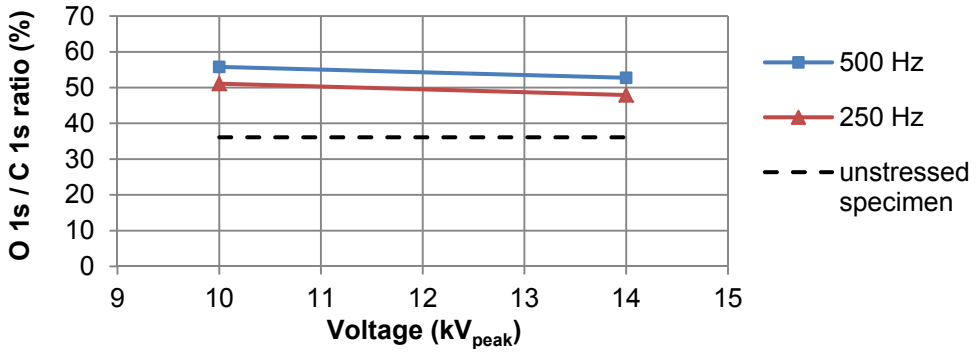

Figure 5.20: Material composition of stressed specimens in oxygen-free environment

Those results imply that gas phase reactions are only of secondary importance compared to surface composition change caused by discharge particles activity. This is supported by XPS analysis of unstressed surfaces and those stressed in air and oxygen-free environments. Whereby, the determined surface compositions indicate the significant importance of initial oxygen content which was about 23% for a virgin specimen (see figure 5.4) opposed to 29% for oxygen-free medium and 30% for specimens stressed in air (see figure 5.21). Hence irrespective of whether oxygen is present in the gas or in the solid phase, it will participate in surface oxidation. These results and the drawn conclusion are consistent with [HUD-92].

5.5.6. Statistical Models

ANOVA statistical models for the sake of investigating all property variables influenced by electrical factors were analyzed. Test voltage magnitude was examined at three levels; 10, 12, and 14 kV_{peak}, while the frequency of the test voltage was studied at two levels 250 and 500 Hz. The selected confidence level is 95% and the adjusted significance level for the hypothesis test is 0.05. All the five examined models are summarized in table 5.12 to explain the main factors of influence on the studied response in each model. The results for each model in the table determine the effective covariates for the examined response. Additionally, the influence of the both stressing factors as well as their interaction is checked.

Table 5.12: Summary of the statistical models and the correlation coefficients for all variables

Model	1	2	3	4	5
Response	Eroded Volume	Eroded Area	Max. Erosion Depth	Total Discharge Energy	Cumulative Charge
Covariates	--	**A_{UV}** • p-value: 0.00 • CC: 0.906	**Q_{cum}** • p-value: 0.00 • CC: 0.924	**Q_{cum} & A_{UV}** • p-values: 0.001 & 0.001 • CCs: 0.996 & 0.951	**E_T** • p-value: 0.00 • CC: 0.996
Impact of Voltage	significant • p-value: 0.00 • CC: 0.794	significant • p-value: 0.00 • CC: 0.728	significant • p-value: 0.006 • CC: 0.866	significant • p-value: 0.003 • CC: 0.791	significant • p-value:0.003 • CC: 0.776
Impact of Frequency	significant • p-value: 0.00 • CC: 0.479	significant • p-value: 0.01 • CC: 0.530	significant • p-value: 0.001 • CC: 0.271	significant • p-value: 0.001 • CC: 0.483	significant • p-value: 0.00 • CC: 0.502
Interaction	significant • p-value: 0.00	significant • p-value: 0.00	significant • p-value: 0.001	significant • p-value: 0.029	Significant • p-value: 0.00

(a)

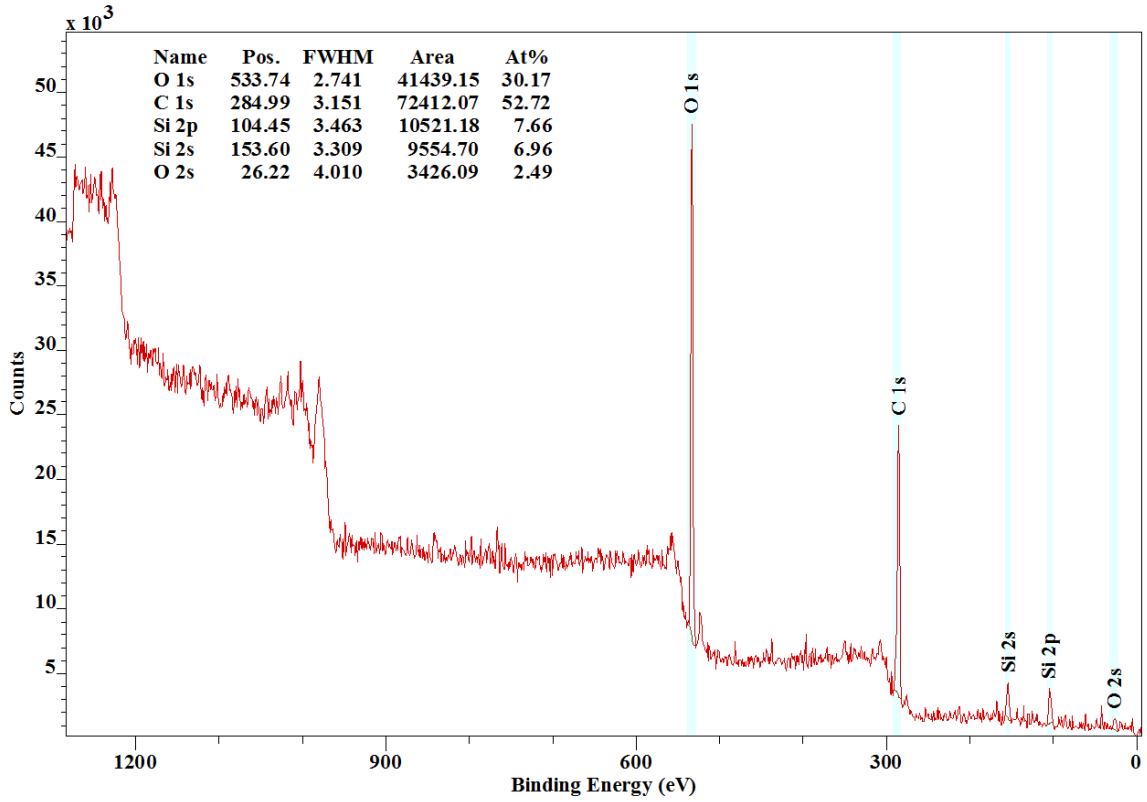

(b)

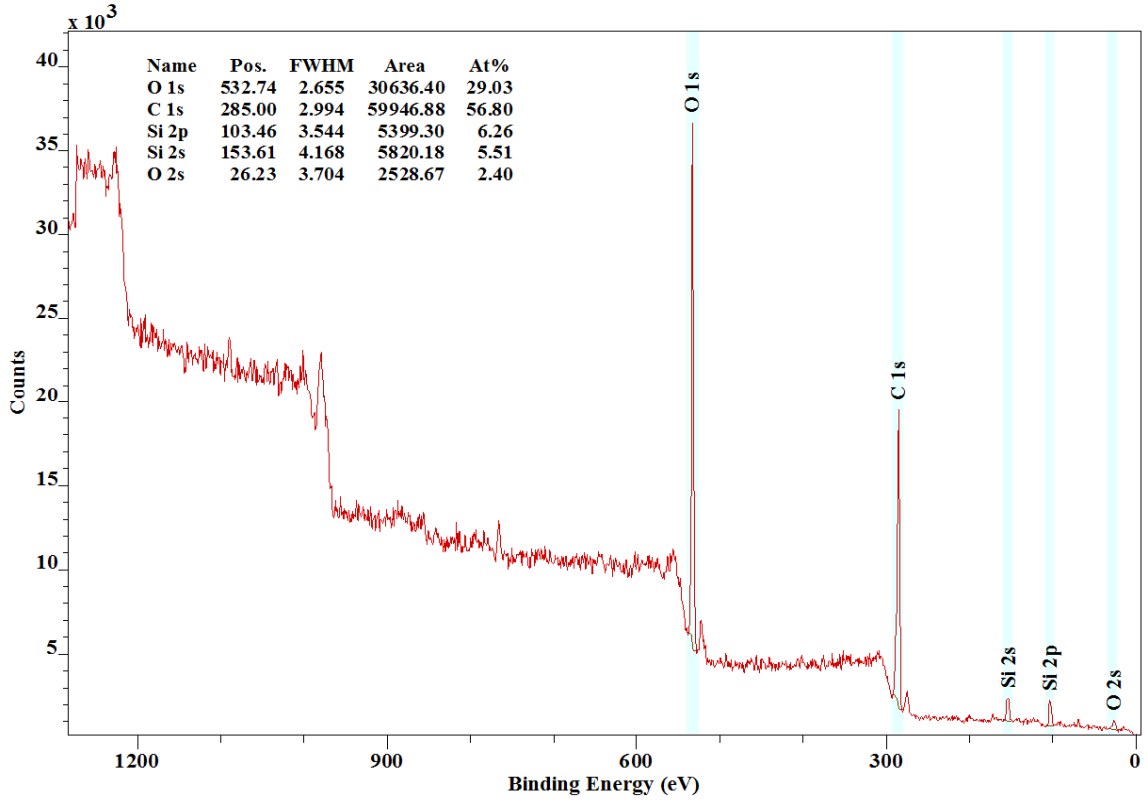

Figure 5.21: Core XPS spectra of a discharge stressed epoxy resin specimen at 10 kV_{peak} and 250 Hz; (a) in air, (b) in oxygen-free medium

One of the examined models is illustrated in detail (i.e. model 1) and the results are then taken from the optimum refitted model (see figure 5.22). This model presents the analysis of variance for eroded volume. It could be inferred that test voltage magnitude and frequency as well as their interaction have a significant influence on eroded material volume, which is confirmed by their p-values. Tukey's test provides grouping information and two sets of multiple comparison intervals; one group for voltage magnitude levels and the other for voltage frequency. In the grouping table, factor levels within the same group are significantly different from each other. Therefore, all levels means have significantly different eroded volume degree. The means of the impact of all stresses differs significantly because all of the 95% confidence intervals exclude zero. Therefore, all stresses in both sets of the Tukey's have significantly different average impact on eroded volume.

From the five models examined concerned with erosion characteristics listed in table 5.12 associated with the correlation coefficients for all examined variables, the following can be concluded:

- Eroded area under oxygen-free environment is significantly controlled by UV illuminated area with correlation coefficient of 0.906. This conclusion is the same as in the case of investigating discharge stresses in air.
- There is an interaction between both electrical influencing factors in terms of eroded volume (model 1) as well as eroded surface area (model 2).
- Although frequency was proven to have a certain impact on maximum erosion depth in model 3, it is weakly correlated with correlation coefficient of 0.271. Therefore, it cannot be stated that maximum erosion depth is influenced by frequency; whereas it is governed by test voltage magnitude with correlation coefficient of 0.866.
- Cumulative charge exhibits a direct impact on maximum erosion depth with a correlation coefficient of 0.924. This indicates that the amount of charge impinging on the surface at a certain point is the factor that determines how deep the erosion is. This result is consistent with the test series concerned with discharge stress in air.
- Total discharge energy and illuminated area have a strong covariance in between with correlation coefficient of 0.951.
- Voltage magnitude and frequency exhibit strong influence on both discharge parameters; beside their interaction which could also be proven.

In general the statistical analysis has led to the same results compared to the case of investigating discharge stresses in air. This can be explained by the fact that material erosion in nitrogen discharge medium is encountered mainly by the bombardment of charged particles (ions electrons and photons) [DIS-92], then it can be assumed that it is also the main mechanism responsible for material erosion in air. Moreover, oxidation of material surface takes place not only in air but also in nitrogen environment because of oxygen existence in the solid phase, which also participates in surface oxidation.

General Linear Model: Eroded Volume versus Voltage; Frequency

```
Factor     Type   Levels  Values
Voltage    fixed       3  10; 12; 14
Frequency  fixed       2  250; 500

Analysis of Variance for Eroded Volume, using Adjusted SS for Tests

Source             DF   Seq SS  Adj SS  Adj MS       F      P
Voltage             2   8,9758  8,9758  4,4879  406,72  0,000
Frequency           1   3,0257  3,0257  3,0257  274,21  0,000
Voltage*Frequency   2   0,9302  0,9302  0,4651   42,15  0,000
Error              24   0,2648  0,2648  0,0110
Total              29  13,1965

S = 0,105045   R-Sq = 97,99%   R-Sq(adj) = 97,58%

Unusual Observations for Eroded Volume
      Eroded
Obs   Volume      Fit   SE Fit  Residual  St Resid
  1  2,43941  2,23062  0,04698   0,20879      2,22 R
  6  1,22123  1,02255  0,04698   0,19868      2,11 R
 16  1,38783  1,14239  0,04698   0,24544      2,61 R

R denotes an observation with a large standardized residual.

Grouping Information Using Tukey Method and 95,0% Confidence

Voltage   N  Mean  Grouping
14       10   1,7  A
12       10   0,7    B
10       10   0,4      C

Means that do not share a letter are significantly different.

Tukey 95,0% Simultaneous Confidence Intervals
Response Variable Eroded Volume
All Pairwise Comparisons among Levels of Voltage
Voltage = 10  subtracted from:

Voltage   Lower  Center   Upper  ----+---------+---------+---------+--
12       0,2152  0,3324  0,4497  (--*---)
14       1,1730  1,2903  1,4075                            (--*--)
                                ----+---------+---------+---------+--
                                  0,35      0,70      1,05      1,40

Voltage = 12  subtracted from:

Voltage   Lower  Center  Upper  ----+---------+---------+---------+--
14       0,8406  0,9578  1,075                   (---*---)
                                ----+---------+---------+---------+--
                                  0,35      0,70      1,05      1,40
Tukey Simultaneous Tests
Response Variable Eroded Volume
All Pairwise Comparisons among Levels of Voltage
Voltage = 10  subtracted from:

         Difference       SE of           Adjusted
Voltage    of Means  Difference  T-Value   P-Value
12           0,3324     0,04698    7,076    0,0000
14           1,2903     0,04698   27,466    0,0000
```

Figure 5.22: The optimum refitted model for eroded volume (Model 1)

6. Electrical Discharge Induced UV radiation

UV radiation is one of the main stresses affecting material degradation and one of the expected mechanisms through which surface erosion of insulating polymers takes place. In this chapter, discharge induced UV radiation was imaged following the test setup A (see figure 2.2) and the images were processed to derive radiation parameters expressing UV characteristics. Using those parameters, UV radiation effect could be quantified under different electrical stresses. Additionally, a novel test setup B was applied to separate UV influence from the combined stresses on material specimen (see figure 2.7). This introduces the possibility to quantify the impact of UV on insulating material in terms of surface erosion.

6.1. Influence of Electrical Stresses on UV Characteristics

6.1.1. Magnitude of Test Voltage

The experiments were carried out with an AC voltage adjusted at 10, 12 and 14 kV_{peak} with frequency of 500 Hz. The chosen upper and lower limits of test voltage were selected according to partial discharge inception voltage and the flashover voltage. With increasing of the voltage an increasingly large luminous zone forms on the specimen surface around the vicinity of the needle electrode as shown in figure 6.1. Those UV emissions can result from recombination and ionization of air or under the influence of the charged particles impinging on insulating material surface. From results shown in figure 6.2, it can be concluded that UV characteristics are dependent on the test voltage.

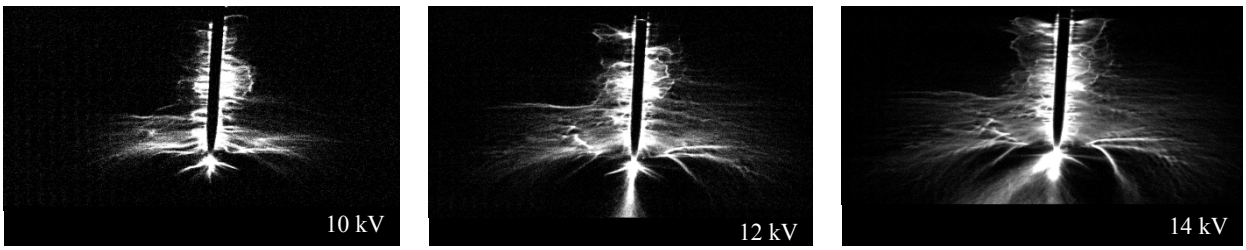

Figure 6.1: Effect of test voltage on UV radiation on specimen surface at 500 Hz and 2 seconds exposure, 20°C, 33 %RH

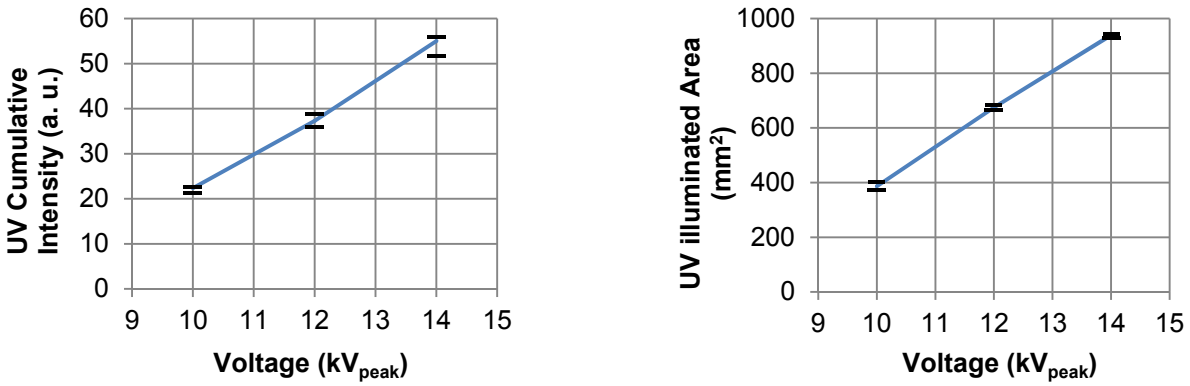

Figure 6.2: UV characteristics under the influence of the test voltage at 500 Hz and 2 seconds exposure, 20°C, 33 %RH

6.1.2. Frequency of the Test Voltage

In order to study the relation between the frequency of the test voltage and characteristics of induced UV radiation, the frequency was adjusted at the values 50, 250 and 500 Hz with a voltage magnitude of 12 kV_{peak}. UV images of corona discharge for different frequency values are shown in figure 6.3. The difference in radiation intensities in the three cases is apparent; with the increase of frequency an increasingly large luminous zone forms on the specimen surface around the vicinity of the needle electrode. Comparing the images, based on the same exposure time (i.e. 2 sec), yields in a change in radiation intensities and illuminated area. The same scale of UV intensity is selected for all images in order to display all discharge streamers even if UV intensity is low.

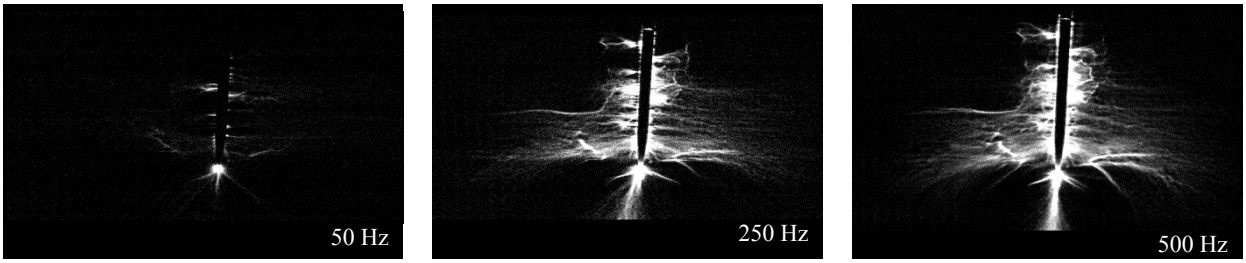

Figure 6.3: Effect of frequency on UV radiation on specimen surface at 12 kV_{peak} and 2 sec exposure, 20°C, 33 %RH

The trend that illuminated area increases with test frequency rise may be dependent on exposure time. In other words, exposure time of 2 seconds may be small for low frequency to build discharges sufficient to produce UV with detectable intensity. If 20 seconds exposure time is selected for the 50 Hz test frequency, then illuminated area may be the same as that at 2 seconds exposure time and 500 Hz. Figure 6.4 shows UV images with the same scale of UV intensity under different test frequencies. It can be seen that increasing exposure time ten times, for the same test frequency 50 Hz, results in larger illuminated area. At small exposure time cumulative intensity in some regions is too small to be detected. Although imaging at 20 seconds exposure time for the same test frequency (i.e. 50 Hz) results in larger UV area, it is still smaller than that at 2 seconds exposure time and 500 Hz. Figure 6.5 presents the calculated illuminated area and cumulative intensity for all conditions. It can be seen that cumulative intensity is higher at 500 Hz test frequency than 50 Hz for the same exposure time. Increasing the exposure time at low frequency compensates the effect of frequency on cumulative intensity.

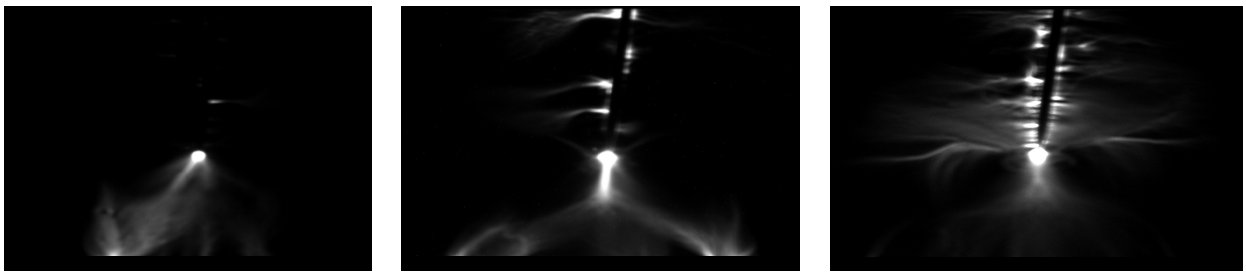

a. 50 Hz, 2 sec. exposure b. 50 Hz, 20 sec. exposure c. 500 Hz, 2 sec. exposure

Figure 6.4: UV images at different test frequencies and exposure times at 12 kV_{peak}, 20°C, 70 %RH

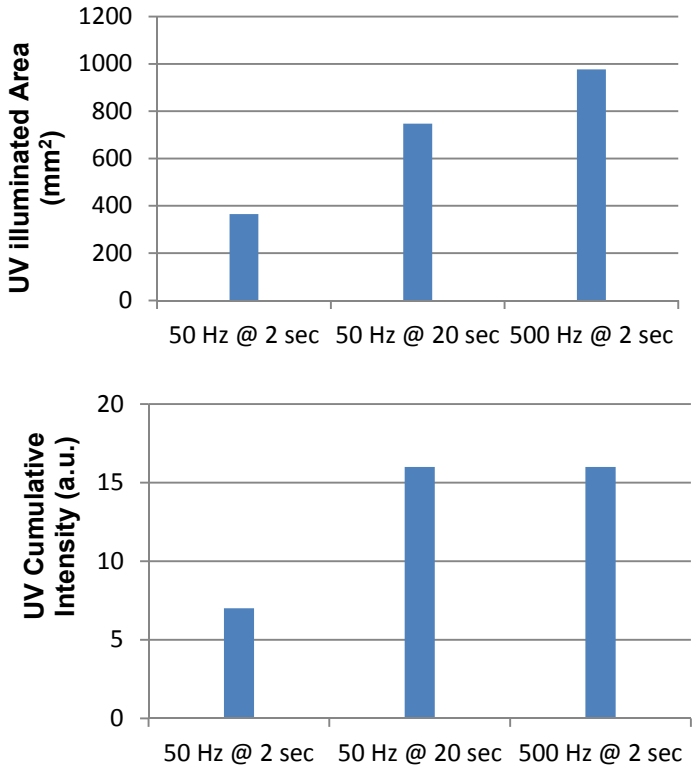

Figure 6.5: The effect of the frequency of test voltage and exposure time on UV characteristics at 12 kV_{peak}, 20°C, 70 %RH

The conclusion from the above analysis is that both UV cumulative intensity and illuminated area is dependent on test frequency at fixed exposure time. The difference in illuminated area between high and low frequencies is referred to:

- UV intensity in some regions for low test frequency is too small to be detected; which can be obviously proven when increasing the exposure time to 20 seconds.
- The increase in supply frequency enhances discharge intensity per second (i.e. number of pulses and discharge magnitude). This leads to more frequent collisions with the gas molecules, higher probability of extending the ionization boundary (i.e. means larger UV illuminated area).

The response of space charge dynamics to increase in the frequency of the test voltage can be deduced from the illustration of the surface PD mechanisms in figure 6.6. In the positive half cycle at the tip of the positive ion cloud the stress due to the space charge cloud superimposes on the background stress. The maximum electric field therefore occurs at the advancing plasma tip [MUR-01], [FOU-99].

Assuming constant space charge decay, an increase in the frequency of the test voltage gives less time for the positive ion space charge to disperse during the full cycle of the supply voltage. With increasing the test frequency, the amount of positive ion space charge available in each discharge event increases. An increase in the amount of the positive ion space charge results in more stress enhancement at the tip of the positive ion space cloud causing faster avalanches and further extension of the discharge streamer (i.e. larger UV area) [NYA-11].

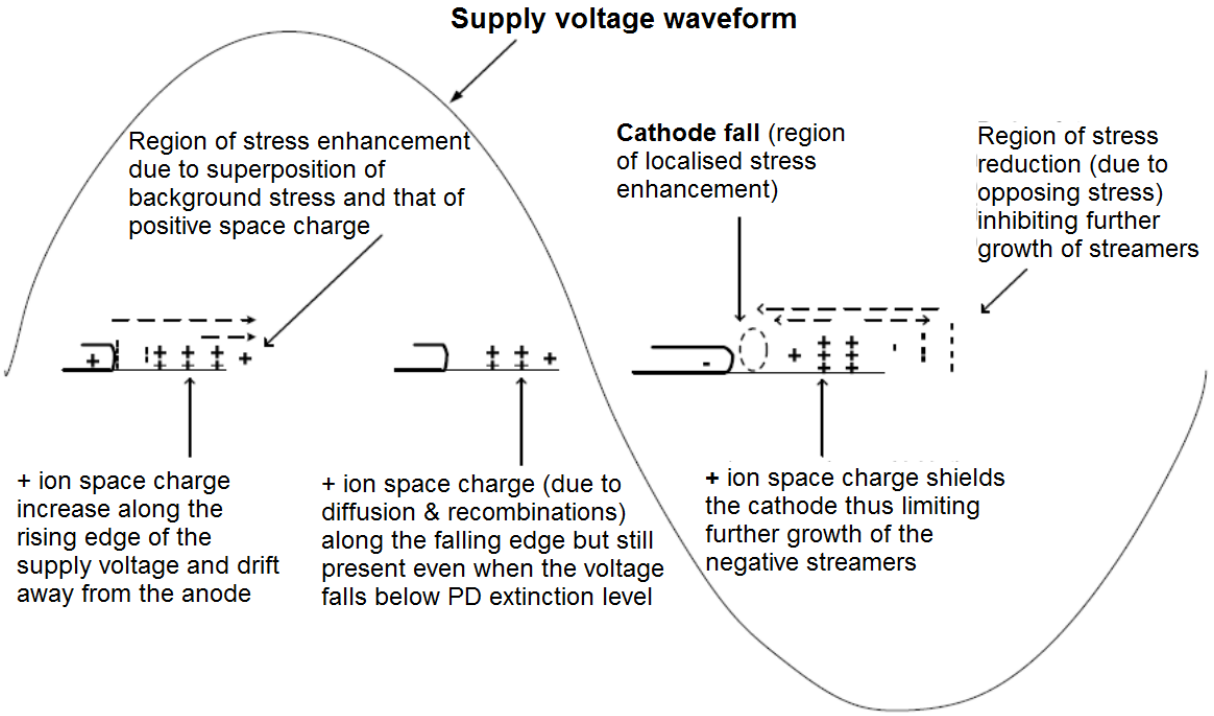

Figure 6.6: Illustration of surface PD mechanisms for needle-to-plate electrode after [NYA-11]

6.1.3. Interaction between Voltage and Frequency

The interaction between magnitude and frequency of the test voltage can be also proven in the form of UV radiation energy associated with corona discharge. It was found that the increase in any of the electrical stress parameters results in an increase in UV radiation intensity. Figure 6.7 displays the interaction plots in terms of both UV illuminated area and UV cumulative intensity. It can be observed that, the effect of voltage magnitude on radiation characteristics is more significant with the increase of the frequency. It can be concluded that an interaction exist between both electrical factors in terms of their impact on UV radiation characteristics.

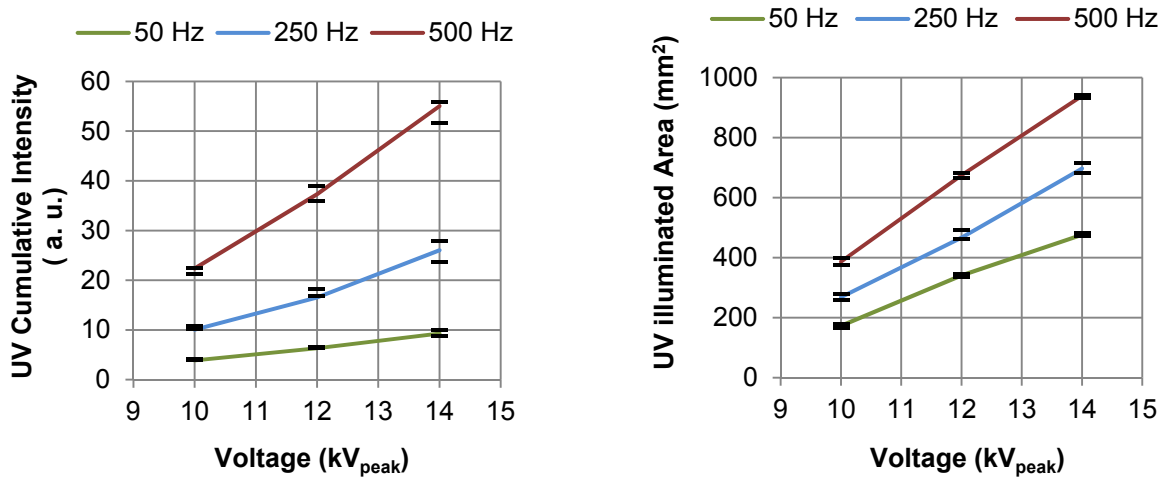

Figure 6.7: Interaction between voltage and frequency in terms of UV characteristics, 2 sec exposure, 20°C, 33 %RH

6.1.4. Statistical Analysis

The statistical models under *ANOVA* tests were examined for the sake of investigating UV characteristics under the influence of electrical stresses. Each factor is studied in 3 levels; 10, 12, and 14 kV_{peak} for test voltage magnitude and 50, 250, and 500 Hz for the frequency. The selected confidence level is 95% and the adjusted significance level for the hypothesis test is 0.05. The examined models are summarized in table 6.1 to explain the main factors of influence on the studied response in each model. The results for each model in the table determine the effective covariates for the examined response. Additionally, the influence of the both stressing factors as well as their interaction is checked.

Table 6.1: Summary of the statistical models and the correlation coefficients for all variables

Model	1	2
Response	UV Intensity	UV illuminated Area
Covariates	$\mathbf{A_{UV}}$, $\mathbf{E_T}$ • p-values: 0.00 and 0.00 • CCs: 0.909 and 0.955	$\mathbf{I_{UV}}$, $\mathbf{E_T}$ • p-values: 0.00 and 0.00 • CCs: 0.909 and 0.887
Impact of Voltage	Significant • p-value: 0.00 • CC: 0.437	Significant • p-value: 0.00 • CC: 0.763
Impact of Frequency	Significant • p-value: 0.00 • CC: 0.825	Significant • p-value: 0.00 • CC: 0.589
Interaction	Significant • p-value: 0.00	Significant • p-value: 0.00

One of the examined models is illustrated in detail (i.e. model 1) and the results are then taken from the optimum refitted model. The optimum refitted model in figure 6.8 presents the analysis of variance for UV intensity. It could be inferred that test voltage magnitude and frequency as well as their interaction have a significant influence on UV intensity, which is confirmed by their p-values. It is also concluded that total discharge energy has a certain impact on UV intensity.

Tukey's test provides grouping information and two sets of multiple comparison intervals; one group for voltage magnitude levels and the other for voltage frequency. In the grouping table, factor levels within the same group are significantly different from each other. Therefore, all levels means have significantly different UV intensity degrees. The impact of all stresses differs significantly because all of the 95% confidence intervals exclude zero. Therefore, all stresses in both sets of the Tukey's have significantly different average impact on UV intensity

From the examined models concerned with UV characteristics versus electrical factors of influence it can be concluded that total discharge energy exhibits a significant influence on UV characteristics other than cumulative charge which failed to be included in the two models. In other words total discharge energy controls UV characteristics, which is physically reasonable because UV radiation is evolved from the conversion of a portion of the discharge

energy. Finally, Electrical stressing factors are strongly affecting UV characteristics and an interaction between both factors significantly exists.

General Linear Model: UV intensity versus Voltage; Frequency

```
Factor     Type   Levels  Values
Voltage    fixed       3  10; 12; 14
Frequency  fixed       3  50; 250; 500

Analysis of Variance for UV intensity, using Adjusted SS for Tests
Source             DF   Seq SS  Adj SS  Adj MS       F      P
illuminated Area    1  8153,00    4,76    4,76  129,35  0,000
Total Energy        1  1020,42    5,28    5,28  143,36  0,000
Voltage             2   626,69   19,86    9,93  269,80  0,000
Frequency           2    33,39   55,06   27,53  748,10  0,000
Voltage*Frequency   4    29,24   29,24    7,31  198,66  0,000
Error              33     1,21    1,21    0,04
Total              43  9863,96

S = 0,191825   R-Sq = 99,99%   R-Sq(adj) = 99,98%

Grouping Information Using Tukey Method and 95,0% Confidence
Voltage   N  Mean  Grouping
14       14  30,0  A
12       15  20,3     B
10       15  12,1        C
Means that do not share a letter are significantly different.

Tukey 95,0% Simultaneous Confidence Intervals
Response Variable UV intensity
All Pairwise Comparisons among Levels of Voltage
Voltage = 10  subtracted from:
Voltage   Lower  Center   Upper  ---------+---------+---------+-------
12        7,394   8,152   8,910  (-*-)
14       17,116  17,889  18,663                              (-*-)
                                 ---------+---------+---------+-------
                                       10,5      14,0      17,5
Voltage = 12  subtracted from:
Voltage  Lower  Center  Upper  ---------+---------+---------+-------
14       8,964   9,737  10,51       (-*-)
                               ---------+---------+---------+-------
                                     10,5      14,0      17,5

Grouping Information Using Tukey Method and 95,0% Confidence
Frequency   N  Mean  Grouping
500        14  38,1  A
250        15  17,8     B
 50        15   6,6        C
Means that do not share a letter are significantly different.

Tukey 95,0% Simultaneous Confidence Intervals
Response Variable UV intensity
All Pairwise Comparisons among Levels of Frequency
Frequency =  50  subtracted from:
Frequency  Lower  Center  Upper  ---+---------+---------+---------+---
250        10,44   11,20  11,96  (-*)
500        30,73   31,50  32,28                                   (-*)
                                 ---+---------+---------+---------+---
                                 12,0      18,0      24,0      30,0
Frequency = 250  subtracted from:
Frequency  Lower  Center  Upper  ---+---------+---------+---------+---
500        19,53   20,30  21,08             (*)
                                 ---+---------+---------+---------+---
                                 12,0      18,0      24,0      30,0
```

Figure 6.8: The optimum refitted model for UV intensity (Model 1)

6.2. Spectrum of UV Radiation from Electrical Discharge

In order to prove the difference between UV radiation spectrum from electrical discharge and that from sunlight, another UV bandpass filter with spectrum range of ***290 nm***: ***380 nm*** (UV-A & UV-B) is mounted on UV camera system instead of the former filter (***250 nm*** to ***380 nm***). Following this procedure makes it possible to describe the UV-C range of UV associated with electrical discharge by comparing UV characteristics of images captured by both filters. In such a way cumulative UV intensity and illuminated area for wavelengths from ***250 nm*** *to* ***290 nm*** are determined by subtraction of UV characteristics calculated for both filter systems.

The results presented below in figure 6.9 supports the existence of short wavelength spectrum in the discharge induced UV radiation. Here, the difference between the two filters in terms of both UV intensity and illuminated area is very clear. It is also noted that the resulting radiation in (c) is originated at the needle boundary and in front of needle tip.

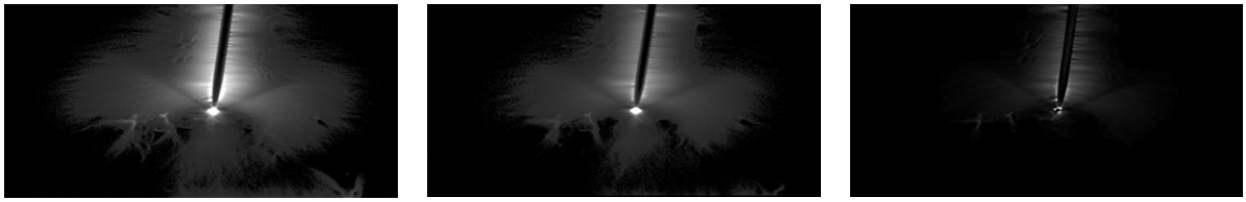

a. Bandpass filter 1
250 nm: 380 nm

b. Bandpass filter 2
290 nm: 380 nm

c. Difference between both filters:
250 nm: 290 nm

Figure 6.9: UV images for the two filters and their subtraction at 12 kVpeak, 500Hz, 5 sec exposure

UV cumulative intensity and UV illuminated area for the energy band of UV radiation in figure 6.9 (c) are determined by the subtraction of the two filters matrices. It was found that UV characteristics for this band exhibit a direct correlation of UV characteristics with respect to both electrical stress parameters (see figure 6.10). Additionally, there is an interaction between voltage magnitude and frequency in terms of cumulative intensity, which does not exist in case of illuminated area.

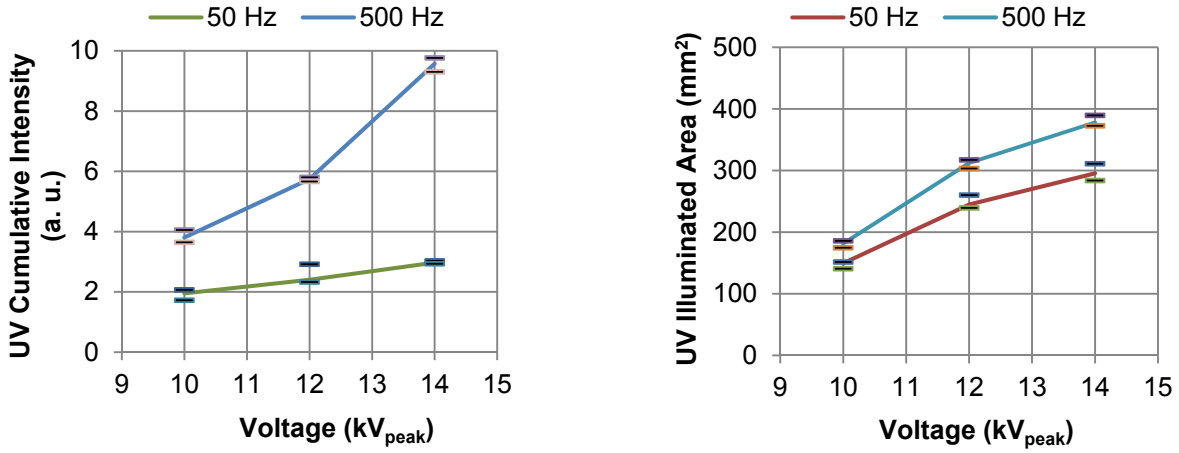

Figure 6.10: UV characteristics in energy band with wavelength 250 nm to 290 nm calculated by subtraction of the two filters' matrices (median, span of 5 samples each)

Two characteristics needs to be defined, the ratio of UV cumulative intensity and UV illuminated area. Those ratios compare the high energy spectrum to the whole spectrum (i.e. Bandpass filter 1) in terms of both UV characteristics as shown in figure 6.11. The rate of increase in illuminated area with electrical stresses for the whole spectrum is higher than that for high energy spectrum. This can be seen in illuminated area ratio exhibiting a decreasing trend with increasing electrical stresses. On the other hand, the ratio of cumulative intensity also shows a decreasing trend with increasing voltage magnitude at low frequencies. However, at higher frequency and voltage magnitudes (i.e. 500 Hz and 14 kV_{peak}), the ratio tends to increase.

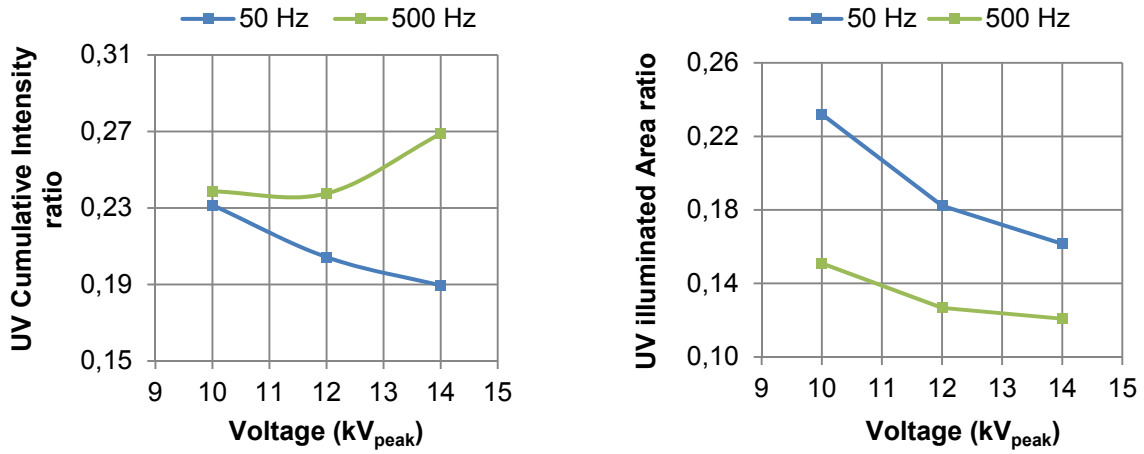

Figure 6.11: Comparing the high energy spectrum to the whole spectrum (i.e. Bandpass filter 1) in terms of both UV characteristics (median of 5 samples each)

The above results confirm the difference between UV radiation spectrum from electrical discharge and that from sunlight. This is also confirmed by [OLL-98] who examined the photo-oxidation and electrical aging of anhydride-cured epoxy resins. Ollier-Dureault conclude that UV radiation stresses associated with electrical aging cannot be simulated by solar UV radiation aging, in the same way photo-oxidation studies cannot be used to deduce the behavior of materials under discharge induced UV radiation.

6.3. UV Characteristics versus Discharge Surface Erosion

UV irradiation on material surface may play an important role in erosion evolution. Therefore, it is necessary to examine the influence of UV irradiation, resulting from electrical discharge, on material surface in terms of erosion characteristics. During erosion evaluation phases following test setup A, which last for 96 hours each, erosion builds up around the vicinity of the needle electrode with different areas dependent on the factors of influence. Therefore, it is assumed that UV radiation with the highest intensities occurring in the vicinity close to needle electrode is taking part in erosion process. Eroded area of the stressed samples is compared to UV irradiated area, as shown in figure 6.12, under different voltages and test frequency of 500 Hz.

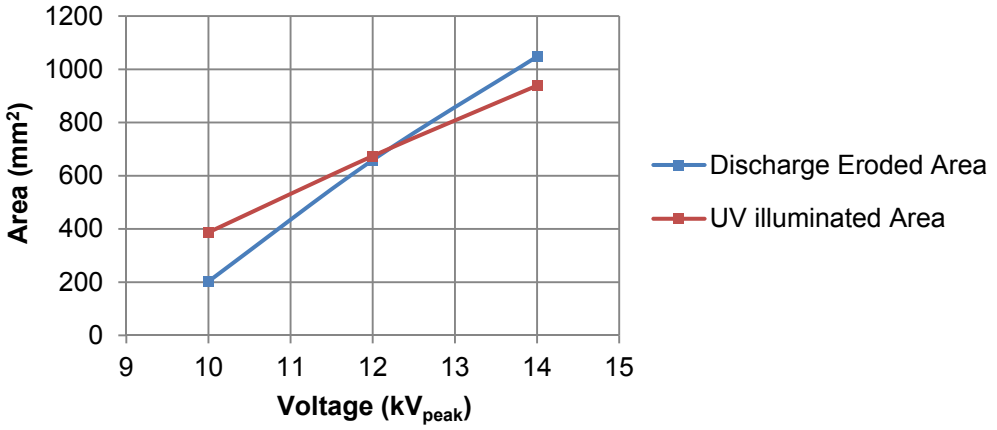

Figure 6.12: UV irradiated area versus eroded area under the influence of test voltage (median), 500 Hz, test setup A

A comparison with the erosion characteristics shows that, the area of UV irradiated regions correlates with the dimensions of eroded areas on insulating material surface. At low voltage magnitudes, UV irradiated area is increasing with a lower rate compared to eroded area. For voltages lower than 12.5 kV_{peak}, UV irradiated area is larger than total eroded area. This means that, only a portion of the irradiated area has enough intensity (i.e. enough photon energy) to take part in material erosion. Whereas working at higher stresses (i.e. voltage higher than 12.5 kV_{peak}) result in eroded area larger than total UV irradiated area. Here it could be stated that UV is not the only stress affecting erosion phenomenon. The same investigation can be also performed for different frequencies at certain voltages, i.e. 10 kV_{peak} and 14 kV_{peak} as shown in figure 6.13. A correlation exists between the eroded area and UV irradiated area. In case of 14 kV_{peak}, eroded area is higher than UV irradiated area and the opposite occurs in case of 10 kV_{peak}, which is in accordance with the results in figure 6.12.

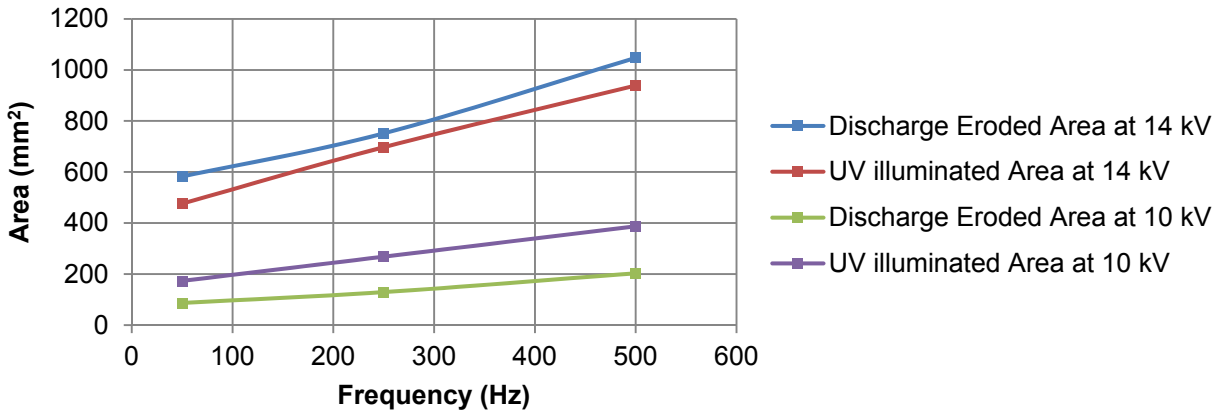

Figure 6.13: UV irradiated area (from test setup A) versus surface eroded area (secondary specimen from test setup B); at 14 kV_{peak} and 10 kV_{peak}

6.4. Quantification of UV Induced Erosion

6.4.1. Erosion Characteristics

The results of this study (i.e. erosion from UV radiation according to test setup B) are presented in figure 6.14. It can be seen that, both eroded area and eroded volume, of the secondary sample, are increasing nonlinearly with both stresses. Nonlinear regression on the obtained erosion characteristics yields equations from [6.1] to [6.3], whereby eroded volume $\boldsymbol{Vol}$ is in mm^3, eroded area $\boldsymbol{A}$ is in mm^2, maximum erosion depth $\boldsymbol{D_{max}}$ is in µm, the test frequency $\boldsymbol{f}$ is in Hz and the voltage $\boldsymbol{V}$ is in volts. From the equations, it could be concluded that the rate of increase of $\boldsymbol{Vol}$ and $\boldsymbol{A}$ with respect to $\boldsymbol{V}$ is much higher than that with respect to $\boldsymbol{f}$. What can be seen as consistent with the graphs is the response of maximum erosion depth, which is independent of test voltage magnitude and guided only by the change in test frequency.

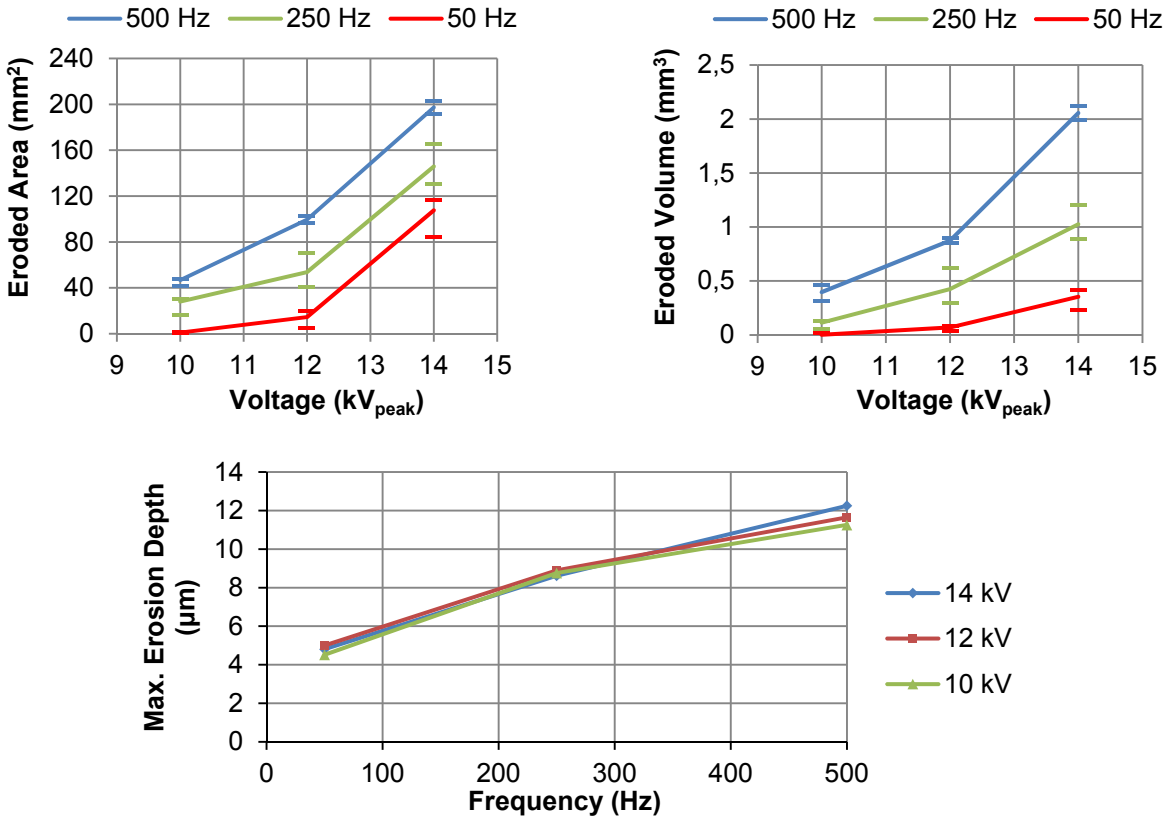

Figure 6.14: Erosion characteristics for secondary samples from UV radiation (median)

$$Vol[mm^3] = 6 \times 10^{-7} \cdot \left[\frac{f[1/s]}{50\ 1/s}\right]^{0{,}705} \cdot \left[\frac{V}{kV_{peak}}\right]^5 \quad [6.1]$$

$$A[mm^2] = 2 \times 10^{-4} \cdot \left[\frac{f[1/s]}{50\ 1/s}\right]^{0{,}306} \cdot \left[\frac{V}{kV_{peak}}\right]^5 \quad [6.2]$$

$$D_{max}[\mu m] = 5 \cdot \left[\frac{f[1/s]}{50\ 1/s}\right]^{0{,}37} \quad [6.3]$$

Concerning maximum erosion depth, it was found to be nearly independent of the test voltage (see figure 6.14). To explain this result, we have to refer to the first test setup in the early chapters examined without the secondary sample. The detected maximum erosion depth in the former test setup was located in front of the needle tip; where a certain enhancement in electric field exists resulting in energetic bombarding charged particles leading to erosion at this point. This is considered as the main stress in this region responsible for erosion evolution. Comparatively, studying the UV influence in terms of erosion on the secondary specimen in the second test setup examined in this chapter is totally different. This is because almost no discharges reaching sample surface under analysis and the main impact is resulting from incident UV radiation. Additionally, the linear change in UV radiation spread with electrical stresses results in no highly stressed points compared to the neighboring ones.

It is also obvious from figure 6.14 that maximum erosion depth depends on test voltage frequency. To introduce an interpretation for this result, the average change in UV characteristics with respect to one step change in the frequency is calculated. Figure 6.15 shows that the change in cumulative intensity is higher than that of illuminated area, which causes that UV intensity per unit illuminated area exhibits an increasing trend with frequency increase. Then, the higher UV intensity per unit illuminated area may explain the increase in maximum erosion depth with frequency increase. This represents evidence that the mechanism by which material erosion takes place in this case is different from the former one in the early chapters.

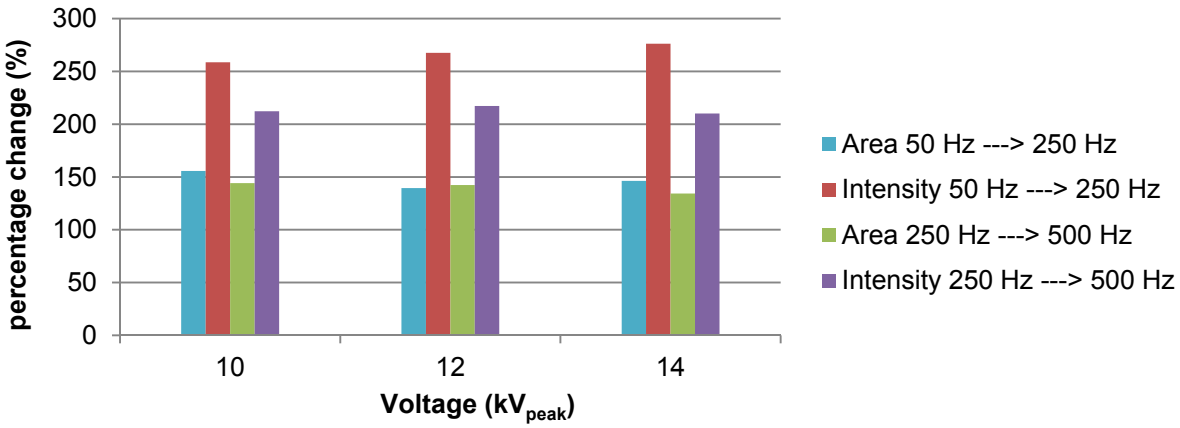

Figure 6.15: Average change in UV characteristics (UV illuminated area and UV cumulative intensity) with respect to one step change in frequency

As a matter of fact the previous work in literature is limited to the surface degradation of polymeric insulators and no clear results were found on the level of surface erosion. Nevertheless, some few researchers proved that the influence of UV on surface degradation is important in the initiation of erosion rate increase and also causes the HTV SIR polymeric materials to undergo a cross-linking reaction [HUH-00], [YOU-05]. Studies on epoxy resin [OLL-98], [LEE-99] have suggested that pendant radicals and easily ionized oxygen-containing degradation products generated by UV radiation in air lead to the decrease in surface resistance. In order to quantify the impact of UV on surface erosion, two parameters are calculated to hold a correlation between UV characteristics and its relative damage. UV erosion yield (Y_A) is the ratio between surface eroded area (A_{eroded}) and UV illuminated area (A_{UV}). UV erosion yield (Y_V) is the ratio between eroded volume (V_{eroded}) and cumulative UV intensity (I_{UV}).

$$Y_A = \frac{A_{eroded}[mm^2]}{A_{UV}[mm^2]} \quad [6.4]$$

$$Y_V = \frac{V_{eroded}[mm^3]}{I_{UV}[a.u.]} \quad [6.5]$$

Both UV erosion yields increase under the influence of either stresses (i.e. voltage or frequency) as shown in figure 6.16. In other words, electrical stresses lead to an increase in UV stress, in terms of both spread and intensity, and hence enhance its ability to cause more damage on material surface. However, at higher voltage stresses, the rate of change for both yields Y_A and Y_V with frequency decreases until reaching zero at 14 kV_{peak}. In other words the enhancement in test voltage magnitude limits the influence of frequency on UV erosion yields.

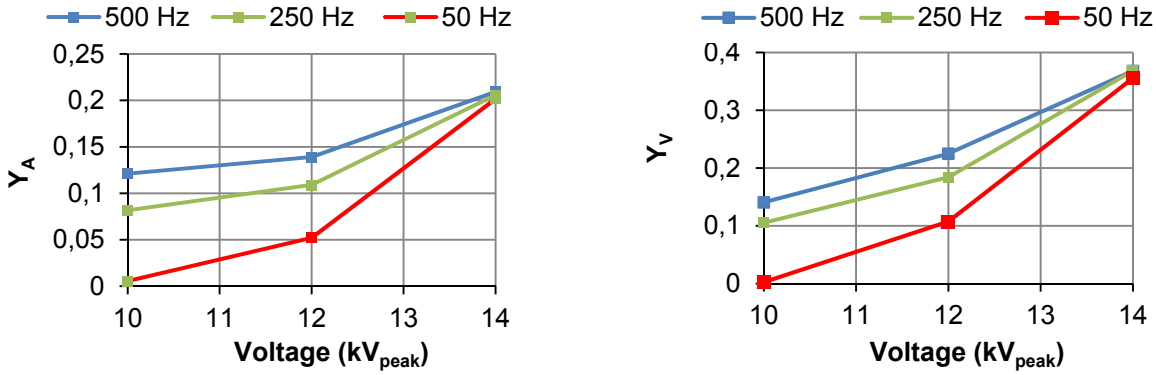

Figure 6.16: UV erosion yields (Y_A and Y_V) at different electrical stresses (median), 20°C and 33 %RH

Figure 6.17 compares erosion of stressed specimens from test setup A under the influence of all stresses including UV to that from secondary specimens from test setup B under the influence of UV. Clearly, it can be noticed that the gap between the lines increases with increasing the electrical stresses. However, erosion in material surface is detected under UV stressed specimens; it is very small compared to the amount of the erosion resulting from discharge stressed specimens. Therefore, it can be assumed that UV in setup A introduces weakening force acting on material surface and increases its susceptibility to erosion under electrical discharge. It could be stated that charged particle bombardment is the dominant mechanism by which erosion takes place.

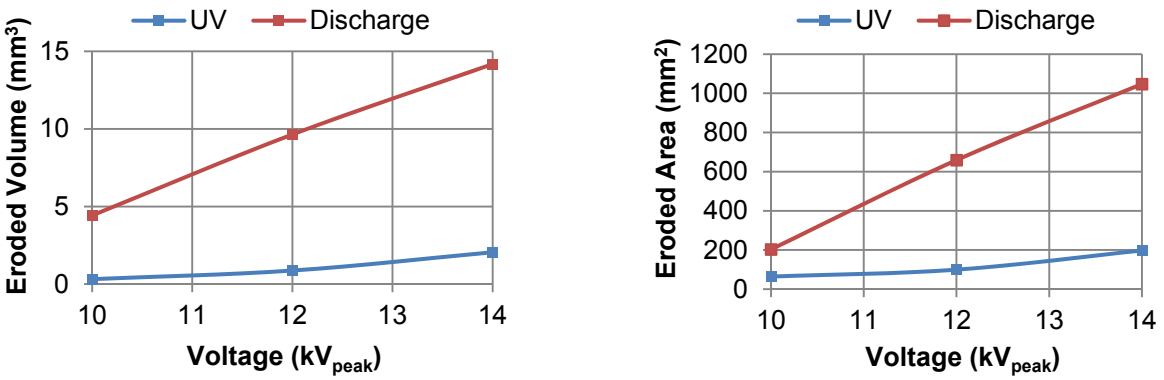

Figure 6.17: UV induced erosion (secondary specimen from test setup B) versus erosion under the influence of all stresses (specimen from test setup A) at 500 Hz

6.4.2. XPS Results

The influence of UV radiation from corona discharges on material surface is studied in terms of material composition through the XPS analysis. Deconvolution of C 1s peak of epoxy resin stressed specimen results in different shifted carbon peaks. Through the analysis of peaks area variation, the impact of UV radiation can be identified. Due to the fact that UV stresses are directly correlated to the applied electrical stresses this study is performed as a function of test voltage magnitude and frequency. These factors are examined on the levels of 50 Hz and 250 Hz for frequency and 10 kV, 12 kV and 14 kV for voltage magnitude. The enhancement in electrical stresses leads to a decrease in the intensity of C–H, C–C peak due to the increase of bond dissociation of such groups under stress to produce more oxygen bonds as listed in table 6.2. Additionally, the area under the peak of oxygen containing hydroxyl groups (C–OH) is increased with electrical stresses. However, the rate of increase of such a group with stress enhancement is less than that under discharge stress (see section 5.2.4).

Table 6.2: Area change in C 1s deconvolution peaks (with respect to the whole envelope area of C 1s peak) and O 1s peak (normalized to that of virgin material specimens) of UV stressed specimens, 20°C, 33 %RH, 96 hours

Analyzed specimens	***Stress parameters***		***C 1s deconvolution***				***relative O 1s peak***
	V kV_{peak}	***f*** Hz	***C – H, C – C %***	***C – OH %***	***C = O %***	***O = C – OH %***	$\frac{O\ 1s}{(O\ 1s)_{virgin}}$
Virgin			65.89	23.17	4.12	6.82	1
Stressed	10	50	62.74	21.73	4.65	10.88	1.40
	10	250	54.62	26.37	5.43	13.58	1.19
	14	50	54.56	29.30	5.18	10.96	1.79
	14	250	49.69	29.32	10.28	10.71	1.64

In the case of UV stressed specimens, the concentration of C=O peak is also increasing with radiation stresses. This could be regarded as a direct impact of photo-oxidation of epoxy resin under the influence of UV radiation stress [SCI-03]. The increase in concentration of this oxygen containing group was not significant in discharge stressed specimens, which supports that erosion under the influence of electrical discharge is mainly dominated by charged particles bombardment. While photo-oxidation mechanism from UV radiation stresses represents a supporting stress to the main one in the evolution of material erosion.

It can be also seen from figure 6.18 that the amount of O 1s / C 1s ratio is larger for UV stressed specimens compared to the unstressed one. This confirms the influence of UV on enhancing the intensity of oxygen bonds. Additionally, it is noted that under low frequency (i.e. 50 Hz), the O 1s / C 1s ratio exhibits a decreasing trend with the increase of test voltage magnitude. From the last column in table 6.2 it is observed that the area of O 1s peak for stressed specimen is much than that for the virgin specimen. Therefore, it can be stated that the change in UV radiation in form of intensity and spread has a significant influence on the oxygen concentration of material surface composition. It is also noted that electrical stresses and hence UV stresses have an influence on oxygen amount. Here the oxygen amount in

material composition exhibits an increasing trend with test voltage magnitude; whereas applying higher test frequency results in a slight decrease in O 1s peak area.

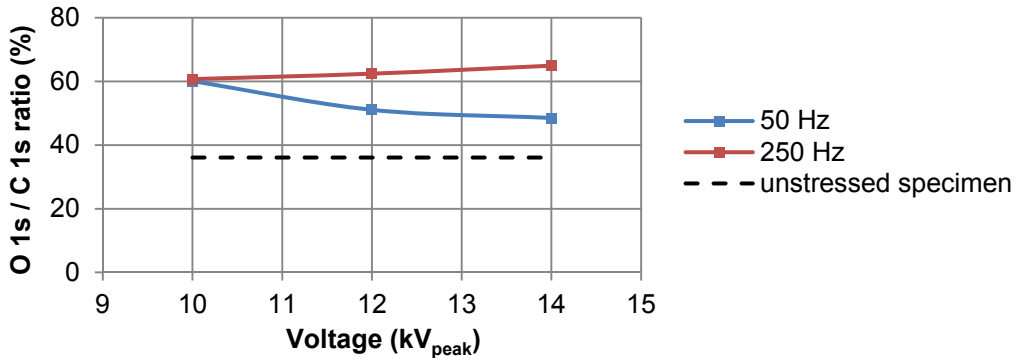

Figure 6.18: Influence of UV radiation on material composition, 20°C and 33 %RH

Comparing the obtained results to the previous work in literature concerning surface degradation of ultraviolet treated polymers helps for better understanding of the examined phenomenon. Many researchers have examined the structural change in the surface of polymeric materials under UV stress using artificial UV environment. Although the range and intensity of generated UV radiation is different from the examined discharge triggered UV, it is worth to compare on the level of surface degradation. Lee et al have studied the surface degradation of UV-treated epoxy composites and found an increase of ester and carboxyl groups as hydrocarbon chains are oxidized [LEE-99]. It was also found that the intensity of these oxygen carbon peaks in the deconvolution models of the C 1s peak are dependent on the UV stresses [SCI-05]. This confirms the photo-oxidation process under UV stresses which is the main reason for the alteration of the oxygen containing groups [HUH-00], [YOU-05].

6.4.3. Statistical Models

The statistical general linear models under *ANOVA* tests were analyzed for the sake of investigating erosion characteristics resulting from UV radiation (taken from test setup A without secondary sample) generated by electrical stresses. Each factor was studied in 3 levels; 10, 12, and 14 kV_{peak} for test voltage magnitude and 50, 250, and 500 Hz for voltage frequency. The selected confidence level is 95% and the adjusted significance level for the hypothesis test is 0.05. The examined models are summarized in table 6.3 to explain the main factors of influence on the studied response in each model. The results for each model in the table determine the effective covariates for the examined response. Additionally, the influence of the both stressing factors as well as their interaction is checked.

One of the examined models is illustrated in detail (i.e. model 1) and the results are then taken from the optimum refitted model. The optimum refitted model in figure 6.19 presents the analysis of variance for maximum erosion depth. It could be inferred that test voltage frequency has a significant influence on maximum erosion depth, which is confirmed by their p-values (less than 0.05). On the other hand test voltage magnitude as well as its interaction with test frequency has no influence on this erosion characteristic.

Table 6.3: Summary of the statistical models and the correlation coefficients for all variables, concerned with the erosion characteristics of the secondary specimen in setup B

Model	1	2	3
Response	Eroded Volume	Eroded Area	Max. Erosion Depth
Covariates	I_{UV} • p-value: 0.00 • CC: 0.906	A_{UV} • p-value: 0.00 • CC: 0.925	--
Impact of Voltage	Significant • p-value: 0.00 • CC: 0.544	significant • p-value: 0.00 • CC: 0.786	insignificant • p-value: 0.256 • CC: 0.298
Impact of Frequency	Significant • p-value: 0.00 • CC: 0.707	Significant • p-value: 0.00 • CC: 0.452	Significant • p-value: 0.00 • CC: 0.914
Interaction	Significant • p-value: 0.00	Significant • p-value: 0.00	insignificant • p-value: 0.625

Tukey's test provides grouping information and two sets of multiple comparison intervals; one group for voltage magnitude levels and the other for voltage frequency. In the grouping table, factor levels within the second group (test frequency) are significantly different from each other. Therefore, all levels means have significantly different values of maximum erosion depth. The impact of all stresses differs significantly for the frequency because all of the 95% confidence intervals exclude zero. Therefore, all stresses in frequency set of the Tukey's have significantly different average impact on maximum erosion depth. On the other, hand factor levels within the first group (test voltage magnitude) share the same letter (A), which is referred to the ineffectual impact of this stress on maximum erosion depth. The 95% confidence intervals for test voltage are overlapping and including zero.

The conclusions are drawn from the above examined models concerned with UV induced erosion characteristics versus electrical factors of influence. UV intensity taken from test setup A without the secondary specimen is the influencing factor that mainly controls eroded volume from UV stresses. In other words, the amount of eroded volume taken from material surface is governed by the strength of incident radiation. This result can be explained by the fact that the degree of damage at each point depends on the incident photon energy, which is directly correlated to UV intensity as well [MAS-06]. The energy contained in UV radiation is capable of directly rupturing polymer chains (chain scission), and, in the presence of oxygen, UV radiation causes oxidation of polymers. UV illuminated area exhibits a significant influence on surface eroded area (secondary specimen). Therefore, it is assumed that the degree of erosion spread on material surface is guided by how much from irradiated surface is UV illuminated. It is worth to mention here that only UV illuminated region with sufficient intensity is susceptible to erosion, which means that not the whole irradiated area is eroded with a detectable amount.

General Linear Model: Max. Erosion Depth versus Voltage; Frequency

```
Factor     Type   Levels  Values
Voltage    fixed       3  10; 12; 14
Frequency  fixed       3  50; 250; 500

Analysis of Variance for Max. Erosion Depth, using Adjusted SS for Tests

Source             DF   Seq SS   Adj SS   Adj MS       F      P
Voltage             2    1,635    2,667    1,334    1,42  0,256
Frequency           2  386,447  387,356  193,678  205,99  0,000
Voltage*Frequency   4    2,477    2,477    0,619    0,66  0,625
Error              35   32,908   32,908    0,940
Total              43  423,468

S = 0,969659   R-Sq = 92,23%   R-Sq(adj) = 90,45%

Grouping Information Using Tukey Method and 95,0% Confidence
Voltage   N  Mean  Grouping
14       14   8,7  A
12       15   8,6  A
10       15   8,1  A
Means that do not share a letter are significantly different.

Tukey 95,0% Simultaneous Confidence Intervals
Response Variable Max. Erosion Depth
All Pairwise Comparisons among Levels of Voltage
Voltage = 10  subtracted from:
Voltage    Lower  Center  Upper    -+---------+---------+---------+-----
12       -0,4073  0,4590  1,325         (------------*-----------)
14       -0,3159  0,5682  1,452          (------------*------------)
                                  -+---------+---------+---------+-----
                               -0,70      0,00      0,70      1,40

Voltage = 12  subtracted from:
Voltage    Lower  Center   Upper    -+---------+---------+---------+-----
14       -0,7749  0,1092  0,9933    (------------*-----------)
                                   -+---------+---------+---------+-----
                                 -0,70      0,00      0,70      1,40

Grouping Information Using Tukey Method and 95,0% Confidence
Frequency   N  Mean  Grouping
500        14  11,8  A
250        15   8,9    B
 50        15   4,6      C
Means that do not share a letter are significantly different.

Tukey 95,0% Simultaneous Confidence Intervals
Response Variable Max. Erosion Depth
All Pairwise Comparisons among Levels of Frequency
Frequency =  50  subtracted from:
Frequency  Lower  Center  Upper    +---------+---------+---------+------
250        3,527   4,393  5,259            (---*---)
500        6,373   7,257  8,141                       (---*----)
                                  +---------+---------+---------+------
                                2,0       4,0       6,0       8,0

Frequency = 250  subtracted from:
Frequency  Lower  Center  Upper    +---------+---------+---------+------
500        1,980   2,864  3,748    (---*----)
                                  +---------+---------+---------+------
                                2,0       4,0       6,0       8,0
```

Figure 6.19: The optimum refitted model for maximum erosion depth (Model 3)

7. Conclusions

The work presented in this thesis helped to achieve the goal of understanding the surface erosion mechanism of epoxy resin insulating material under the influence of corona discharge. Additionally, the stressing factors of influence on the erosion process have been identified and their impacts on material surface have been quantified. One of the important stresses involved in the surface erosion is UV radiation associated with corona discharges. Therefore, a novel test setup, on the level of surface erosion studies, has been introduced in order to examine the influence of UV radiation separately while minimizing the impact of charged particles bombardment.

For the goals above to achieve, a needle-to-plane electrode arrangement was designed to produce electric field stress tangential to the specimen surface. In such a way, the proposed test setup with such electrode arrangements could possess significant advantages over that according to IEC 60343. First and foremost, it was possible to examine the impact of UV radiation separately on material surface using this test setup. Second is the focus on a well-defined area with a local discharge activity. Finally, the used test setup provides a dominating tangential field component which seems to be more representative to service conditions.

The investigated influencing factors are electrical stressing factors, i.e. test voltage magnitude and frequency, as well as environmental factors, i.e. temperature and humidity. Discharge intensity is defined by two parameters; total discharge energy and cumulative charge; whereas surface erosion severity is characterized by three quantities; surface eroded area, eroded volume and maximum erosion depth.

Both electrical stressing factors have proven to have a dominant role for the erosion. It was found that discharge intensity in terms of the effectiveness in extracting more particles from material surface, represented by total discharge energy and cumulative charge, is positively correlated to both stressing factors. Significant interaction exists between both factors in terms of erosion characteristics as well as discharge parameters.

Under the influence of electrical stresses both discharge parameters, i.e. energy and charge, have a direct influence on eroded volume. On the other hand, the covariance between eroded area and UV illuminated area reflects the correlation between the spread of electric discharge and the surface eroded area. Maximum erosion depth of the eroded samples was proven to be dominated by the corresponding cumulative charge magnitude.

One of the influencing factors expected to influence discharge behavior as well as the erosion severity are the ambient conditions in the discharge zone. The analysis is performed between temperature and humidity of discharge medium. It was clear that temperature rise increase discharge parameters but with a slow rate of change. On the other hand, it was proven that cumulative charge and total discharge energy are slightly affected by humidity change in inverse proportional relationship. The interaction between both factors in terms of discharge parameters was proven.

7. Conclusions

Both environmental factors, i.e. temperature and relative humidity, have a strong impact on erosion characteristics of the stressed specimens at the same applied voltage. The amount of eroded material, represented by eroded volume, exhibits an increasing trend with both factors. On the other hand, eroded surface area was found to be mainly governed by humidity degree. However, temperature has no separate influence on this erosion characteristic, but it is clearly still important in the form of an interaction with humidity. Finally, maximum erosion depth is not humidity dependent at room temperature; whereas it depends much more on discharge intensity. This proves that erosion in the high electric field region (maximum erosion depth location) is mainly guided by discharge.

The effect of oxygen-free environment on discharge parameters was studied. It was found that both voltage and frequency exhibit a significant influence on discharge parameters in form of direct correlation. Significant interaction exists between both stresses concerning the examined parameters. This behavior was found to be quite similar to that of discharge parameters calculated for air as discharge medium. Electrical stressing factors of influence were found to be directly correlated to material erosion characteristics, eroded area and volume. There is also clear evidence on interaction between both stresses in terms of erosion parameters.

For specimens not directly affected by electrical discharge but UV radiation from discharge, it was found that total discharge energy exhibits a significant influence on UV characteristics. In other words, total discharge energy controls UV characteristics. Electrical stressing factors are strongly affecting UV characteristics and the interaction in between is significant. UV intensity is the influencing factor that mainly controls eroded volume from UV stresses. In other words, the amount of eroded volume taken from material surface is governed by the strength of incident radiation. On the other hand, UV illuminated area exhibits a significant influence on surface eroded area. The frequency of the test voltage is strongly affecting maximum erosion depth; whereas voltage magnitude has no influence on this characteristic.

ESCA analysis has revealed many observations regarding the bond dissociation of carbon groups and the change in the degree of oxidation in material surface under all the examined stresses. It could be concluded that each stressing factor has its characteristic fingerprint, through which the resulting damage from each of them can be distinguished.

8. Bibliography

[ABD-00] Abdel-Salam, M., Anis, H., El-Morshedy, A. and Radwan, R.:
High Voltage Engineering Theory and Practice
Marcel Dekker Inc., 2000, ISBN: 0824704029

[ADD-02] Addison, P. S.:
The Illustrated Wavelet Transform Handbook
Napier Univ., Edinburgh, UK: Institute of Physics Publishing Bristol and Philadelphia, 2002, ISBN: 0750306920

[AHM-78] Ahmed, F.S. and Ahmed, A.S.:
Breakdown of Solid Insulating Films by Partial Discharge Using Sinusoidal and Pulse Voltages
In: IEEE Transactions on Electrical Insulation, Vol.13, No.5, pp.337-342, Oct. 1978

[AMI-06] Amin, M. and Salman, M.:
Aging of Polymeric Insulators (An Overview)
In: Reviews on Advanced Materials Science, No. 2, Vol. 13, pp.93-116, 2006.

[AND-07] Anderson, J., Sonerud, B., Serdyuk, Y., Gubanski, S. M. and Hillborg, H.:
Evaluation of Polymeric Materials to Corona and Ozone
In: XVth International Symposium on High Voltage Engineering, Slovenia, pp.1-6, 2007

[ANG-08] Anglhuber, M., Rätzke, S. and Kindersberger, J.:
Erosion von Kunststoffoberflächen bei Koronabelastung
ETG Fachtagung „Grenzflächen in elektrischen Isoliersystemen“, ETG-Fachbericht 112,VDE-Verlag GmbH Berlin Offenbach, Würzburg, pp.15-20, 16-17 Sep. 2008

[ANG-12] Anglhuber, M.:
Untersuchung zum Verhalten nanoskalig gefüllter Epoxidharzformstoffe unter elektrischer Beanspruchung
Dissertation: Lehrstuhl für Hochspannungs- und Anlagentechnik der Technische Universität München, 2012

[ARO-11] Arora, R. and Mosch, W.:
High Voltage and Electrical Insulation Engineering
IEEE Press Series on Power Engineering, Wiley, 2011, ISBN: 9781118008966

[ASH-88] Ashcroft, W. R.:
Chemistry and Technology of Epoxy Resins
Ellis, B. Ed., Blackie Academic & Professional, London, 1993.

[AUG-04] Augustsson, C.:
NM Epoxy Handbook
Nils Malmgren AB.2004

[BAR-87] Bartnikas, R.:
Electrical Properties of Solid Insulating Materials: Measurement Techniques
Engineering Dielectrics, Vol. II b: ASTM STP 926, 1987

[BAT-63] Batzer, H., Ernst, O. and Strieli, R.:
Cycloaliphatische Epoxidharze
In: Elektronische Zeitschrift B, Vol.15, pp.595-599, 1963

[BEY-86] Beyer, M.; Boeck, W.; Möller, K. and Zaengl, W.:
Hochspannungstechnik: theoretische und praktische Grundlagen
Berlin, Heidelberg Springer, 1986

[BOL-95] Bolon, D. A.:
Epoxy Chemistry for Electrical Insulation
In: IEEE Electrical Insulation Magazine, Vol.11, No.4, pp.10-18, July/Aug. 1995

[BOU-11] Boudenne, A., Ibos, L., Candau, Y. and Thomas, S.:
Handbook of Multiphase Polymer Systems
Wiley, ISBN: 9780470714201, 2011

[BRY-99] Brydson , J.A.:
Plastic Materials, 5th edition
Butterworth-Heinemann, ISBN: 9780750641326, 1999

[BUI-69] Bui-Ai, Guyetand A., and Pham Van Vui:
On the Working Life of Insulators Subjected to Partial Discharges
In: C. R. Academy of Science, Paris, Vol.268, 824-827, 1969

[CAV-07] Cavallini, A., Fabiani, D. and Montanari, G.C.:
Time-Evolution o Nanostructured Epoxy Resin Degradation Due to Surface Partial Discharge Activities
In: IEEE Annual Report Conference on Electrical Insulation and Dielectric Phenomena (CEIDP), pp.256-259, 14-17 Oct. 2007

[CHE-81] Cherney, E. A. and Stonkus, D. 1.:
Non-Ceramic Insulators for Contaminated Environments
In: IEEE Transactions on Power Apparatus and Systems, Vol.100, No.1, pp.131-142, Jan. 1981

[CIG-04] Cigré WG D1.14:
Material Properties for Non-Ceramic Outdoor Insulation
Technical brochure No.455, WG D1.14, August 2004

[CIG-12] Cigré WG D1.14:
Resistance to Weathering and UV Radiation of Polymeric Materials for Outdoor Insulation
Technical brochure No.488, WG D1.14, Feb. 2012

[COO-60] Cooper, G. D. and Prober, M.:
The Action of Oxygen Corona and of Ozone on Polyethylene
In: Journal of Polymer Science, Vol.44, pp.397-409, 1960

[DAK-74] Dakin, T. W.:
Application of Epoxy Resins in Electrical Apparatus
In: IEEE Transactions on Electrical Insulation, Vol. EI-9, No.4, pp.121-128, Dec. 1974

[DAN-76] Daniel, C.:
Applications of Statistics to Industrial Experimentation
Wiley, New York, 1976, ISBN: 9780471194699

[DAV-76] Davies, O. L. and Goldsmith, P. L.:
Statistical Methods in Research and Production
Longman, New York, 1976, ISBN: 978-0582450875

[DE-90] De Mattos Mehland, E. L. and de TourreiI, C. H.:
Multiple Stress Aging of HV Polymeric Insulation
In: IEEE Transactions on Electrical Insulation, Vol.25, No.3, pp.521-526, June 1990

[DIS-92] Dissado, L. A. and Fothergill, J. C.:
Electrical Degradation and Breakdown in Polymers
IEE, Peter Peregrinus Ltd., 1992, ISBN: 0863411967

[DOM-92] Domininghaus, H.:
Die Kunststoffe und ihre Eigenschaften
VDI Verlag, 1992, ISBN: 9783540264330

[DON-94] D. L. Donoho, I. M. Johnstone,
Ideal Spatial Adaptation via Wavelet Shrinkage
In: Biometrika, Vol.81, pp.425-455, 1994

[DU-08] Du, B. X., Yong, L. and Wang, R. L.:
Effects of Corona Discharge on Surface Deterioration of Silicone Rubber Insulator under Reduced Pressures
In: International Symposium on Electrical Insulating Materials, Piscataway, USA, pp.271-274, 2008

[ELE-85] Eletskii, A., and Smirnov, B.:
Dissociation of Molecules in Plasma and Gas: The Energy
In: Pure and Applied Chemistry, Vol.57, pp.1235-1244, 1985

[ELI-86] Elias H. G. and Vohwinkel F.:
New Commercial Polymers 2
Gordon and breach science publisher, 1986, ISBN: 9782881240782

[FAB-09] Fabiani, D., Cavallini, A., Montanari, G.C. and Testa, L.:
Extraction of aging markers for nanostructured epoxy resin aged under surface discharges
In: IEEE Electrical Insulation Conference, Montreal, QC, Canada, pp.387-391, 31 May-03 June 2009

[FOU-99] Fouracre, R.A., MacGregor, S.J. and Tuema, F.A.:
An Investigation into the Mechanisms of Surface Discharges
In: 12th IEEE International Conference on Pulsed Power, Vol.2, pp.1380-1383, 27-30 June 1999

[GAM-87] Gamez-Garcia, M. , Bartnikas, R. and Wertheimer, M.R.:
Synthesis Reactions Involving XLPE Subjected to Partial Discharges
In: IEEE Transactions on Electrical Insulation, Vol. EI-22, No.2, pp.199-205, Apr. 1987

[GRI-06] Grindling, J.:
Simulation zur Verarbeitung von reaktiven Non-Post-Cure-Epoxidharz-Systemen im Druckgelieren und konventionellen Vergießen
Dissertation: Fakultät für Maschinenbau der Universität Paderborn, 2006, ISBN: 3832255834

[GUB-92] Gubanski, S.:
Properties of Silicone Rubber Housings and Coatings
In: IEEE Transactions on Electrical Insulation, Vol.27, No.2, pp.374-382, Apr.1992

[HAC-99] Hackam, R.:
Outdoor HV Composite Polymeric Insulators
In: IEEE Transactions on Dielectrics and Electrical Insulation, Vol.6, No.5, pp.557-585, Oct. 1999

[HAL-93] Hall, E.,
History and Bibliography of Polymeric Insulator
In: IEEE Transactions on Power Delivery, Vol.8, No.1, pp.376-385, Jan. 1993

[HAR-08] Harsch, M.:
Methoden und Ansätze zur spannungsarmen Vernetzung von Epoxidharzen
Dissertation: Fachbereich für Maschinenbau und Verfahrenstechnik der Technischen Universität Kaiserslautern, 2008

[HAU-92] Hauschild, W. and Mosch, W.:
Statistical Techniques for High-voltage Engineering
P. Peregrinus Ltd, IEE Power Engineering Series Vol.13, 1992, ISBN: 086341205X

[HEB-99] Martin Heber
Untersuchungen an heterogenen oxidischen Katalysatoren mittels Ultraviolett-Photoemission
Dissertation: Fachbereich Physikalische Chemie , Chemie Ruhr Universität Bochum, Herbert Utz Verlag, 1999, ISBN:3896755757

[HER-04] Herman, F. M.:
Encyclopedia of Polymer Science and Technology
Wiley & Sons, 3rd Edition, Vol.2, 2004, ISBN: 0471275077

[HIL-98] Hillborg, H. and Gedde, U. W.:
Hydrophobicity Recovery of Polydimethylsiloxane after Exposure to Corona Discharge
In: Elsevier Journal of Polymer, Vol.39, pp.1991-1998, 1998

[HIL-99] Hillborg, H. and Gedde, U. W.:
Hydrophobicity Recovery of Polydimethylsiloxane after Repeated Exposure to Corona Discharges: Influence of Crosslink Density
In: IEEE Conference on Electrical Insulation and Dielectric Phenomena (CEIDP), Austin, TX, USA, pp.751-755, 1999

[HIN-09] Hinde, D. D.:
Corona Discharges on the Surfaces of High Voltage Composite Insulators
Dissertation: Queensland University of Technology, School of Engineering Systems, 2009.

[HUD-92] Hudon C. and Bartnikas R.:
Surface and Gas Phase Reactions Arising with Epoxy Exposed to Partial Discharges
In: IEEE Conference on Electrical Insulation and Dielectric Phenomena (CEIDP), pp.725-734, 18-21 Oct. 1992

[HUH-00] Huh, C., Youn, B. and Lee, S.:
Degradation in Silicone Rubber Used for Outdoor Insulator by UV Radiation
In: 6th International IEEE Conference on Properties and Applications of Dielectric Materials, Vol.1, No., pp.367-370, 21 - 26 June 2000

[HUI-91] van der Huir, R.:
Untersuchung volumen- und Oberflächenspezifischer Eigenschaften polymerer Isolierstoffe für den Hochspannungs-Freilufteinsatz
Dissertation: Technische Universität Braunschweig, 1991

[IJU-02] Ijumba, N. M., Britten, A. C. and Swartz, J. P.:
The Hydrophobicity of Silicone Rubber Insulators Subjected to Water Droplet Corona under HVDC Potential
In: IEEE International Conference on Power System Technology, China, pp.1884-1889, 2002

[JOH-79] Johnston, D. R., LaForte, J. T., Podhorez, P. E. and Galpern, H. N.:
Frequency Acceleration of Voltage Endurance
In: IEEE Transactions on Electrical Insulation, Vol.14, No.3, pp.121-126, 1979

[KAN-03] Kanarev, P., Normov, D.A.:
Energy Balance of Fusion Processes of the Ozone Molecule
In: The Kuban State Agrarian University, Russia, 2003
http://guns.connect.fi/innoplaza/energy/story/Kanarev/ozone/index.html

[KAO-04] Kao, K.C.:
Dielectric Phenomena in Solids: With Emphasis on Physical Concepts of Electronic Processes
Academic Press, 2004, ISBN: 0123965616

[KAT-87] Katz, H.S., Milewski, J.V.:
Handbook of Fillers for Plastics
Van Nostrand Reinhold Company, New York, 1987, ISBN: 0442260245

[KIM-92] Kim, S. H., Cherney, E. A. and Hackam, R.:
Hydrophobic Behavior of Insulators Coated With RTV Silicone Rubber
In: IEEE Transactions on Electrical Insulation, Vol. 27, No.3, pp.610-622, June 1992

[KIM-99] Kim, J., Chaudhury, M. K. and Owen, M. J.:
Hydrophobicity Loss and Recovery of Silicone HV Insulation
In: IEEE Transactions on Dielectrics and Electrical Insulation, Vol.6, No.5, pp.695-702, Oct. 1999

[KIN-13] Kindersberger, J.:
High Voltage Technology
Lecture Notes, TU München, Fall 2013

[KIN-96] Kindersberger, J., Schutz, A., Karner, H. C. and Huir, R. V. D.:
Service Performance, Material Design and Applications of Composite Insulators with Silicone Rubber Housings
In: Cigré 33-303, pp.1-5, 1996

[KOZ-04] Kozako, M., Fuse, N., Ohki, Y., Okamoto, T. and Tanaka, T.:
Surface Degradation of Polyamide Nano-Composites Caused by Partial Discharges using IEC (B) Electrodes
In: IEEE Transactions on Dielectrics and Electrical Insulation, Vol.11, No.5, pp.833-839, Oct. 2004

[KOZ-05a] Kozako, M., Kido, R., Imai, T., Ozaki, T., Shimizu, T. and Tanaka, T.:
Surface Roughness Change of Epoxy/TiO_2 Nanocomposites Due to Partial Discharges
In: IEEE International Symposium on Electrical Insulating Materials (ISEIM), Vol.3, pp.661-664, 5-9 June 2005

[KOZ-05b] Kozako, M., Kuge, S., Imai, T., Ozaki, T., Shimizu, T. and Tanaka, T.:
Surface Erosion Due to Partial Discharges on Several Kinds of Epoxy Nanocomposites
In: IEEE Annual Report Conference on Electrical Insulation and Dielectric Phenomena CEIDP, pp.162-165, 16-19 Oct. 2005.

[KRE-89] Kreuger, F. H.:
Partial Discharge Detection in High-Voltage Equipment
Butterworths, 1989, ISBN: 9780408020633

[KÜC-09] Küchler, A.:
Hochspannungstechnik: Grundlagen - Technologie - Anwendungen
Springer Science & Business Media, 2009, ISBN: 9783540784128

[KUF-00] Kuffel, J. and Kuffel, E. and Zaengl, W.S.:
High Voltage Engineering Fundamentals
Elsevier Science, 2000, ISBN: 9780080508092

[KUM-03] Kumagai, S. and Yoshimura, N.:
Hydrophobic Transfer of RTV Silicone Rubber Aged in Single and Multiple Environmental Stresses and the Behaviour of LMW Silicone Fluid
In: IEEE Transactions on Power Delivery, Vol.18, No.2, pp.506-516, Apr. 2003

[KUM-09] Kumara, S., Serdyuk, Y. V. and Gubanski, S. M.:
Charging of Polymeric Surfaces by Positive Impulse Corona
In: IEEE Transactions on Dielectrics and Electrical Insulation, Vol.16, No.3, pp.726-733, June 2009

[KUM-12] R. Kumar, P. Patel
Signal Denoising with Interval Dependent Thresholding Using DWT and SWT
In: International Journal of Innovative Technology and Exploring Engineering (IJITEE), Vol.1, pp.47-50, Nov. 2012

[LEE-99] Lee, B.S. and Lee, D.C.:
Surface Degradation Properties of Ultraviolet Treated Epoxy/Glass Fiber
In: IEEE Transactions on Dielectrics and Electrical Insulation, Vol.6, No.6, pp.907-912, Dec. 1999

[LEN-08] Leng, Y.:
Materials Characterization: Introduction to Microscopic and Spectroscopic Methods
John Wiley, Singapore, 2008, ISBN: 0470822988

[LIU-06] Liu, J., He, W., Zhou, L. and Yang, F.:
Application of Ultraviolet Detector in Discharge Detection
In: International Journal of Emerging Electric Power Systems, Vol.7, pp.1-6, 2006

[LUO-13] Luo, Y., Wu, G., Liu, J., Zhu, G., Wang, P., Cao, K.,
Damage Processes of Polyimide Film Caused by Surface Discharge
In: IEEE International Conference on Solid Dielectrics (ICSD), pp.325-328, 30 June - 04 July 2013

[MA-02] Ma, X., Zhou, C. and Kemp, I. J.:
Interpretation of Wavelet Analysis and its Application in Partial Discharge Detection
In: IEEE Transactions on Dielectrics and Electrical Insulation, Vol.9, No.3, pp.446–457, June 2002

[MA-11] Ma, B.:
Effects of Corona and Ozone Exposure on Properties of Polymeric Materials for High Voltage Outdoor Applications
Dissertation: Department of Materials and Manufacturing Technology, Chalmers University Of Technology, Göteborg, Sweden 2011, ISBN: 9789173855655

[MAC-97] Mackevich, I. and Shah, M.:
Polymer Outdoor Insulation Materials Part I: Comparison of Porcelain and Polymer Electrical Insulation
In: IEEE Electrical Insulation Magazine, Vol. 13, No. 3, pp, 5-11, May - June 1997

[MAL-03] Mallon, P. E., Greyling, C. J., Vosloo, W. and Jean, Y. C.:
Positron Annihilation Spectroscopy Study of High-Voltage Polydimethylsiloxane (PDMS) Insulators
In: Elsevier Journal Radiation Physics and Chemistry, Vol.68, pp.453-456, 2003

[MAR-08] Martin, R.:
Ageing of Composites
Elsevier Science, Woodhead Publishing Series in Composites Science and Engineering, 2008, ISBN: 9781845694937

[MAS-78] Mason, J. H.:
Discharges
In: IEEE Transactions on Electrical Insulation, Vol.13, No.4, pp.211-238, Aug. 1978

[MAS-06] Massey, L.K.:
The Effect of UV Light and Weather: On Plastics and Elastomers, 2nd Edition
Elsevier Science, Plastics Design Library, 2006, ISBN: 9780815519256

[MAY-73] Mayoux, C. and Bui, A.:
Scanning Electron Microscope Observations of the Effects of Discharges on PE
In: IEEE Transactions on Applied Physics, Vol.44, No.8, pp.3423-3424, Aug. 1973

[MAY-76] Mayoux, C. J.:
Partial Discharge Phenomena and the Effect of Their Constituents on Polyethylene
In: IEEE Transactions on Electrical Insulation, Vol.11, No.4, pp.139–148, Dec. 1976

[MAY-88] May, C. A.:
Epoxy Resins Chemistry and Technology
Marcel Dekker Inc., New York, Second Edition, 1988, ISBN: 0824776909

[MCM-68] McMahon, E.J.:
The Chemistry of Corona Degradation of Organic Insulating Materials in High-Voltage Fields and under Mechanical Strain
In: IEEE Transactions on Electrical Insulation, Vol.3, No.1, pp.3-10, Feb. 1968

[MEI-05] Meincken, M., Berhane, T. A. and Mallon, P. E.:
Tracking the Hydrophobicity Recovery of PDMS Compounds Using the Adhesive Force Determined by AFM Force Distance Measurements
In: Elsevier Journal of Polymer, Vol.46, pp.203-208, 2005

[MOR-99] Moreno, V. M. and Gorur, R. S.:
AC And DC Performance of Polymeric Housing Materials for HV Outdoor Insulators
In: IEEE Transactions on Dielectrics and Electrical Insulation, Vol.6, No.3, pp.342-350, June 1999

[MOR-00] Moreno, V. M. and Gorur, R. S.:
An Experimental Approach to the Estimation of the Long Term Corona Performance of Non-Ceramic Insulator Housings
In: IEEE International Symposium on Electrical Insulation (ISEI), Anaheim, CA, USA, pp.193-196, 2000

[MOR-01a] Moreno, V. M. and Gorur, R. S.:
Effect of Long-Term Corona on Non-Ceramic Outdoor Insulator Housing Materials
In: IEEE Transactions on Dielectrics and Electrical Insulation, Vol.8, No.1, pp.117-128, Mar. 2001

[MOR-01b] Moreno, V. M. and Gorur, R. S.:
Corona Induced Degradation of Non-Ceramic Insulator Housing Materials
In: IEEE Conference on Electrical Insulation and Dielectric Phenomena (CEIDP), Ontario, Canada, pp.640-643, 2001

[MUR-01] Murooka, Y., Takada, T. and Hiddaka, K.:
Nanosecond Surface Discharge and Charge Density Evaluation Part I: Review and Experiments
In: IEEE Electrical Insulation Magazine, Vol.17, No.2, pp.6-16, Mar - Apr 2001

[NAI-13] Naidu, S. and Kamaraju, V.:
High Voltage Engineering
McGraw-Hill Education, 2013, ISBN: 9781259062896

[NAS-71] E. Nasser
Fundamentals of Gaseous Ionization and Plasma Electronics
John Wiley & Sons Inc., 1971, ISBN: 047163056X

[NIA-14] Niayesh K. and Gockenbach E.:
On the Aging Mechanism of Solid Insulating Materials Exposed to Repetitive High Voltage Pulses
In: IEEE Transactions on Dielectrics and Electrical Insulation, Vol.21, No.1, pp.304-310, Feb. 2014

[NYA-11] Nyamupangedengu, C.:
PD-Type-Dependent Spectral Bandwidth in Solid Polymer Dielectrics
Dissertation: Faculty of Engineering and the Built Environment, University of the Witwatersrand, Johannesburg, South Africa, 2011

[OLA-05] Olah, A., Hillborg, H. and Vancso, G. J.:
Hydrophobic Recovery of UV/Ozone Treated Polydimethylsiloxane: Adhesion Studies by Contact Mechanics and Mechanism of Surface Modification
In: Elsevier Journal of Allied Surface Science, Vol.239, pp.410- 423, 2005

[OLL-98] Ollier-Durbault, V. and Gosse, B.:
Photo-Oxidation and Electrical Aging of Anhydride-Cured Epoxy Resins
In: IEEE Transactions on Dielectrics and Electrical Insulation, Vol.5, No.6, pp.935-943, Dec. 1998

[OLY-67] Olyphant, M.:
Internal Corona Testing of Casting Resins
In: IEEE Transactions on Electrical Insulation, Vol.2, No.2, pp.92-101, Aug. 1967

[PAT-00] Patsch, R., Berton, F. and Jung J.:
Space Charge, Local Electric Field and Partial Discharges
In: 8th IEE International Conference on Dielectric Materials, Measurements and Applications, No.473, pp.519-522, 17-21 Sep. 2000

[PAT-99] Patsch, R., Berton, F. and Jung J.:
Pulse-Sequence-Analysis - Chances to Characterize Defects
In: IEEE International Conference on Electrical Insulation and Dielectric Phenomena (CEIDP), Vol.1, pp.243-248, 17-20 Oct. 1999

[PFE-91] Pfeiffer, W.:
High-frequency Voltage Stress of Insulation
In: IEEE Transactions on Dielectrics and Electrical Insulation, Vol.26, No.2, pp.239-246, Apr. 1991

[PIN-02] Pinnangudi, B.N., Gorur, R.S. and Kroese, A. J.:
Energy Quantification of Corona Discharges on Polymer Insulators
In: IEEE Conference on Electrical Insulation and Dielectric Phenomena (CEIDP), pp.315-318, 2002

[PIN-05] Pinnangudi, B.N., Gorur, R.S. and Kroese, A. J.:
Quantification of Corona Discharges on Non-Ceramic Insulators
In: IEEE Transactions on Dielectrics and Electrical Insulation, Vol.12, No.3, pp.513-523, June 2005

[RAM-12] Ramanujam M.:
Photo-oxidation and Weathering of LDPE Studied by Surface and Bulk Analysis
Dissertation: Fakultät III Prozess-wissenschaften, Technische Universtität Berlin, Berlin, 2012

[SCH-81] Schnabel, W.:
Polymer Degradation: Principles and Practical Applications
Carl Hanser GmbH, 1981, ISBN: 3446132643

[SCI-03] Scierka, S., Forster, A. and Kosik, W.:
An XPS Study on the Effects of Pigment on the UV Degradation of an Epoxy System
In: 81st Annual Meeting Technical Program of the Federation of Societies for Coatings Technology (FSCT), Pennsylvania Convention Center, Philadelphia, PA, 13–14 Nov. 2003

[SEI-98] Seifert, J.:
Grenzflächen- und Verbundprobleme in mineralisch gefüllten Epoxidharzformstoffen
Dissertation: Fakultät für Maschinenbau und Elektrotechnik der Technischen Universität Carolo-Wilhelmina zu Braunschweig, 1998, ISBN: 978-3826547300

[SHI-00] Shim, I, Soraghan, J. J., Siew, W.H.:
Digital Signal Processing Applied to the Detection of Partial Discharge: An Overview
In: IEEE Electrical Insulation Magazine, Vol.16, No.3, pp.6-12, May – June 2000

[SHI-01] Shim, I, Soraghan, J. J., Siew, W.H.:
Detection of PD Utilizing Digital Signal Processing Methods, Part 3: Open-Loop Noise Reduction
In: IEEE Electrical Insulation Magazine, Vol.17, No.1, pp.6-13, Jan. - Feb. 2001

[SHU-95] Shugg, W. T.:
Handbook of Electrical and Electronic Insulating Materials
Second Edition, IEEE Press, IEEE Dielectrics and Electrical Insulation Society, Piscataway, 1995, ISBN: 978-0780310308

[SON-08] Sonobe, T.:
Electric Power System Suppressing Corona Discharge from Viewpoint of Environment
US Patent 7,447,567, 2008, http://www.google.de/patents/US7447567

[SOR-97a] Sorqvist, T. and Vlastos, A. E.:
Outdoor Polymeric Insulators Long Term Exposed to HVDC
In: IEEE Transactions on Power Delivery, Vol.12, No.2, pp.1041-1048, Apr. 1997

[SOR-97b] Sorqvist, T. and Vlastos, A. E.:
Performance and Aging of Polymeric Insulators
In: IEEE Transactions on Power Delivery, Vol.12, No.4, pp.1657-1665, Oct. 1997

[STA-68] Stamm H. and Hanella K.:
Elektrische Gießharze
Ausgewälte Probleme der Hochspannungstechnik, Berlin, Verlag Technik VEB, 1968

[SUW-98] Suwarno, Salama, Sirait, K. T. and Kaerner, H. C.:
Dielectric Properties and Surface Hydrophobicity of Silicone Rubber under the Influence of the Artificial Tropical Climate
In: IEEE International Symposium on Electrical Insulating Materials, pp.607-610, 27-30 Sep. 1998

[TAN-06] Tanaka, T., Nose, A., Ohki, Y. and Murata, Y.:
PD Resistance Evaluation of LDPE/MgO Nanocomposite by a Rod-to-Plane Electrode System
In: IEEE 8th International Conference on Properties and applications of Dielectric Materials, pp.319-322, June 2006

[TAN-07] Tanaka, T., Yazawa, T., Ohki, Y., Ochi, M., Harada, M. and Imai, T.:
Frequency Accelerated Partial Discharge Resistance of Epoxy/Clay Nanocomposite Prepared by Newly Developed Organic Modification and Solubilization Methods
In: IEEE International Conference on Solid Dielectrics, Winchester, UK, pp.337-340, 8-13 July 2007

[TAN-08a] Tanaka, T., Ohki, Y., Ochi, M., Harada, M. and Imai, T.:
Enhanced Partial Discharge Resistance of Epoxy/Clay Nanocomposite Prepared by Newly Developed Organic Modification and Solubilization Methods
In: IEEE Transactions on Dielectrics and Electrical Insulation, Vol.15, No.1, pp.81-89, 2008

[TAN-08b] Tanaka, T., Matsuo, Y. and Uchida, K.:
Partial Discharge Endurance of Epoxy / SiC Nanocomposite
In: IEEE Annual Report Conference on Electrical Insulation and Dielectric Phenomena (CEIDP), pp.13-16, 26-29 Oct. 2008

[TAN-11] Tanaka, T., Bulinski, A., Castellon, J., Frechette, M., Gubanski, S., Kindersberger, J., Montanari, G.C., Nagao, M., Morshuis, P., Tanaka, Y., Pelissou, S., Vaughan, A., Ohki, Y., Reed, C.W., Sutton, S. and Han, S.J.:
Dielectric Properties of XLPE/SiO2 Nanocomposites based on CIGRE WG D1.24 Cooperative Test Results"
In: IEEE Transactions on Dielectrics and Electrical Insulation, Vol.18, No.05, pp.1482-1517, Oct. 2011

[TAN-86] Tanaka, T.:
Internal Partial Discharge and Material Degradation
In: IEEE Transactions on Electrical Insulation, Vol.21, No.6, pp.899-905, Dec. 1986

[TRI-39] Trichel, G. W.:
The Mechanism of the Positive Point-to-Plane Corona in Air at Atmospheric Pressure
In: Journal of Physical Review, American Physical Society, Vol.55, pp.382-390, 1939

[TSA-02] Tsai, Shu-Jen Steven
Power Transformer Partial Discharge (PD) Acoustic Signal Detection using Fiber Sensors and Wavelet Analysis, Modeling, and Simulation
Master of Science, Virginia Polytechnic Institute and State University, 2002, Blacksburg, Virginia, U.S.A, URN: etd-12062002-152858

[VEN-07] Venkatesulu, B. and Thomas, M. J.:
Long-term Accelerated Multistress Aging of Composite Outdoor Polymeric Insulators
In: IEEE International Conference on Solid Dielectrics, Winchester, UK, pp.188-191, 8-13 July 2007

[WU-07] Wu, N.:
Microscopy and Spectroscopy: Chapter 3: X-ray Photoelectron Spectroscopy
Mechanical and Aerospace Engineering, West Virginia University, 2007

[YOS-99] Yoshimura, N., Kumagai, S. and Nishimura, S.:
Electrical and Environmental Aging of Silicone Rubber used in Outdoor Insulation
In: IEEE Transactions on Dielectrics and Electrical Insulation, Vol.6, No.5, pp.632-650, Oct 1999

[YOU-05] Youn, B. and Huh, C.:
Surface Degradation of HTV Silicone Rubber and EPDM Used for Outdoor Insulators under Accelerated Ultraviolet Weathering Condition
In: IEEE Transactions on Dielectrics and Electrical Insulation, Vol.12, No.5, pp.1015-1024, 2005

[ZAE-64] Zaengl, W.:
Das Messen hoher, rasch veränderlicher Stoßspannungen
Dissertation: Technische Universität München, 1964

[ZAE-77] Zaengl, W.:
Ein Beitrag zur Schrittantwort kapazitiver Spannungsteiler mit langen Messkabeln
In: ETZ-A, Bd. 98, pp. 792-795, 1977

[ZHU-06a] Zhu, Y., Haji, K., Otsubo, M. and Honda, C.:
Surface Degradation of Silicone Rubber Exposed to Corona Discharge
In: IEEE Transactions on Plasma Science, Vol.34, No.4, pp.1094-1098, 2006

[ZHU-06b] Zhu, Y., Otsubo, M., Honda, C. and Tanaka, S.:
Loss and Recovery in Hydrophobicity of Silicone Rubber Exposed to Corona Discharge
In: Elsevier Journal of Polymer Degradation and Stability, Vol.91, pp.1448-1454, 2006

[ZHU-06c] Zhu, Y., Otsubo, M. and Honda, C.:
Degradation of Polymeric Materials Exposed to Corona Discharges
In: Elsevier Journal of Polymer Testing, Vol.25, pp.313-317, 2006

Standards:

[IEC 60343] Recommended Test Methods for Determining the Relative Resistance of Insulating Materials to Breakdown by Surface Discharges
Second edition, 1991

[IEC 62039] Selection Guide for Polymeric Insulating Materials for Outdoor Use under HV Stress
First edition, 2007

[ISO 483] Plastics - Small enclosures for conditioning and testing using aqueous solutions to maintain the humidity at a constant value, Nov. 2005

9. List of Abbreviations

ANOVA	Analysis of Variance
ATH	Aluminum Trihydrate
CC	Correlation Coefficient
Db	Daubechies Mother Wavelet
DGEBA	Diglycidyl Ether of Bisphenol A
DWT	Discrete Wavelet Transform
EP	Epoxy Resin
EPDM	Ethylene Propylene Diene Monomer Rubber
EPR	Ethylene Propylene Rubber
ESCA	Electron Spectroscopy Chemical Analysis
EVA	Ethylene Vinyl Acetate
FEM	Finite Element Method
FT	Fourier Transform
GFR	Glass Fiber Reinforced
GIS	Gas Insulated Systems
GITS	Gas Insulated Transmission System
GLM	General Linear Model
HTV	High Temperature Vulcanized
LHS	Leybold Heraeus Spectrometer
LPDE	Low Density Polyethylene
MAD	Median Absolute Deviation
PD	Partial Discharge
PE	Polyethylene
PDMS	Polydimethylsiloxane
ppw	parts per weight
RH	Relative Humidity
R-PD	Reverse Partial Discharge
RTV	Room Temperature Vulcanized
SEM	Scanning Electron Microscopy
SER	Solid Epoxy Resins
SIR	Silicone Rubber
SNR	Signal-to-Noise Ratio
STFT	Short Time Fourier Transform
UV	Ultraviolet
XPS	X-ray Photoelectron Spectroscopy

10. List of Symbols

A	Eroded Area
A_i	Area of infinitesimal element
A_{UV}	UV illuminated Area
C	Capacitance
D_{max}	Maximum erosion depth
dw	Change in discharge energy per pulse
E_0	Electric field strength at the ionization boundary
E_b	binding energy
E_g	Electric field strength without space charge
E_k	kinetic energy
E_T	Total discharge energy
f	Test frequency
f_{low}	Low frequency magnitude
f_{high}	High frequency magnitude
H	Relative humidity in discharge medium
hv	photon energy
I_{noise}	Base noise threshold level
I_{pixel}	Pixel intensity
I_{UV}	UV intensity
n	Number of discharges per second, polymerization degree
N_{UV}	number of illuminated pixels
P	Pressure
P_{loss}	Dielectric loss
Q_{cum}	Cumulative charge
Q_i	Charge magnitude per pulse
t_{low-eq}	Low frequency equivalent stress time
t_{high}	High frequency stress time
$tan\delta$	Loss factor
V	Test voltage magnitude
V_i	Pulse inception voltage
Vol_i	Volume of infinitesimal element
Vol	Eroded volume
w	Wavelet coefficient value

10. List of Symbols

$\boldsymbol{Y_A}$	UV erosion yield in terms of eroded area
$\boldsymbol{Y_V}$	UV erosion yield in terms of eroded volume
$\boldsymbol{\alpha}$	Ionization coefficient
$\boldsymbol{\alpha_e}$	Effective ionization coefficient
$\boldsymbol{\varepsilon_r}$	Relative Permittivity
$\boldsymbol{\lambda}$	Wavelength, DWT threshold level
$\boldsymbol{\lambda_m}$	Mean free path
$\boldsymbol{\vartheta}$	Celsius Temperature of discharge medium
$\emptyset$	work function